1-1-2013

Diffusion Of Gold Nanoparticles In Synthetic And Biopolymer Solutions

Indermeet Kohli
Wayne State University,

DYNAMICS OF GOLD NANOPARTICLES IN SYNTHETIC AND BIOPOLYMER SOLUTIONS

by

INDERMEET KOHLI

DISSERTATION

Submitted to the Graduate School

of Wayne State University,

Detroit, Michigan

in partial fulfillment of the requirements

for the degree of

DOCTOR OF PHILOSOPHY

2013

MAJOR: PHYSICS

Approved by:

_____

Advisor Date

_____

_____

_____

_____

DEDICATION

This thesis is dedicated to my family and specially to my husband, Kiranjeet Singh, for his invaluable guidance, encouragement and support.

ACKNOWLEDGMENTS

It is my pleasure to have this opportunity to thank the numerous people who supported me during my academic career. First, I would like to express my gratitude towards Dr. Ashis Mukhopadhyay for all his help and guidance in my research work. I consider myself fortunate to have him as my Ph.D. advisor. His comments and feedback during my experiments, the preparation of manuscripts as well as during the writing of this thesis have been of critical importance. He was always available to talk and I would like to sincerely thank him for all the valuable, thought provoking and fruitful discussions related not only to Physics, but also to matters involving my future career outside Wayne State University. I appreciate him for all his support and encouragement. I would also like to thank Dr. Peter Hoffmann, Dr. Takeshi Sakamoto and Dr. Michael Solomon to have graciously agreed to be a part of my Ph.D. committee. Special thanks must go out to Dr. Ratna Naik to have given me an opportunity to conduct research at Wayne State University. I really appreciate her for being so supportive and considerate from the very beginning.

I would like to thank Dr. Venkatesh Subba Rao and Dr. Rami Omari, my senior lab colleagues, for familiarizing me with the instruments and materials. My research would not have been very smooth without their guidance. I also wish to acknowledge my other lab colleagues - Sharmine Alam, Bhavdeep Patel, Andrew Aneese and Laura Gunther for their help, assistance and interaction during the course of my research. Finally, I would like to acknowledge my family for supporting me throughout all of my academic pursuits.

TABLE OF CONTENTS

LIST OF FIGURES

LIST OF TABLES

CHAPTER 1

INTRODUCTION

The classical systems of colloidal particles, polymeric solutions and melts, amphiphiles, and liquid crystals that have been studied since years are categorized as soft matter.[1] In this chapter, I have outlined the common characteristics of soft matter systems followed by properties of polymeric systems. It will also cover the importance of my research and the organization of this thesis.

1.1 SOFT MATTER

The materials corresponding to the states of matter that cannot be classified as either simple liquids or crystalline solids are termed as soft matter. Some examples of soft matter that we are familiar with from everyday life are glue, tomato ketchup, paste, soap etc. Human body also consists of soft matter such as proteins, polysaccharides and nucleic acid. Soft matter systems exhibit many unique properties. They have a tendency to self assemble in order to minimize the free energy, but unlike other materials, the lowest free energy equilibrium state corresponding to these materials is not of dull uniformity. Various complex structures arise owing to the rich phase behavior caused by subtle balances of energy and entropy in these systems.[1]

These materials display a combination of time dependent elastic and viscous response which is classified as viscoelasticity. If a stress is applied at time t=0 and kept constant thereafter, the first response of a viscoelastic material will be elastic. At time scale greater than τ, the relaxation time, a liquid like behavior is exhibited and the material starts to flow with the strain increasing linearly with time. The relaxation time

"τ" marks the ending of solid like behavior and beginning of liquid like behavior.[2] A good example of viscoelastic material is "silly putty", which if dropped on a hard surface, as a ball, bounces back elastically; whereas flows like a highly viscous liquid if stress is applied to it slowly.

Soft matter systems possess mesoscopic dimensions which correspond to length scales larger than atomic size (> 0.1 nm), but smaller than macroscopic objects (< 10 μm). Despite of being greater than atomic sizes these are small enough to follow Brownian motion.[1, 2] My research work in soft matter physics was mainly focused on the polymeric systems.

1.2 POLYMERS

"Poly" means many and "mer" means part. Giant molecules, that are made up of many repeating units are called polymers. These repeating units are called monomers and are connected to each other by covalent bonds. The process by which monomers are bonded together to form a polymer is called polymerization.

Polymers may exhibit different properties owing to their degree of polymerization, microstructure, and architecture. The number of monomers N, that forms a polymer molecule, is termed as the degree of polymerization. If M_{mon} is the mass of each monomer molecule, then the molecular weight M_w of the polymer will be the product of degree of polarization N and molar mass of monomer M_{mon}.[3]

$$M_w = N\, M_{mon} \qquad 1.2.1$$

Polymer's microstructure is determined by the organization of monomers along the fixed chain. Depending on the type of monomers, polymers can be classified as homo

or heteropolymers with homopolymers consisting of only one type of monomer, and heteropolymers with many different types of monomers. Copolymer is a heteropolymer with only two different types of monomers. Based on the sequence of monomers, copolymers exhibit different microstructures as shown in figure 1.2.1.[3]

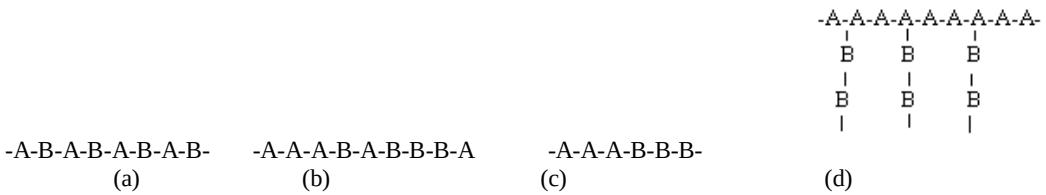

Figure 1.2.1: (a) alternating copolymers (b) random copolymers (c) block copolymers (d) graft copolymers

Polymer architecture depends on monomer structure, linear or branched, as well as the way the polymer was synthesized. Figure 1.2.2 represents different types of polymer architectures. It affects many of the physical properties of the polymeric system, like viscosity etc. Linear polymers, for example: high density polyethylene, can be completely characterized by their degree of polymerization N. Branched polymers possess side chains along with the main chain, and the branches affect the way in which

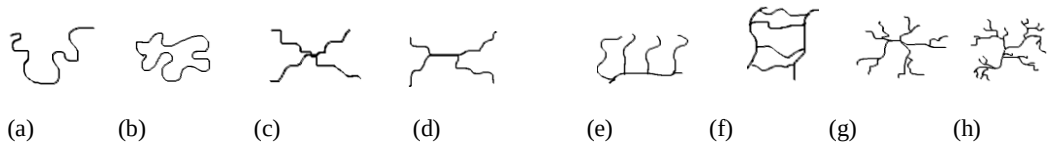

Figure 1.2.2: (a) linear, (b) ring, (c) star-branched, (d) H- branched, (e) comb, (f) ladder, (g) dendrimer (h) randomly branched

molecules move relative to each other. If many branch points are introduced to a polymer system, a macroscopic volume network can be created. Vulcanized rubber is an example of one such macroscopic network.[1]

Polymer chain dimensions as well as thermodynamics of dilute polymer solutions are altered by the quality of the solvent. This can be justified by considering that the presence of solvent molecules modifies the interactions between polymer chains.[2] A solvent is considered to be good if the solvent-monomer interaction is favored over the monomer-monomer interaction. In this case, the chain expands in order to maximize its monomer-solvent contacts, and the polymer adopts a swollen coil conformation. On the other hand, a poor solvent is one in which monomer-monomer interaction is favored and the chain contracts in order to minimize its interactions with the solvent. Very often, in poor solvents, polymers precipitate to minimize solvent contact rather than adopting a highly compact conformation. To counterbalance the effect of becoming compact, the excluded volume effect comes to play. In the case where these two effects are perfectly balanced, the polymer chain adopts unperturbed dimensions, and the corresponding solvent is known as theta solvent.[2]

The root mean square end-to-end distance in a good solvent, according to Flory is given as:

$$< r^2 >^{\frac{1}{2}} \sim N^{\upsilon} \qquad 1.2.2$$

where N is the degree of polymerization. The exponent υ in case of good solvent is υ = 3/5 since the chain expands, and in case of theta solvent, υ = ½. In the case of poor solvent, υ = 1/3 implying that the attractive polymer/solvent interactions dominated the

repulsive excluded volume effect and thus the chain collapsed and formed a compact globule.[1] The exact value for Flory exponent in a good solvent is .588. Expansion factor α, which is the ratio between the perturbed and unperturbed dimensions for a good solvent is $\alpha > 1$, for a poor solvent $\alpha < 1$ whereas for a theta solvent $\alpha = 1$.[2]

One of the interesting properties of polymeric systems is glass transition. Glass is classified as a non-crystalline solid. Although it has short-range order, it possesses elastic properties that make it resemble with solids. It can be obtained by cooling the material, starting from a temperature above its melting point. There are two possibilities for the system to be in while it is being cooled, it can either crystallize or remain in a liquid state. Polymers being viscoelastic exhibit a super cooled metastable state, and in some cases the rearrangement of the structure of the super cooled state is unable to catch up with the cooling rate. This implies that the cooling rate is fast enough that it doesn't give enough time to the liquid to crystallize. Under such conditions, the system is no longer in equilibrium and forms a glassy solid. This is called glass transition. The temperature range in which glass transition takes place depends on the heating/cooling conditions of the experiment, though most commonly it is marked by one particular temperature called glass transition temperature T_g.[1, 2]

T_g is the temperature below which the state of the amorphous substance exhibits the properties of solid (glass phase) and above which it behaves like a viscous liquid. As the glass transition temperature is approached, the viscosity becomes too large. Due to this high viscosity, the movement of the molecules is restricted and they get interlocked.

As a result, no appreciable change in the structure is noticed for a long time and it appears as if the liquid has frozen at a temperature below T_g.

The change from liquid to glass is marked by discontinuities in thermodynamic quantities that are dependent on free energy, being its second derivatives. Figure 1.2.3 shows volume as a function of temperature, which shows a discontinuous change at the T_g, which is dependent on experimental conditions. In case the liquid forms a crystal, the path marked "crystal" will be followed by it, and at a melting temperature T_m there will be a discontinuous change in the volume attributing to the formation of crystal phase (first order). On the other hand, if the cooling rate is fast enough then the liquid will be cooled below its freezing point without crystallizing. It will follow path "Glass (1)". A change in the slope of the graph can be noticed at some temperature below freezing point, which corresponds to T_g. If the cooling rate is a lower than that for glass (1), then the path "Glass (2)" will be followed. It appears to be similar to second order but that is not true thermodynamically since transition temperature depends on the rate at which experiment is performed.[1] The dynamics of a system are greatly altered when measured near the T_g of the corresponding system.

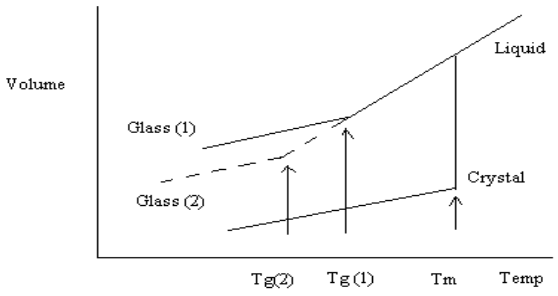

Figure 1.2.3: Volume vs. Temperature. Glass(1) and Glass (2) represent the two different paths followed by the polymeric system depending on the rate of cooling.

Polymeric systems include polymer solutions and polymer melt, where polymer melt corresponds to a state of liquid polymer (melted). My research work was focused on studying polymer solution dynamics using gold nanoparticles as probes. In the case of simple liquids, the translational diffusion coefficient (D) of isolated spherical particles is given by the well-known Stokes−Einstein (SE) relation,

$$D = k_B T/6\pi\eta_o R_o, \qquad 1.2.3$$

where k_B is the Boltzmann constant, T is the absolute temperature, R_o is the radius of the spherical particle, and η_o is the solvent viscosity. On the other hand in case of polymer solutions, where there are probe particles, polymer and solvent molecules, various length scales are involved and the applicability of this relation becomes complicated. This discussion will be revisited in the following chapters.

1.3 SIGNIFICANCE OF RESEARCH

Understanding the transport properties of nanoparticles in solutions of macromolecules is relevant for many interdisciplinary fields of study as well as important for many technological applications. For instance, nanoparticles have been used to enhance the lifetime of plastics, which was a major concern in the field of bioengineering and microelectronics. It has been demonstrated that when nanoparticles are dispersed in a polymer matrix, they tend to move towards the source of any crack. Such a response of nanoparticles results in development of more durable and self healing plastics.[4] Thus, these studies are significant in the development of novel composite systems that contain nano sized inclusions.

Recently in the field of biophysics, gold nanoparticle are being used for cancer diagnostics as well as therapy owing to their unique optical properties.[5] It is thus important to study their dynamics in physiological environments. Polymer solutions can mimic such crowded systems and provide insight for understanding nanoparticle motion in complex fluids and biological systems, figure 1.3.1.[6]

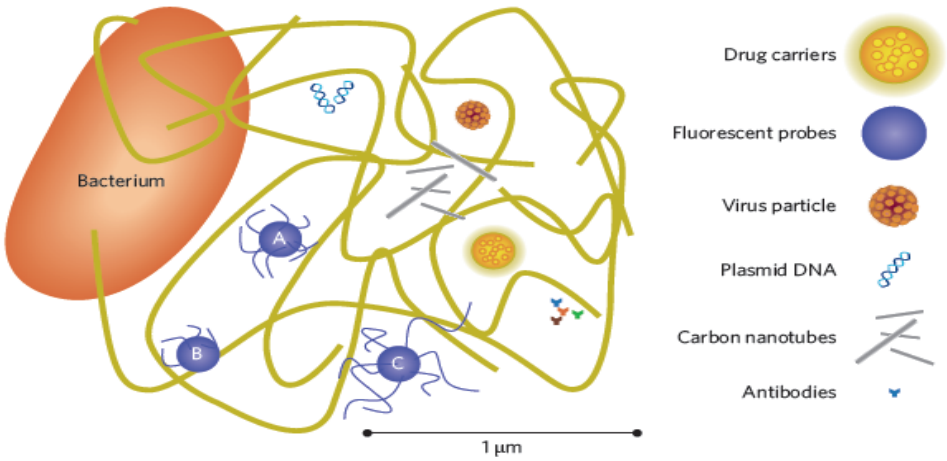

Figure 1.3.1: Scaled representation of mucin network. Understanding length scale dependent transport properties of nanoparticles in polymer solutions is relevant to dynamics of drug delivery carrier through these complex spatial structures (Cu 2009).

In the field of soft matter physics and nanotechnology[7], these studies play a vital role in confirming the accuracy of theories of particle dynamics and explaining the discrepancies between microrheology theory and experiments.

1.4 THESIS DETAILS

This thesis will investigate three important topics in soft condensed matter Physics. First, we shall investigate how different length scales of a polymer solution

affect the dynamics of nanoparticles. Adsorption of nanoparticles at the surface of biopolymers like proteins will be the second component of this thesis. The final section of this thesis will be the study of the effect of macromolecular crowding on nanoparticle dynamics; here, attention will be paid to branched polymer systems and particulate solutions.

This dissertation will be organized as follows. Chapter 2 will provide some background information with the previous work done in the fields relevant to my projects. Chapter 3 will comprise the experimental techniques used to study soft matter systems, more specifically fluorescence correlation spectroscopy (FCS) that I had employed for my experiments. Chapter 4-6 will be on the various experiments that I had performed along with the respective results. Specifically, Chapter 4 covers my investigation of the effect of length scales on the diffusion of nanoparticles in polymer solutions, Chapter 5 focuses on the interaction and diffusion of nanoparticles in protein solutions, Chapter 6 covers nanoparticle behavior in branched polymer solutions, and Chapter 7 will consist of conclusion and future research plan. The last section in the thesis will be an appendix covering the research work that I had performed in collaboration with Dr. Lawes' group, and some of the current research being performed in my group.

CHAPTER 2

BACKGROUND

2.1 POLYMERIC SYSTEMS

The investigation of particle diffusion in polymeric systems started as early as 1960s. During the subsequent twenty years, the important principles, that form the basis of modern polymer physics, were developed. As of today, a lot of theoretical as well as experimental work has been done to describe polymer melt and solution dynamics.

A considerable discussion about dilute polymer solutions as well as polymer melt properties has been done in the literature.[8-10] A rational reason for the same is that polymer melt properties have important industrial applications, for example, in processes like injection molding, film casting etc. Properties of the polymer melt are substantially determined by the polymer molecular weight. The techniques employed to determine polymer's molecular weight, for instance measuring intrinsic viscosity, work in dilute solution regime, thereby rendering study of these dilute solutions important. The focus of this thesis is on the probe diffusion in non dilute polymer solutions, that is the regime between dilute polymer solutions and polymer melts. A lot of work has been done so far on probe diffusion in polymeric systems, and it is not possible to list all of it. The following section of the chapter will cover the theoretical and experimental results that are most relevant to my research. Section 2.2 and 2.3 will provide background pertinent to chapter 4 and 6, where we have discussed probe diffusion in linear polymer, slightly branched polymer and particulate solutions. Section 2.4 will provide background for chapter 5 corresponding to probe dynamics in biopolymer solutions.

2.2 PREVIOUS THEORETICAL WORK

2.2.1 HYDRODYNAMIC THEORIES

According to the physical concepts applied, the theories describing probe diffusion in polymeric systems can be divided into two broad classes.[11] The first class of theories was based on hydrodynamic interactions between particles and polymers.[12, 13] For dilute polymer solutions, with probe size $2R_o$ greater than the chain size $2R_g$ (R_g denotes polymer radius of gyration), the chains were considered "hard spheres" with size equal to their hydrodynamic radii. Here, the diffusing probes experienced hydrodynamic interaction with these effective hard spheres. In case of semidilute polymer solutions, the polymers were modeled as fixed friction centers of monomer beads.[12] The hydrodynamic drag experienced by the moving probe particles due to the fixed monomer beads was assumed to be screened at a length scale of the order of solution correlation length. In this class of theories,[12, 14-17] the relaxation of polymer matrix was not taken into account and a stretched exponential dependence of terminal diffusion coefficient on polymer concentration and particle size was predicted.

The second class of theories treated the polymer solutions as "porous" systems and was based on the concept of "obstruction effect".[18-22] A distribution of distances from an arbitrary point in the system to the nearest polymer characterized the "pore size". A suspension of random rigid fibers was considered to obtain this distribution.[18] It was assumed that the diffusion coefficient of the probe particles was linearly proportional to the fraction of relatively larger "pores" in polymer solutions. At higher concentrations, when polymers overlap, the probe particles could no longer diffuse through "pores" with

relatively smaller size, and the linear assumption failed. Polymers being flexible and coil like exhibited different dependence of "pore" size on concentration than that of solution of rigid fibers. Besides, particles with size larger than the distance between obstacles (correlation length), were not permanently hindered by obstacles as the polymer dynamics affected the spacing between the obstacles.

The scaling theory for probe diffusion in polymeric systems was developed by Brochard-Wyart and de Gennes.[23] Here, a concentrated polymer solution was considered as a transient statistical network of mesh length ξ (correlation length, average distance between monomer on one chain to the nearest monomer on another chain). A scaling form for the viscosity experienced by probes in polymer solutions was introduced. According to this theory, if probe size $R_o < \xi$, the viscosity should depend on probe size as $\eta(R_o/\xi)$, and if probe size $R_o >> \xi$ the particle should experience full solution viscosity. Thus, ξ was concluded to be the crossover length scale for the viscosity experienced by the nanoprobes. A lot of theoretical work was done to establish the functional form for viscosity dependence on probe size and concentration.[12, 23-25]

Phillies followed the hydrodynamic model to describe probe dynamics. He suggested a stretched exponential functional form for concentration dependence of particle diffusion in polymer solutions

$$D = D_o \exp(-\beta\varphi^{\nu}) \qquad 2.2.1$$

here D_o is particle diffusion in the limit of low concentration, and β and ν are scaling parameters.[24] For a wide range of polymer molecular weights, it was observed that $\nu \sim M^{-1/4}$ and $\beta \sim M^{1}$. This stretched exponential relation worked, within experimental error,

for all polymer concentrations and it was thus assumed that there is no significant change in the nature of polymer motion in dilute or semidilute concentration regime. This was contrary to the predictions of scaling models for polymer self diffusion, where polymer solutions were divided into various concentration regimes and polymer motion was assumed to vary from regime to regime. In case of dilute solutions, where distance between polymer chains is much larger compared to the polymer radius of gyration R_g, scaling theories predicted that single chains diffused as isolated hydrodynamic ellipsoids. In the semidilute regime, where polymer chains overlap, polymer dynamics were assumed to be controlled by chain "reptation", in which polymer chains move parallel to their own backbones. Phillies model however did not consider reptation. In his model, it was assumed that the hydrodynamic interactions are the dominant dynamic chain-chain interactions. A similar mechanism was considered to have been adopted by hard spheres as the one that the polymer chains would follow in order to enhance another chain's drag.The model was thus applicable to polymers and probes of different architectures. Hydrodynamic screening was also not included, and it was assumed that interaction between pair of polymer chains was unaffected by the presence of intervening plymers. Cukier [12] considered the effect of screening in his hydrodynamic model and suggested a functional form for Brownian motion of probes in semidilute concentration regime as

$$D = D_o \exp(-\kappa R_o) \qquad 2.2.2$$

where κ is the hydrodynamic screening length and depends on polymer concentration c (g/ml) as $\kappa \propto c^{1/2}$. All the theories considering hydrodynamic interactions predicted a strong exponential (or stretched exponential) dependence of diffusion coefficient on

polymer concentration. However, a recent scaling theory developed by Cai *et al.*[11] considered coupling between particle motion and polymer dynamics, and suggested a power law dependence of diffusion coefficient. The theoretical arguments proposed by them have been outlined in section 2.2.2.

Fan *et al.* provided an analytical solution to the hydrodynamic resistance experienced by spherical particles moving through a polymer solution.[16] They suggested that owing to the loss of configurational entropy near the wall, the polymer segment density gradually increases from a negligible value at the particle surface to a bulk value far away from the particle. This corresponded to an effective depletion layer within which the viscosity was expected to have increased from solvent viscosity at the solid surface to bulk viscosity in polymer solution.

2.2.2 SCALING THEORY

Cai *et al.* [11] extended the scaling theory for particle mobility in polymer melts, developed by the Brochard-Wyart and de Gennes,[23] in order to understand the dynamics of nanoparticles experiencing thermal motion in polymer solutions. As we used this theory in one of our papers (Macromolecules, 2012), I will discuss it in detail below. According to their theory,[11] particle mobility in polymer liquids was dependent on particle size relative to two important length scales: correlation length ξ ant the tube diameter (entanglement length) a. Dilute solutions refers to the concentration where polymer chains are isolated and have no interactions, and semidilute marks the onset of the regime where chains start to penetrate though there is no effective entanglement. At the overlap concentration φ^*, which marks the crossover from dilute to semidilute regime,

the correlation length ξ is on the order of polymer size. It decreases as a power of polymer concentration as

$$\xi(\varphi) \approx b\varphi^{-\nu/(3\nu-1)} \qquad 2.2.3$$

where b is the Kuhn monomer length and ν is the Flory exponent. This exponent depends on solvent quality. The correlation length scales as $\xi(\varphi) \propto \varphi^{-1}$ ($\nu = 1/2$) in the case of theta solvent, and as $\xi(\varphi) \propto \varphi^{-0.76}$ ($\nu = 0.588$) in the case of athermal solvent.

The second important length scale was the tube diameter (entanglement length) a. In case of athermal or good solvent it was given by

$$a(\varphi) \approx a(1)\varphi^{-\nu/(3\nu-1)} \sim \varphi^{-0.76} \sim \xi \qquad 2.2.4$$

where a(1) corresponds to the tube diameter in polymer melt and is approximately 5 nm. The entanglement length has a different concentration dependence in case of theta solvent given by

$$a(\varphi) \approx a(1)\varphi^{-2/3} \qquad 2.2.5$$

Relative to these two length scales, the particles were divided into three different length regimes, small particles ($2R_o < \xi$) where particle diameter is smaller than the polymer correlation length, intermediate sized particles ($\xi < 2R_o < a$) where a is the tube diameter for entangled polymer liquids, and large sized particles ($2R_o > a$). Having divided the particles into three length regimes, they explained size dependence of the mean square displacement and particle diffusion coefficient.

2.2.2.1 MEAN SQUARE DISPLACEMENT

(a) Small Sized Particles:

It was suggested by the theory, that for small sized particles ($2R_o < \xi$), regime I in figure 2.2.1(a), particle diffusion was similar to that in pure solvent and was not much

affected by polymers. The mean-square displacement in this case, as shown in figure 2.2.1(b), was given by

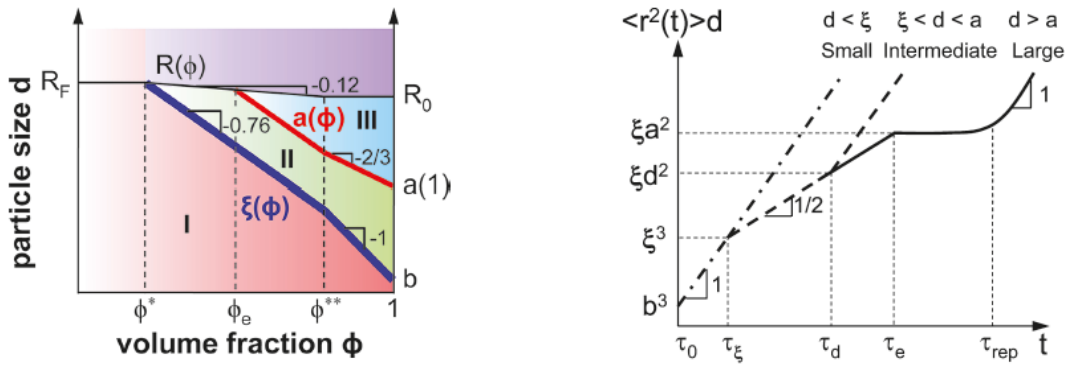

Figure 2.2.1: (a) Three regimes for mobility of probe particles with size d ($2R_o$ in the text) in the polymer solution with volume fraction φ shown in the (φ,d) parameter space: regime I for small particles ($2R_o < \xi$), regime II for intermediate particles ($\xi < 2R_o < a$), and regime III for large particles ($2R_o > a$). Solid lines represent crossover boundaries between different regimes. Thick and medium lines correspond to the dependences of ξ and a on volume fraction φ in good solvent, while thin lines at top describes concentration dependence on polymer size R(φ) (R_g in text). Dashed lines represent concentrations - dilute regime $0 < \varphi < \varphi^*$ where φ^* represents polymer overlap concentration, semidilute unentangled solution regime $\varphi^* < \varphi < \varphi_e$ where φ_e represents concentration at which polymer start to entangle, the semidilute entangled solution regime with $\varphi_e < \varphi < \varphi^{**}$, and the concentrated entangled solution regime with $\varphi^{**} < \varphi < 1$. (b) Time dependence of the product of mean-square displacement $<\Delta r^2(t)>$ and particle size d ($2R_o$ in the text) for small, intermediate and large sized particles. Here, τ_o is the relaxation time for monomer, τ_ξ is the relaxation time for correlation blob, τ_d relaxation time of polymer segment with size comparable to particle size(τ_x in text), τ_e relaxation time of entanglement strand and τ_{rep} the relaxation time of whole polymer chain (Reprinted with permission from Macromolecules 2011, 44, 7853-7863. Copyright (2011) American Chemical Society)

$$<\Delta r^2(t)> \approx D_s t, \text{ for } t > \tau_o \qquad 2.2.6$$

where τ_o is the monomer relaxation time and is given by $\tau_o \approx \eta_s b^3/(k_B T)$. The particle diffusion in this regime was inversely proportional to solvent viscosity η_s and particle size, and was given by

$$D \approx k_B T/(\eta_s R_o) \qquad 2.2.7$$

(b) Intermediate Sized Particles:

For intermediate sized particles ($\xi < 2R_o < a$), regime II figure 2.2.1(a), particle motion was not affected by chain entanglements, but was affected by subsections of polymer chains. The mean square displacement of these particles was proposed to be time scale dependent, figure 2.2.1(b). At short times ($t < \tau_\xi$) particle motion was diffusive and the particle felt local solution viscosity which was similar to that of the solvent viscosity. This diffusive behavior continued up to the time scale τ_ξ, which was the relaxation time of correlation blob with size ξ and was given by $\tau_\xi \approx \eta_s \xi^3/(k_B T) \approx \tau_o (\xi/b)^3$. In the intermediate time scale, ($\tau_\xi < t < \tau_x$), the particle experienced subdiffusion and felt a time-dependent viscosity coupled to fluctuation modes of polymer solution. The polymer mode with a relaxation time t corresponded to the motion of a section of chain containing $(t/\tau_\xi)^{1/2}$ correlation blobs. The effective viscosity felt by the particle, for time scale $\tau_\xi < t < \tau_x$, corresponded to the viscosity of a solution with polymer size comparable to the chain section size $\xi(t/\tau_\xi)^{1/4}$. It was greater than the solvent viscosity by a factor of number of correlation blobs in the respective chain section.

$$\eta_{eff}(t) = \eta_s (t/\tau_\xi)^{1/2} \qquad 2.2.8$$

The effective diffusion coefficient of these particles was given by

$$D_{eff} \approx k_B T/(\eta_{eff}(t) R_o) \approx D_s (t/\tau_\xi)^{-1/2} \qquad 2.2.9$$

and the corresponding mean square displacement for the particles would be

$$\langle \Delta r^2(t) \rangle \approx D_{eff}\, t \approx D_s (t\tau_\xi)^{1/2}, \text{ for } \tau_\xi < t < \tau_x \qquad 2.2.10$$

The subdiffusive regime continued until the time scale $\tau_x \approx \tau_\xi (2R_o/\xi)^4$ which corresponded to the time at which the size of the chain section that determined the viscosity was of the order of particle size $\xi(\tau_x/\tau_\xi)^{1/4} \approx 2R_o$.

At longer times ($t > \tau_x$), the motion was diffusive again ($<\Delta r^2(t)> \approx Dt$) with diffusion coefficient

$$D \approx k_B T/(\eta_{eff}(\tau_x) R_o) \approx k_B T\xi^2/(\eta_s R_o^3) \qquad 2.2.11$$

the effective viscosity (η_{eff}) felt by the particle here was given by a polymer liquid consisting of chains comparable to the particle size

$$\eta_{eff} \sim \eta_s(R_o/\xi)^2 \qquad 2.2.12$$

Intermediate sized particles were relatively more interesting, thus in our experiments we focused on testing the predictions of the scaling theory in this particular length regime.

(c) Large Sized Particles:

Large sized particles ($2R_o > a$) got trapped in the entanglement mesh. The time scale at which the arrest of particle occurred was of the order of relaxation time of entanglement strand

$$\tau_e \approx \tau_\xi (a/\xi)^4 \approx \tau_o (\xi/b)^3 (a/\xi)^4 \qquad 2.2.13$$

At short time scale $t < \tau_e$, large sized particles experienced the same time dependent motion as that of intermediate sized particles in the first two regimes. At time scale longer than τ_e, the motion of large particles could proceed by two mechanisms. The first one was related to the reptation of the surrounding polymers. It could lead to the release

of topological constraints at a time scale τ_{rep}, the reptation time, proportional to cube of number of entanglements per chain.

$$\tau_{rep} \approx \tau_e (N/N_e)^3 \qquad 2.2.14$$

where N_e is the number of monomers per entanglement strand.

The second mechanism involved the hopping of particles between neighboring entanglements due to fluctuations in entanglement mesh. Hopping mechanism was favored by particles with size comparable to tube diameter ($2R_o \approx a$). Large particles got trapped by entanglements at time scale shorter than τ_{rep} and the mean square displacement, figure 2.2.1(b), of these particles was given by

$$<\Delta r^2(t)> \approx a^2\xi/R_o, \text{ for } \tau_e < t < \tau_{rep} \qquad 2.2.15$$

At longer times ($t > \tau_{rep}$), particle motion was Brownian resulting from chain reptation and was affected by bulk viscosity η of the polymer solution, which increased with degree of polymerization N and polymer concentration. The mean square displacement was given by

$$<\Delta r^2(t)>_{rep} \approx (k_BT/\eta R_o)t, \text{ for } t > \tau_{rep} \qquad 2.2.16$$

The diffusion due to chain reptation as experienced by these particles was given by

$$D_{rep} \approx k_BT/(\eta R_o) \approx a^2\xi/(\tau_{rep}R_o), \text{ for } 2R_o > a \qquad 2.2.17$$

2.2.2.2 DIFFUSION COEFFICIENT

(a) Diffusion dependence on particle size

As shown in figure 2.2.2(a), it was concluded from the scaling theory that the small sized particles follow SE relation and the diffusion was determined mainly by the solvent viscosity η_s. On the other hand, diffusion of intermediate sized particles showed a

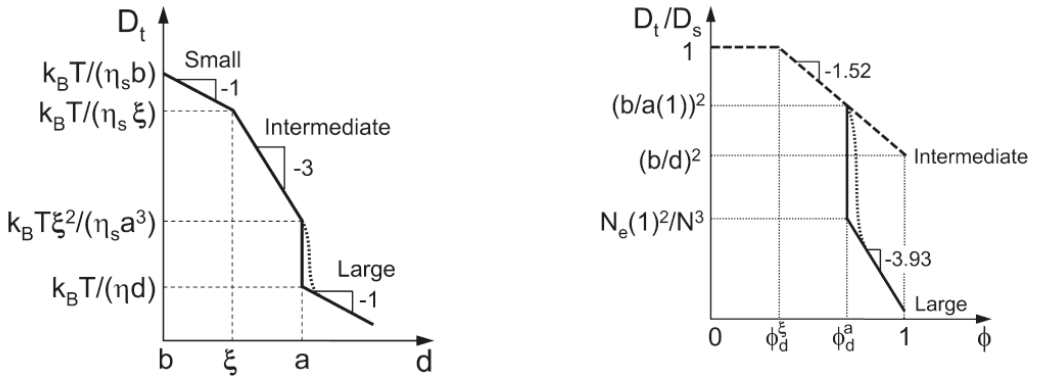

Figure 2.2.2 : (a) Dependence of particle diffusion coefficient on particle size d ($2R_o$ in text). (b) Concentration dependence of terminal diffusion D_t (D in text) normalized by their diffusion in pure solvent. ϕ_d^{ξ} and ϕ_d^{a} (represented by ϕ^{ξ} and ϕ^{a} in text respectively) correspond to crossover concentration at which correlation length ξ and tube diameter a are on the order of particle size (Reprinted with permission from Macromolecules 2011, 44, 7853-7863. Copyright (2011) American Chemical Society).

stronger size dependence as the effective viscosity η_{φ}, felt by these particles increased as the square of particle size $(R_o)^2$. The diffusion coefficient of these intermediate sized particles was thus inversely proportional to the cube of the particle size, $D(R_o) \propto R_o^{-3}$. Large particles felt full solution viscosity η and the diffusion coefficient in this case was determined by chain reptation. The particles with size on the order of tube diameter experienced a sharp drop in the diffusion coefficient. The dotted line in figure 2.2.2(a), shows broadening of this crossover contributed by particle diffusion caused by hopping mechanism. As mentioned earlier, large particle mobility was affected by hopping as well as chain reptation. The particle needed to overcome an entropic energy barrier in order to hop from one entanglement cage to another. This energy barrier increased with the ratio of particle size to tube diameter. Thus as long as particle size was comparable to tube diameter, hopping mechanism controlled particle diffusion and $D \sim \exp(-R_o/a)$. An

important point here was that hopping dominated diffusion does not probe the bulk viscosity of the polymer solution. On the other hand, for $2R_o >> a$ the diffusion was dominated by chain reptation process and particles experienced the macroscopic viscosity of the polymer solution.

(b) Diffusion dependence on polymer concentration:

The theory also predicted the effect of polymer concentration on particle diffusion as shown in figure 2.2.2(b). There were two important concentration dependent length scales involved correlation length $\xi(\varphi)$ and tube diameter $a(\varphi)$. Thus, two crossover concentrations should be considered. The first one was ϕ^{ξ} at which the correlation length was comparable to particle size, $\xi \approx 2R_o$. It was estimated by the expression,

$$\phi^{\xi} \approx \begin{cases} (2R_o/b)^{-1}, & \text{for theta solvent} \\ (2R_o/b)^{-1.32}, & \text{for athermal solvent} \end{cases} \qquad 2.2.18$$

The other important concentration was ϕ^{a} at which tube diameter was on the order of particle size, $a(\phi) \approx 2R_o$. In theta solvent $a(\phi) \approx a(1)\phi^{-2/3}$, and in athermal solvent $a(\phi) \approx a(1)\phi^{-0.76}$ The crossover concentration was estimated by making use of the expression

$$\phi^{a} \approx \begin{cases} (2R_o/a(1))^{-3/2}, & \text{theta} \\ (2R_o/a(1))^{-1.32}, & \text{athermal} \end{cases} \qquad 2.2.19$$

Between ϕ^{ξ} and ϕ^{a}, the particle size corresponded to the intermediate size regime. According to the theory, for volume fraction below ϕ^{ξ} the particle diffusion probed solvent viscosity η_s and was independent of polymer concentration, equation 2.2.7. For volume fraction above ϕ^{ξ}, particle diffusion was affected by segmental motion of polymers and was given by

$$D \approx k_B T\xi^2/(\eta_s R_o^3) \approx \frac{k_B T b^2}{(\eta_s R_o^3)} \varphi^{-2\nu/(3\nu-1)}, \quad \text{for } \phi^{\xi} < \phi < 1 \text{ and } b < 2R_o < a(1) \qquad 2.2.20$$

Thus, in case of intermediate sized particles, the particle diffusion should decrease with solution concentration as a power of -2 for theta solvent ($\nu = 1/2$), and as a power of -1.52 for athermal solvent ($\nu = 0.588$).

At a solution concentration above ϕ^a, the particles fall in large particle regime $2R_o > a$ and experienced full solution viscosity. The diffusion in this regime was controlled by chain reptation and followed

$$D \approx D_{rep} \approx a^2\xi/(\tau_{rep} R_o) \qquad 2.2.21$$

Using the relation $\tau_e \approx \tau_o (\xi/b)^3 (a/\xi)^4$, and $\tau_{rep} \approx \tau_e (N/N_e(\varphi))^3$, the definition of $\xi(\varphi)$ equation 2.2.3, $a(\varphi)$ equation 2.2.4 and the relation

$$N_e(\varphi) \approx N_e(1) \begin{cases} \phi^{-4/3}, & \text{theta} \\ \phi^{-1.32}, & \text{athermal} \end{cases} \qquad 2.2.22$$

the expression for D_{rep}, equation 2.2.17 was simplified to obtain its dependence on solution concentration

$$D(\varphi) \approx \frac{k_B T}{(\eta_s R_o)} \frac{N_e(1)^2}{N^3} \begin{cases} \varphi^{-14/3}, & \text{theta} \\ \varphi^{-3.93}, & \text{athermal} \end{cases} \quad \text{for } \phi^a < \phi < 1 \text{ and } 2R_o > a(1) \qquad 2.2.23$$

2.2.3 COMPUTATIONAL STUDIES

Liu *et al.* did molecular dynamics (MD) simulation to investigate nanoparticle diffusion in polymer melt.[9] They used standard bead-spring model proposed by Kremer and Grest[26] to represent the polymer chain. Figure 2.2.3 represents the effect of nanoparticle size on its dynamics in the dilute limit. This particular simulation considered 100 chains of length N = 60, with the radius of gyration $R_g = 4.0\sigma$, where σ is the size of the monomer. The diffusion, D, of the nanoparticles was obtained by various parallel

simulations with different initial configurations. The reduced viscosity value of $\eta^* \approx 42.5$, was obtained from the literature corresponding to a polymer melt with monomer number density of 0.84.[27] This value was used to calculate the diffusion coefficient of nanoparticles in polymer melt using SE relation, which is also shown in figure 2.2.3 for comparison with MD simulation. It was reported that SE diffusion coefficient gradually approximates the MD data with the increase in R_o/R_g, and becomes same as the ratio approaches unity. At lower R_o/R_g, SE prediction is an order of magnitude slower than that of MD simulation.

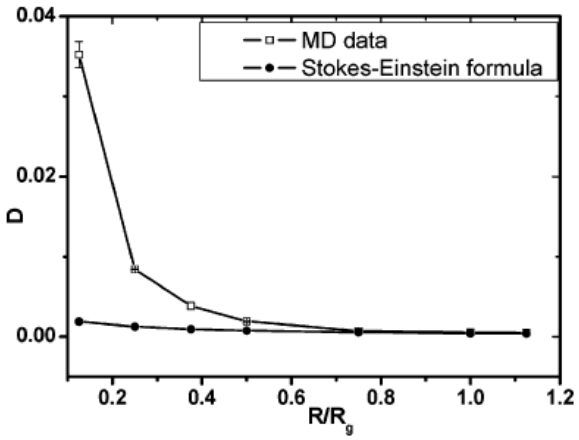

Figure 2.2.3: The diffusion coefficient D of nanoparticles as a function of R/R_g. R here corresponds to particle radius R_o. Open squares represent MD data; full dots represent SE prediction with slip boundary conditions (Reprinted with permission from J. Phys. Chem. C 112, 6653-6661. Copyright (2008) American Chemical Society)

It was justified by considering that the SE formula takes into account the macroscopic viscosity of the polymer melt in order to calculate the diffusion, whereas particles with relatively small values of R_o/R_g, experience microscopic viscosity which

leads to underestimation of diffusion coefficient of these particles by SE. It was suggested that the small nanoparticles experienced nanoviscosity because when they diffused through the polymer melt, they did not necessarily have to wait for the polymer chains to relax, which is coupled to the polymer macroviscosity. As R_o/R_g increased, the solvent behaved as a continuum on the length scale of chain size R_g, causing the bigger particles to experience macroviscosity.

They also studied the dependence of diffusion coefficient on the hydrodynamic radius of the particles in the regime $R_o/R_g < 1$. As shown in figure 2.2.4, it was observed that the diffusion coefficient of these small particles was inversely proportional to the

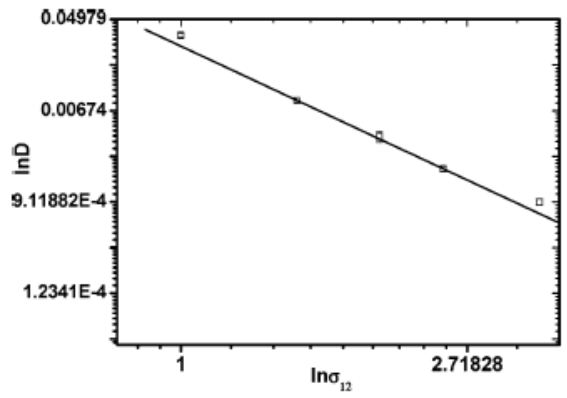

Figure 2.2.4: Ln(D) vs. Ln (σ_{12}), where D is the diffusion coefficient of nanoparticles and σ_{12} is the hydrodynamic radius (R_o). The slope of the fitted line is about -3 suggesting that diffusion coefficient is inversely proportional to cube of hydrodynamic radius for particles in regime $R_o/R_g < 1$ (Reprinted with permission from J. Phys. Chem. C 112, 6653-6661. Copyright (2008) American Chemical Society)

cube of the hydrodynamic radius of these particles. This is contrary to SE relation where the diffusion coefficient is inversely proportional to the particle hydrodynamic radii. It

was suggested that the friction between particle and polymer, in case of these small particles, was caused by monomer rubbing the nanoparticle surface. The resulting friction will then be proportional to particle surface, making local viscosity scale as R_o^2.

Ganesan *et al.* also presented computer simulation results suggesting that the polymer radius of gyration R_g is the length scale controlling the transition from nanoviscosity to macroviscosity.[10] They specifically considered the situation where probe size was greater than that of correlation length, but smaller or comparable to that of the polymer size. It was claimed that for smaller R_o/R_g ratios, the presence of entanglements was not necessary to observe reduction in viscosity, however, the entangled systems showed a much stronger effect.

2.3 PREVIOUS EXPERIMENTAL WORK

Along with theoretical research, a lot of experimental work has also been done over the years to understand particle motion in polymer solutions. As mentioned earlier, only the most relevant work will be mentioned in this section. In late 1970's Langevin and Rondelez investigated sedimentation rates of various nanoparticles with radii 2.5 - 17.5 nm in aqueous poly(ethylene oxide) solutions.[28] They found that the retardation factor s/s_o, where s_o is the sedimentation coefficient of the particle in neat solvent and s is that of the probe in the polymer solution, followed a scaling law: $s/s_o = \psi(R_o/\xi)$ with $\psi \sim 1$ for $R_o/\xi << 1$, and ψ was found to be of the form $\exp(-Ac^y)$. The factor A was reported to be proportional to particle size, and value of the exponent $y \approx 0.62$, as shown in figure 2.3.1, for PEO solutions. This work followed de Gennes' theory where a dense polymer solution was considered to be a transient statistical network of mesh size ξ.[8, 23] Although

it was reported that for probe size smaller than ξ, particles experienced the scaled viscosity, Langevin and Rondelez did not observe particle following macroviscosity at higher polymer concentrations.

Won *et al.* performed dynamic light scattering experiments to investigate dynamics of 200 nm polystyrene (PS) spheres in dilute, semidilute and entangled solution

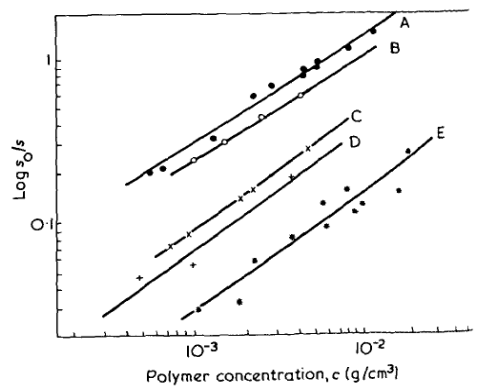

Figure 2.3.1: Log s_o/s vs. log c where c is the polymer concentration. A, slope 0.67; B, slope 0.65; C, 0.75; D, slope 0.75; E, slope 0.70. ●, Ludox in PEO M =300000; ○ , Ludox in PEO M = 140000; x , EMV viruses PEO M = 300000; +, TBSV PEO M = 300000; *, BSA PEO M = 300000 (Langevin 1978).

of poly(vinyl methyl ether) (PVME) with $M_w = 1.3*10^6$.[29] As shown in figure 2.3.2, they observed positive deviation from SE relation as the concentration approached overlap concentration, c^*. It was qualitatively justified by considering that the fluid within a distance on the order of correlation length ξ, from the probe surface, had different composition than that of bulk solution. Thus, the diffusion of the probe over distance comparable to ξ did not experience bulk viscosity. The corresponding depletion zone in a dilute solution was expected to extend to a distance on the order of R_g ($c=c^*$ corresponds to $\xi \approx R_g$) . Whereas, in case of a semi dilute solutions, the extent of this depletion zone

was expected to decrease with the solution correlation length, ξ. Thus at significantly high concentrations, in the entangled regime, SE behavior should be recovered and it indeed was.

Ye *et al.* also reported positive deviation from SE prediction, in their study of probe diffusion in non adsorbing poly(ethylenepropylene) (PEP) solutions, by conducting

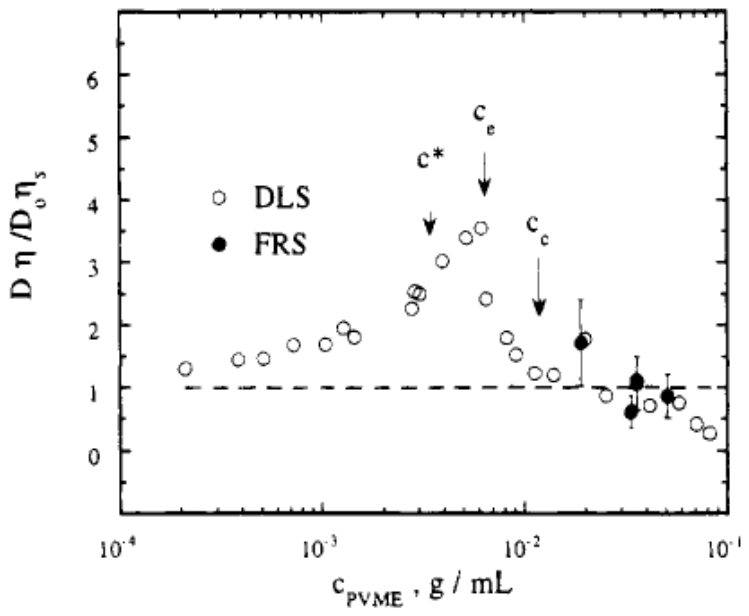

Figure 2.3.2: The product of diffusion coefficient and solution viscosity normalized by corresponding values at infinite dilution as a function of matrix concentration. The dashed line represents SE prediction. c^*, c_e, and c_c correspond to overlap, entanglement and critical concentration respectively, where $c_c \approx 2\ c_e$ (Reprinted with permission from Macromolecules 27(25), 7389-7396. Copyright (1994) American Chemical Society)

DLS and sedimentation experiments.[30] They argued that it was caused by the reduction in the local viscosity experienced by the colloidal particles when their size was comparable to or smaller than correlation length of the polymer solution. Figure 2.3.3 shows the comparison between measured values to that predicted by SE relation.

Michelman *et al.* performed fluorescence correlation spectroscopy experiments to explore the regimes $2R_o \sim \xi$ and $2R_o >> \xi$.[31] Figure 2.3.4 is a schematic of three regimes of probe size relative to correlation length ξ in a polymer solution, representing $2R_o << \xi$, $2R_o \sim \xi$, and $2R_o >> \xi$ in (a), (b), and (c) respectively. They measured the translational diffusion coefficients of various probes (Rhodamine6G, Alexa546, TAMRA, (R)-phycoerythrin, rhodamine-labeled dextran, bovine serum albumin, polystyrene beads) in

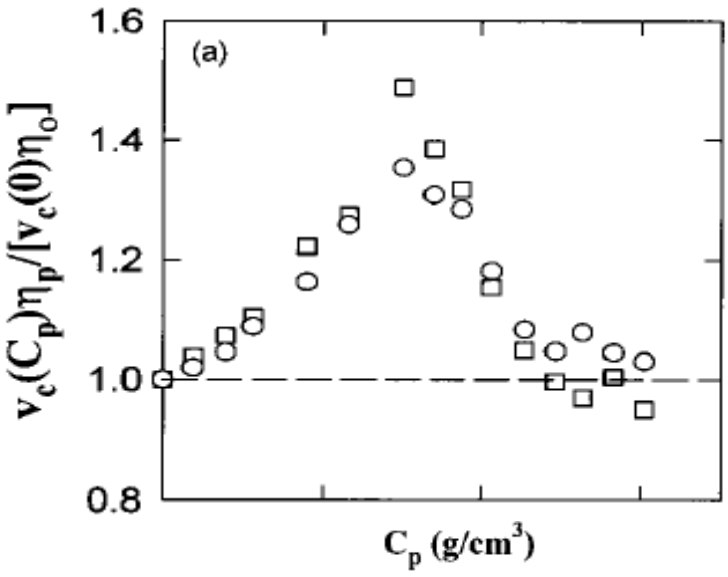

Figure 2.3.3: Measured $v_c(C_p)\eta_p/ v_c(0)\eta_0$ as a function of polymer concentration C_p, where v_c corresponds to the sedimentation velocity and η_p and η_0 represent the polymer solution viscosity and viscosity at infinite dilution respectively. Dashed line corresponds to SE prediction (Reprinted with permission from Macromolecules 31(17), 5785-5793. Copyright (1998) American Chemical Society)

dilute and semidilute poly(vinyl) alcohol (PVA) solutions. It was observed that for particles much larger than correlation length, the scaled diffusion varied exponentially with concentration, $\frac{D}{D_0} = \exp(-bc)$, with b=0.61. Also, for these large polystyrene

particles the decay in the diffusion coefficient was attributed to the increase in the bulk viscosity of PVA solutions, thus following Stoke's Einstein relation. On the other hand, for particles on the order of correlation length the diffusion was reported to be well fit with stretched exponential function as , $\frac{D}{D_0} = \exp(-Rc^n)$. All the probes in this size regime exhibited similar exponent in the range 0.73-0.84 corresponding to a good solvent. It was suggested that the probes on the order of ξ experience some local dynamics.

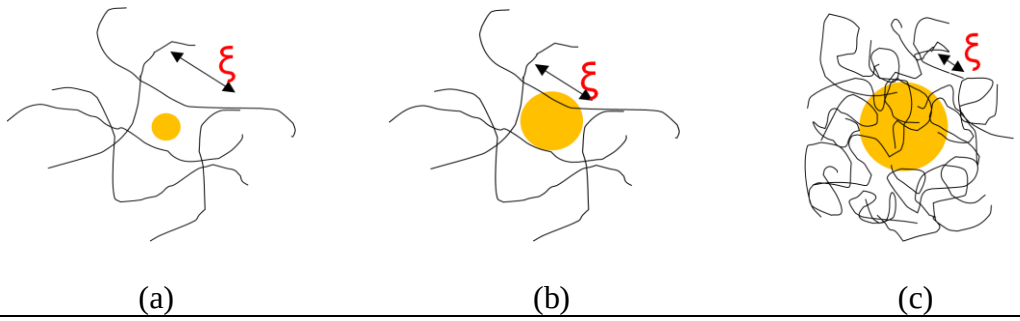

Figure 2.3.4: Schematic diagram depicting three regimes of relative sizes of probes and correlation length, indicated by arrow, of polymer solution in which they are diffusing. In (a) probe is much smaller than correlation length, $2R_o << \xi$. In (b) probe is on the order of correlation length, $2R_o \sim \xi$. In (c) probe is much larger than correlation length, $2R_o >> \xi$

Holyst *et. al.* [32] conducted experiments to investigate the length scale dependent dynamics of nanoparticles using capillary electrophoresis and fluorescence correlation spectroscopy. Many different nanoscopic probes, like dye molecules and proteins, were used in their experiments and had diameters ranging from 1.7 to 114 nm. Poly(ethylene glycol) with molecular weight ranging from 6 to 20 kg/mol were used. It was observed that probes with diameter smaller than polymer radius of gyration experienced

nanoviscosity, which was orders of magnitude smaller than the macroviscosity of the polymer solution. They concluded from their experiments that contrary to the theoretical assumption, the crossover length scale is not related to the blob size ξ. It was rather given by the polymer radius of gyration, R_g as suggested by the MD simulations. They also suggested that de Gennes' scaling form, $\eta(R/\xi)$ is applicable to all probe sizes provided R is identified as the gyration radius or probe diameter depending on the length regime the probe falls into.

Although the relative particle to polymer size chosen for their experiments was such that sufficient data was collected in both $R>R_g$ and $R<R_g$ regime, the use of different probe molecules could have potentially affected the specific probe-polymer chemistry. In addition, the experimental probes used here, being protein molecules, were flexible and porous. This would have allowed the probes to adopt different conformation depending on solvent conditions. In order for them to attain a compact globular structure, the solvent used should have been a poor solvent. This in turn could have altered the probe polymer interaction causing a change in the polymer density distribution near the particle surface, thus affecting particle dynamics.

All the conflicting results regarding the crossover length scale for nanoviscosity to macroviscosity, and the role of various parameters, such as mesh size, effect of entanglement, matrix dynamics, polymer probe interaction, etc. demand further investigation.[28-35] But investigating nanoparticle dynamics in a systematic manner remains challenging. This discussion will be continued in chapter 4.

2.4 PREVIOUS WORK ON BIOPOLYMERS

The information in this section is the background relevant to chapter 5, where I discuss probe interaction and diffusion in biopolymer solutions. Certain inorganic nanoparticle have diagnostic as well as therapeutic applications. Studies have shown that once introduced into plasma, these nanoparticles get coated with a number of biomolecules present in the medium.[36] These biomolecules form a corona and in turn alter the surface properties of the nanoparticles.[37] Thus, understanding the dynamics of these nanoparticles in biopolymers, like proteins, are important for their safe application in living organisms. [38]

Rocker *et al.*[38] studied the interaction of human serum albumin with small polymer coated (10-20 nm) sized FePt nanoparticles and quantum dots. They analyzed

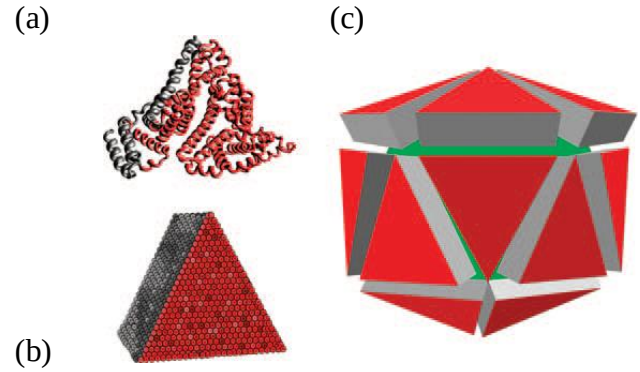

Figure 2.4.1: Structure for HSA (a) Representation of polypeptide chain. (b) Approximated as an equilateral triangular prism. (c) Surface of polymer coated Fe-Pt nanoparticle (green) covered by a monolayer of about 20 HSA molecules (red triangular prisms) (Rocker 2009).

the nanoparticle-protein interactions qualitatively as well as quantitatively. Figure 2.4.1, shows the structure of human serum albumin (HSA) which can be approximated to be an equilateral triangular prism with side 8 ~ nm and height ~ 3 nm.[39] A change in particle

radius ΔR =3.3 nm was reported, and it was concluded that human serum albumin forms a monolayer at the surface of carboxyfunctionalized nanoparticles.

Casals *et al*.[37] reported a time dependent conjugation of blood serum proteins to the nanoparticle, by exposing gold nanoparticles to cell culture medium with 10% fetal bovine serum. They observed that the coating process was slower for lower serum concentrations. It was also concluded that there was an evolution from a loosely bound to an irreversible attached protein layer over time. Mass spectrometry was used to confirm that albumin was the most abundant component of the protein corona. Earlier studies have also suggested that bovine serum albumin binds spontaneously at the surface of citrate stabilized gold nanoparticles.[40]

Two possible mechanisms have been sugested in the literature for the spontaneous adsorption of BSA on citrate caped AuNPs. BSA is a globular protein consisting 583 amino acids, with 60 lysine residues, 17 disulphide bridges, a single tritophan, and a free thiol (cysteine-34).[41] It can either follow an electrostatic attraction mechanism,[37, 40] caused by attraction between negatively charged citrate capped AuNPs with the positively charged lysine residues, or via a thiol ligand displacement reaction[42] through the unpaired cysteine. Casal *et al.* observed that the formation of protein corona was slower for the relatively smaller negatively charged AuNPs.[37] This was inconsistent with the ligand replacement mechanism as the smaller particles should have better access to the free thiol and result in rapid corona formation. Thus, they interpreted the BSA adsorption on citrate capped AuNP to have followed an electrostatic attraction mechanism.

Systematic study of interaction of BSA with nanometer-sized AuNPs and investigation of their interaction mechanism would be potentially useful in the areas ranging from Biophysics to drug delivery. This discussion will be revisited in chapter 5.

The following chapter will cover the experimental technique - Fluorescence correlation spectroscopy, that was employed for this thesis work. It will include the experimental set up as well as the underlying theory.

CHAPTER 3

FLUORESCENCE CORRELATION SPECTROSCOPY

3.1 INTRODUCTION

Fluorescence correlation spectroscopy (FCS) is a fluctuation correlation method that is capable of measuring the dynamics of molecular processes by observing spontaneous microscopic fluctuations in molecular positions and number density.[43] In most spectroscopic techniques, the average intensity is the quantity of interest. However, in FCS, the quantity of interest is the fluctuation in fluorescence intensity from the average, figure 3.1.1. Madge, Elson and Webb were the first to develop FCS in early 70's to measure the dynamics of DNA-drug interactions.[44] FCS has now become a desirable measurement technique for various processes, and has a variety of applications in the field of biophysics, analytical chemistry and cell biology.[45] Some recent applications of FCS include investigation of biological systems, studying processes such as enzymatic reactions within living cell etc.[46]

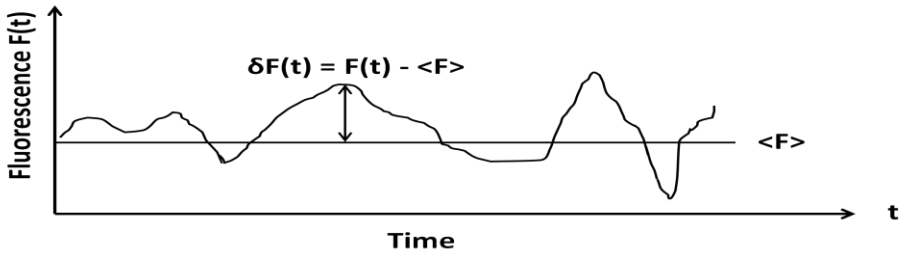

Figure 3.1.1: Fluctuation of fluorescence due to molecular dynamics

FCS monitors tiny fluctuations of fluorescent molecules as they diffuse in and out of the laser focus. These fluctuations may be due to Brownian motion, externally induced

flow, chemical reactions or some other such processes.[44, 47] The fluorescence signal can be analyzed through temporal autocorrelation. The autocorrelation function (ACF), equation 3.1.1, quantifies these fluctuations. It measures the similarity of the function with itself after a time lag.

$$G(\tau) = \frac{<\delta F(t).\delta F(t+\tau)>}{<F(t)>^2} \quad (3.1.1)$$

where τ is the time lag, ⟨⟩ is time-average, F(t) is the observed fluorescence intensity and δF(t) is the fluctuation in the fluorescent intensity. The ACF has been normalized by diving it by the square of the average intensity. Figure 3.1.2 represents the development of an autocorrelation curve. The analysis of the ACF has been discussed in detail under the FCS theory section.

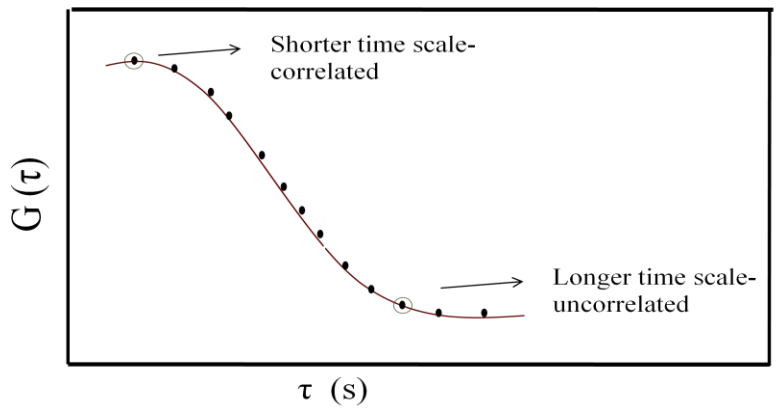

Figure 3.1.2: The development of an autocorrelation curve. The ACF calculates the self-similarity of a fluctuation as a function of time lag. By fitting the curve to a particular model, the diffusion coefficient and concentration of fluorescent dyes may be calculated

FCS and dynamic light scattering (DLS) can be considered to be similar, but there are a few major differences. FCS involves fluorescence emission which is inherently

inelastic, whereas DLS involves elastic or quasi-elastic scattering. FCS exhibits single molecule sensitivity and thus requires very low, nano-molar, sample concentration. DLS experiments require much higher sample concentration. The small focal volume of FCS allows a very local study of cellular samples. Such features render FCS to be relatively more desirable spectroscopic technique.

The photon emission rate of FCS is directly proportional to average number of fluorescent molecules $\langle N \rangle$ in the sampling volume. Therefore, larger the $\langle N \rangle$ (higher concentration of molecules) smaller will be the statistical noise. On the contrary, the amplitude of correlation function is inversely proportional to $\langle N \rangle$, therefore $\langle N \rangle$ should not be too large either. It was found that above-mentioned two effects canceled each other exactly in a wide range of concentrations.[45] In order to obtain a successful autocorrelation curve $\langle N \rangle$ should vary between 0.1 and 1000; which corresponds to a fluorescent dye concentration of 10^{-6} to 10^{-10} M, focal volume being about 1*f*L(10^{-15}L).

It is often possible that the system under investigation does not exhibit fluorescence. In such a case, the system is labeled with a fluorescent dye. Fluorescein and laser dyes were the very first fluorescent dyes used for FCS; these were also being used for other forms of microscopy.[48] Since these dyes were unable to withstand high laser powers, these became unsuitable for FCS. A fluorescent dye can get irreversibly photo bleached after emitting a limited number of photons. The dyes more suitable for FCS applications should have low photo bleaching, high extinction coefficient and high fluorescence quantum yield. Some dyes with these properties that are being used for labeling purposes are derivatives of Rhodamine: tetramethylrhodamine (TMR) and

carboxyrhodamine (Rh6G).[45] The introduction of these relatively more photostable dyes allows an FCS experiment to run for longer time span. The following sections present the theory and experimental set up for FCS.

3.2 FCS THEORY

FCS is used to investigate molecular dynamics by analyzing the fluctuations in the fluorescence emission. The laser beam is tightly focused to excite a small volume (~ femtoliter) in the sample solution. When the fluorescent molecules move into the focus volume, they absorb the energy from excitation light and emit fluorescent light which is collected by the PMT. The dynamics of the system under investigation is determined by auto-correlating the fluctuations of the fluorescent intensity. The autocorrelation function (ACF), equation 3.1.1, quantifies these fluctuations. The fluctuation in the fluorescent intensity $\delta F(t)$ is given by

$$\delta F(t) \equiv F(t) - \langle F(t) \rangle \qquad 3.2.1$$

If only one fluorescent species is present in the sampling volume, the detected fluorescence fluctuation is given as

$$F(t) = kQ \int dr \, . E(r) C(r,t), \qquad 3.2.2$$

where k is a constant, Q is a product of absorptivity, fluorescence quantum efficiency, and the detection efficiency of the optical system, E(r) is the spatial intensity profile of the excitation light, and C(r,t) is the dye concentration at a particular position and time. We will consider an experimental situation where change in intensity is caused by only concentration fluctuations. These might occur due to diffusion, mass transport or chemical reaction. Under thermal equilibrium, these concentration fluctuations are caused

solely by diffusion (thermal motion). In this case, change in fluorescent particle concentration ($\delta C(r,\ t) = C(r,\ t) - \langle C \rangle$) is related to the diffusion coefficient D by Fick's law given by

$$\frac{\partial \delta C(r,t)}{\partial t} = D\nabla^2 \delta C(r,t) \qquad 3.2.3$$

A solution to eqn 3.2.3 is given by

$$\delta C(r,t) = \frac{\langle C \rangle}{\sqrt{4\pi D t}} exp\left(-\frac{r^2}{4Dt}\right) \qquad 3.2.4$$

Following relation holds for translational motion in two dimensions, assuming the sample is stationary,

$$\langle \delta C(r,t).\delta C(r',t+\tau) \rangle = \frac{\langle C \rangle}{4\pi D t} exp\left(-\frac{(r-r')^2}{4Dt}\right) \qquad 3.2.5$$

Substituting 3.2.1 and 3.2.2 in 3.1.1, we can get

$$G(\tau) = \frac{\int dr \int dr' E(r)E(r')\langle \delta C(r,t).\delta C(r',t+\tau) \rangle}{(\langle C \rangle \int E(r)dr)^2} \qquad 3.2.6$$

Using eqn 3.2.6 along with 3D Gaussian model with two photon excitation, where

$$E(r) = E(x,y,z) = E_o \exp\left(-\frac{4(x^2+y^2)}{w_o^2} - \frac{4z^2}{z_o^2}\right) \qquad 3.2.7$$

where w_o is the beam waist and z_o is the beam height, an expression for autocorrelation can be obtained

$$G(\tau) = \frac{1}{2\sqrt{2}\langle N \rangle} \frac{1}{1+(\frac{8D\tau}{\omega_0^2})\sqrt{1+(\frac{8D\tau}{z_0^2})}} = \frac{G(0)}{1+(\frac{8D\tau}{\omega_0^2})\sqrt{1+(\frac{8D\tau}{z_0^2})}} \qquad 3.2.8$$

The average number of molecules within excitation volume and concentration can be calculated as follows

$$< N >= \frac{1}{2\sqrt{2}G(0)}, and \qquad < C >= \frac{2\sqrt{2}}{\pi\sqrt{\pi}w_0^2 z_0 G(0)} \qquad 3.2.9$$

Thus from FCS measurements we can estimate diffusion coefficient as well as concentration values. Equation 3.2.8 gives the autocorrelation function for 3D diffusion

(a)

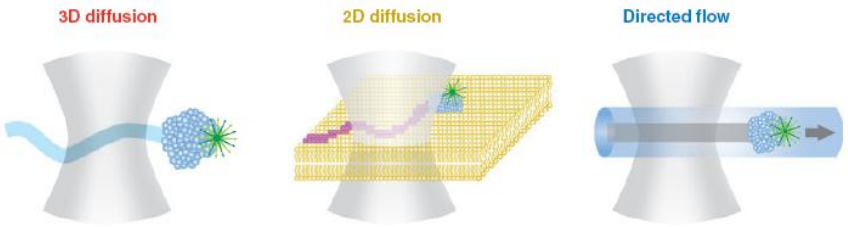

(b)

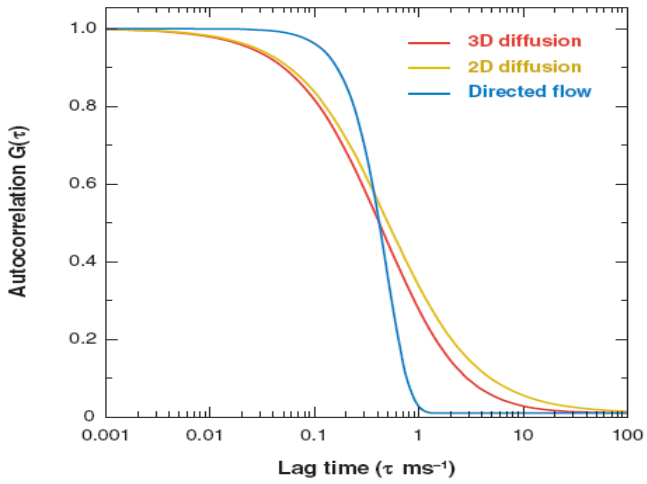

Figure 3.2.1: (a, b): Model autocorrelation curves for different kinds of particle motion: free diffusion in three dimensions (red), free diffusion in two dimensions, e.g., for membrane-bound molecules (yellow) and directed flow (Cyan) (Haustein 2007)

for two-photon excitation. Suitable models for ACF have been developed considering the dimensionality of the system under investigation, the properties of laser set up, and the

means by which fluorophores move. Figure 3.2.1 represents model autocorrelation curves for different processes.[49]

3.3 EXPERIMENTAL SET UP FOR FCS

All FCS setups measure the fluctuations in the fluorescence emission; however, construction of a particular FCS set up varies in accordance to the experiments of interest. The most important component of a typical FCS set up is the laser, which serves as the excitation source for the fluorophores. This laser light source can be either continuous (one-photon excitation) or pulsed (two-photon). A schematic of two-photon FCS set up, employed in this thesis work, is displayed in figure 3.3.1.

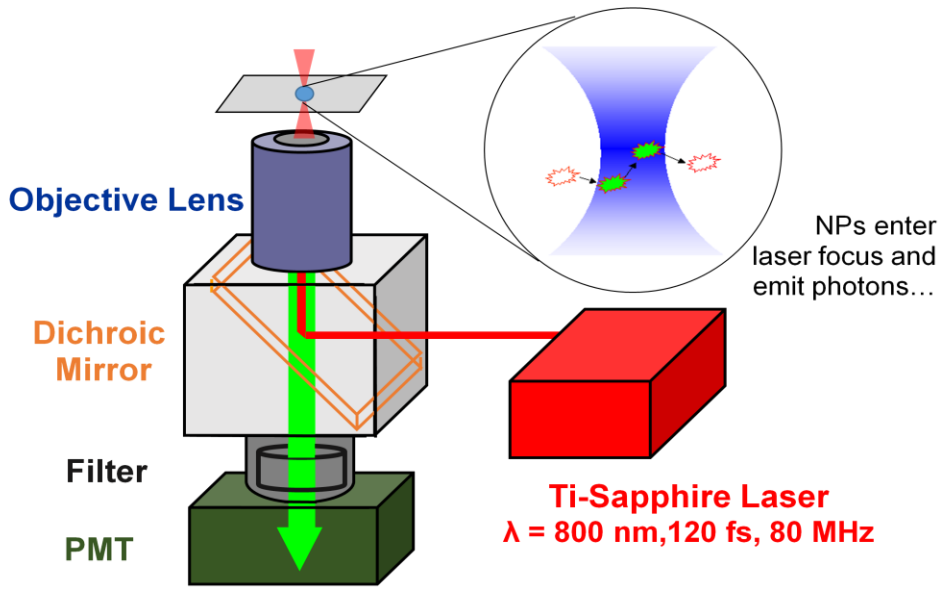

Figure 3.3.1: Two photon FCS set up for translational diffusion measurements

When the laser is pulsed at a very high frequency, the fluorophores in the excitation volume are able to absorb two photons. The absorption of both photons occurs

within 10^{-16} seconds. The photon pair possesses the energy required for excitation, simplest case being the one with the wavelength of each photon being approximately twice that of the actual transition. This is in contrast to confocal FCS set up that utilizes one-photon excitation. Since the probability of two-photon excitation is proportional to the square of excitation energy, we need to use high–peak-power laser sources with pulses of femtoseconds to picoseconds which will provide high instantaneous photon flux at the sample. In addition, light intensity decreases quadratically with increase in distance from focal plane. Both these factors together allow the laser to excite a very small volume around the focus. Thus in case of two-photon, unlike one-photon, smaller excitation volume is attained without the use of pinholes. In addition to this, localizing the fluorescent excitations will confine the photo damage, if any, to a very small volume. This makes two-photon set up more desirable for biological samples that are relatively sensitive to photo damage. Another advantage of a two-photon FCS over its one-photon counterpart arises from the fact that the wavelength of excitation and emission light will be considerably different. For example, an 800 nm photon will be used to excite transitions at 400 nm and emitted light will be around 500 nm. Since the emitted photons have lower wavelength relative to the incident photons, the emission will be well separated from scattered light which can be easily filtered out.[50, 51]

Following figure 3.3.1, the energy required to excite the fluorophores is provided by a femtosecond Ti-sapphire laser (Mai Tai, Spectra-Physics) that generates 100 fs width laser pulses of wavelength 800nm at a frequency of 80MHz. Neutral density filters (NDF) were used to change the power of the laser beam. A Zeiss inverted microscope

(Axiovert S200TV, Carl Zeiss) served as the optical platform for the experiments. The laser beam was focused on the sample through a high numerical aperture (N.A.= 1.25, 100X) objective. In order to achieve better focusing the objective needed to be back-filled with an expanded beam. The laser beam being small (~ 2 mm), needed to be expanded. This was attained by placing a beam expander, which is a pair of two achromatic lenses separated by a distance equal to the sum of their focal lengths, in the laser path before it entered the microscope. The beam is then reflected off a dichroic mirror. It is a special mirror formed of multilayer dielectric coating that reflects wavelength above a certain value (transition wavelength) and transmits all below it. The transition wavelength of the dichroic mirror should be relevant to the fluorophore, and should fall between the excitation and emission wavelength of the fluorophore. The so chosen dichroic mirror separates the path of light by reflecting the excitation light (coming from laser) into the objective and transmitting the fluorescence emission light (coming from sample) into the detector.

The beam reflected from the dichroic mirror is collected by a high numerical aperture microscope objective through which it is focused on the sample. The objective excites a very small volume (~ femtoliter), within the sample solution, with the aid of pulsed laser. On passing through the laser focus, fluorophore absorbs two and emits one photon. Since wavelength of emitted light is shorter than excitation wavelength, it transmits through the dichroic mirror. This emitted light is collected by the photomultiplier tube (PMT) having single photon sensitivity. There is another

wavelength selective element, a short pass filter that is placed between the dichroic mirror and PMT so as to stop any leakage or scattered light from entering the PMT.

An integrated data acquisition system (ISS, IL) was used to record and analyze the output from the photo multiplier tubes (PMT). The data acquisition card records the fluctuations of fluorescent intensity. A software package calculates the auto correlation function (ACF). This ACF can be used to extract important information about dynamics of sample under study.

The technique described in this chapter was employed to do the experiments covered in this thesis. Chapter 4-6 will cover the research work that I performed as a graduate student at Wayne State University.

CHAPTER 4

GOLD NANOPARTICLE DYNAMICS IN SYNTHETIC POLYMER SOLUTIONS

4.1 DIFFUSION OF NANOPARTICLES IN SEMIDILUTE POLYMER SOLUTIONS: THE EFFECT OF DIFFERENT LENGTH SCALES

The Following material was originally published in Macromolecules (2012)[52]

Understanding the transport properties of nanoparticles (NPs) in solutions of macromolecules is important for several interdisciplinary fields of studies as well as relevant for many technological applications. For example, in colloidal physics, the diffusion and sedimentation of particles play a vital role for the dispersion stability, analytical separation and chromatography[53]. In biophysics, there is growing interest to understand how biopolymers such as proteins move through crowded cytoplasmic environments[6]. The dynamics in this situation can affect cellular functions, such as kinetics of enzymatic reactions, the formation of DNA or protein complexes, and self-assembly of various supramolecular structures, like fibrillar aggregates[46]. In the areas of soft matter physics and nanotechnology, these studies are important for proper interpretation of microrheology experiments[7] and development of novel composite systems that contained nanosized inclusions[54].

For these reasons, diffusion of NPs in polymer solutions has received a lot of attention theoretically[10, 12, 17, 24, 28, 55] as well as experimentally[28, 32-34, 55-57]. In simple liquids, the translational diffusion coefficient (D) of isolated spherical particles is given by the well-known Stokes−Einstein (SE) relation, $D = k_BT/6\pi\eta_oR_o$, where k_B is the

Boltzmann constant, T is the absolute temperature, and η_o is the solvent viscosity. It is assumed in this relation that the radius of the particle (R_o) is much greater than solvent molecules[33]. But in a ternary mixture containing polymer, solvent and the particle, there are several length-scales involved and application of SE relation becomes complicated in certain regimes. In semidilute solutions, where the polymer concentration is above the overlap volume fraction (ϕ^*), the matrix forms a transient network of overlapping chains characterized by an average mesh size called the correlation length (ξ)[3, 8]. It is a decreasing function of polymer volume fraction (ϕ), $\xi \sim \phi^{-0.76}$ for uncharged polymers in good solvent and is independent of the polymer molecular weight (M_w). The correlation length introduces a new length scale in addition to particle radius and the radius of gyration of the polymer chain (R_g). Theoretical approaches by de Gennes and his coworkers have identified three regimes depending on the relative size ratio, R_o/ξ[8, 23]. If $R_o/\xi << 1$, the particles can slip easily through the mesh and they detect only the neat solvent viscosity (η_o). In the opposite limit, the diffusion is governed by the macroscopic viscosity (η_m) of the solution, which is commonly measured in a rheometer. In the transition regime, $R_o/\xi \sim 1$, the local viscosity (η_ϕ) experienced by the particle depends upon the length scales at which it is probed, and generally $\eta_o < \eta_\phi < \eta_m$. In this scenario, ξ can be considered as the 'cross-over length scale' and η_ϕ depends upon ϕ, but independent of M_w. A scaling relation of the form $D_o/D = \eta_\phi/\eta_o \sim F(R_o/\xi)$ has been suggested, where D_o is the diffusion coefficient of the particle in the neat solvent[28]. Some theoretical models have suggested a functional form, $F(R_o/\xi) \sim \exp(R_o/\xi)$. But there are conflicting reports in the literature regarding the validity of these predictions[28-31, 33-35, 56].

A competing model of probe diffusion was developed by Phillies[24]. He argued that hydrodynamic interactions dominate over topological constraints on probe diffusion and proposed an equation of the form $D/D_o \sim \exp(-\beta\phi^{\nu})$[24, 25, 58]. Though regarded mostly as an empirical equation, it fits a wide range of concentration from dilute to concentrate as well as probes and polymers with different architectures (linear, branched, globular, star-shaped, etc.)[55]. Phillies noted that β depends upon M_w, but is independent of R_o, and ν depends upon solvent quality ranging from 0.5 to 1. Hydrodynamic screening theory by Cukier predicts a similar form, $D/D_o \sim \exp(-\kappa R_o/\xi)$, which yields the exponent $\nu=0.76$[7]. Recent theoretical approaches have considered the effect of depletion layer for neutral polymer-probe interaction[16]. Such a layer has a thickness of the order of ξ, where the segmental density of the chain increases from zero to the bulk value[16]. Assuming that the local viscosity is a function of monomer concentration, it gradually increases from the solvent viscosity (η_o) close to the probe surface to macro-viscosity (η_m) in the bulk[59]. The analysis also showed a stretched exponential function for $F(R_o/\xi)$ in semidilute solution[17]. None of these theories consider explicitly the dynamical characteristics of the polymer matrix. A recent scaling theory by Cai *et. al.* have considered the effect of chain relaxation on the mobility of particles[60]. They have derived the power law dependencies of polymer concentration and particle size on diffusion coefficient. In parallel to the theoretical approaches, there have been molecular dynamics simulations as well, which found that the cross-over length scale between nano- and macroviscosity is not ξ, but R_g[9, 10, 61]. For unentangled melts, in regime $R_o < R_g$, local viscosity (η_ϕ) is dominated by monomer units rubbing the nanoparticle surface, making it proportional to the particle

area (R_o^2), which yields $D \propto 1/R_o^3$ and independent of chain length. In the large particle limit, hydrodynamic contribution dominates giving $D \propto 1/R_o$ and its numeric value is given by SE relation of diffusion coefficient (D_{SE})[9, 61].

Experimentally, dynamic light scattering (DLS)[30, 57, 59, 62], fluctuation correlation spectroscopy (FCS)[31, 32, 56, 63], fluorescence recovery after photobleaching (FRAP)[33], and sedimentation[28, 30, 35, 57] are most popular in this area of research. A recent review of experiments could be found in Ref. [32] and some of the earlier works were well summarized in Ref. [29]. We will briefly mention only few results, which will help readers to put our work in perspective. DLS experiments by Lodge group[29] have found that for polystyrene spheres ($R_o \approx 200$ nm) in solutions of poly(viny1 methyl ether) with $R_g \approx 54$ nm, the ratio D/D_{SE} increases with the polymer concentration and reaches the maximum value of ≈3 near ϕ^*. But sufficiently above the entanglement concentration, ϕ_e ($\approx 3\phi^*$), the SE behavior was recovered. DLS experiments measured the diffusion at a short length scale compared to R_o, which is perturbed significantly by the depletion layer and may not record the average bulk behavior[16, 29, 30, 57, 59]. Sedimentation and FCS experiments, in contrast, probe the long-time and large-scale motion of the particles[28, 57]. Sedimentation experiments have found that the particles experience the single-chain viscosity rather than the solvent viscosity when $R_o < \xi$[30]. In the intermediate region, D_o/D does not have the simple scaling form $F(R_o/\xi)$ and depends upon M_w[35]. As the polymer concentration is increased and the limit, $R_o >> \xi$ is reached, the particle feels the macroscopic viscosity as suggested by de Gennes theory. In these experiments, particle size (R_o= 4-5 nm) was smaller than the radius of gyration, (R_g = 8 nm) of the chain. But a

significant number of other experiments have reported deviation from SE equation when $R_o < R_g$. Hoyst group has performed FCS experiments with poly(ethylene glycol) (PEG) in water using probes as molecules with different sizes, such as fluorescent dyes, proteins, and silica spheres[32]. They concluded that for $2R_o < R_g$, the measured nanoviscosity was orders of magnitude smaller than macroviscosity, however, macroviscosity governs the probe dynamics if $2R_o > R_g$. In the crossover regime ($2R_o \sim R_g$), they observed a scale-dependent diffusion, which they explained in terms of non-uniform viscosity within the depletion layer[59]. The SE relation for larger probes in polyvinyl (PVA) solution was also verified in another FCS experiments by Michelman–Ribeiro *et al*[31].

All the conflicting results regarding the crossover length scale and the roles of various parameters, such as mesh size, matrix dynamics, effect of entanglement, polymer-probe interaction, etc. demand further investigations. But it remains a challenge to study nanoparticle dynamics in a systematic manner, more specifically in the length regime $\xi \leq R_o < R_g$. One of the reasons is the paucity of suitable probes in the size range of 5-20 nm[33]. For smallest sized probes (R_o~1-2 nm) different dyes (e.g., rhodamine, alexa), for intermediate sizes ($R_o \sim$ 3-5 nm) fluorescently labeled molecules (e.g., dextran, lysozyme, bovine serum albumin), and for larger sizes ($R_o \sim$ 5-100 nm) quantum dots, silica and polystyrene spheres were used in previous experiments[31-33, 58, 59, 62]. For the intermediate size, which is the focus of this study, the probes used so far were flexible and porous[33]. They can change their size depending upon the solvent condition or as the polymer concentration is varied. The solvent needs to be the poor solvent for the probe

molecules, so that they adopt a compact globular structure. The use of different molecules can change the specific probe-polymer chemistry. As a result the polymer density distribution near the particle surface may be altered and the properties of the depletion layer can be modified[7, 16, 30]. This can alter the viscous drag experienced by the particle and change the particles' diffusivity. There is evidence in computer simulation that diffusion coefficient could decrease with increasing interaction strength[61].

In contrast to experiments by other groups, we have used rigid and impenetrable probes (gold spheres) with radius between 2.5 nm to 10 nm. The solvent (water) is a good solvent for the polymer at the room temperature and the probe particles can also be readily dispersed into it. The use of the same probe but with different sizes eliminates the possibility of specific probe-polymer interaction that could change diffusion. Another distinguishing aspect of this research is the use of fluctuation correlation spectroscopy (FCS), which has the advantage of using extremely low particle concentrations (~few nM). This is about 4-5 orders of magnitude smaller compared to other methods such as DLS or FRAP. The average particle-particle separation is much higher, so that the mutual interactions between the particles can be neglected and only true self-diffusion was measured. The low concentration of particles also reduces the possibility of polymer-induced probe aggregation from depletion interaction. Because of the specificity of this technique, scattering from the matrix polymer does not significantly complicate the experiment or its interpretation. This is an issue in DLS experiments, where for smaller particles ($R_o < R_g$) and low concentration of particles, the autocorrelation function could be dominated by the dynamics of the polymer network.

In this paper we have used FCS to understand the nanoparticle dynamics in semidilute poly(ethylene glycol) (PEG) water solutions. The use of very small sized spherical probes well within the range $\xi \leq R_o < R_g$ made this study unique. Our results will be important to test theories of polymer dynamics and understand the relationship between micro- and macroscopic viscosities of complex fluid systems. They will also have implications in other fields, where there is complex coupling between two or more characteristic length scales that govern their dynamics.

4.2 EXPERIMENTAL SECTION

PEG samples of two different molecular weights 5 kg/mol (M_w/M_n = 1.08) and 35 kg/mol (M_w/M_n = 1.15) were purchased from Polymer Sources, Inc. Gold nanoparticles (Au NPs) of radius 2.5, 5 and 10 nm were purchased commercially from Corpuscular, Inc. Au NPs were particularly useful for our experiments as they do not photo-bleach like fluorescent dyes or blink like semiconductor quantum dots and their size can be tuned as desired. The scattering signal from small NPs is typically very low, but they have high luminescence efficiency upon multi-photon excitation[32]. The polydispersity of these nanoparticles is about 10% as was verified by transmission electron microscopy (TEM) experiments (Figure 4.5.1). The choice of the polymer molecular weights and particle sizes allow us to investigate the size regime that we are interested and also the transition process for the particles experiencing the nanoviscosity to macroviscosity. Many different concentrations of PEG (ϕ=0-0.37) in water-Au NPs mixture as solvent were prepared using a digital balance with resolution of 1 mg. PEG has the advantage over other polymers such as polystyrene, which needs to be dissolved in organic solvents.

These sometimes give a lot of background fluorescence and thus reduces signal-to-noise ratio. Control experiments indicated no strong interactions (e.g., ionic, covalent, etc.) between gold particles and PEG are present, which would have led to adsorption of polymers onto surfaces.

A Zeiss inverted microscope served as the experimental platform. Near infrared light from an 800 nm, 80 MHz, femtosecond Ti: Sapphire laser (Mai Tai, spectra physics) was focused on the sample through a high numerical aperture (N.A.= 1.25, 100X) objective. Emitted light was collected through the same objective and detected by two single photon counting modules (Hamamatsu). An integrated data acquisition system (ISS, IL) was used to record and analyze the output. As NPs diffuse in and out of the laser focus, the number of these particles fluctuates. This fluctuation (F) is quantitatively studied through the autocorrelation function (ACF) G(τ) given by,

$$G(\tau) = \frac{<\delta F(t).\delta F(t+\tau)>}{<F(t)>^2} \qquad 4.2.1$$

If the cause of the fluctuation is Brownian diffusion, the diffusion coefficient (D) can be calculated from the ACF by using,

$$G(\tau) = \frac{G(0)}{1+(\frac{8D\tau}{\omega_0^2})\sqrt{1+(\frac{8D\tau}{z_0^2})}} \qquad 4.2.2$$

In the above equation, G(0) is the magnitude of ACF at short time which is inversely proportional to the number of particles within the laser focus, ω_o is the half-width, and z_o is the half-height of the laser focus. We determined by a calibration experiment that $\omega_o \approx 0.25$ μm and $z_o \approx 1$ μm.

4.3 RESULTS AND DISCUSSION

Before presenting the results, calculations of the important length scales of the system would be useful. The radius of gyration, R_g of the PEG in water as a function of M_w is given by $R_g = 0.02\ M_w^{0.58}$ (nm)[64], which corresponds to R_g=2.8 nm and 8.6 nm for 5K and 35K PEG. Since R_o ranges from 2.5 to 10 nm, R_o/R_g was varied from 0.9 to 4 for 5K and 0.3 to 1.2 for 35K PEG samples. The overlap volume fraction, ϕ^* which marks the onset of semidilute regime was determined by using the relation, $\phi^* = 3M_w/(4\pi\rho N_A R_g^3)$, where ρ is the polymer density and N_A is the Avogadro's number[8]. We estimated that ϕ^*=0.08 for PEG 5K and ϕ^*=0.02 for PEG 35K. Our measurements were carried out in the range of ϕ=0.09-0.37, all of which were in the semidilute regime. The correlation length (ξ) as a function of polymer concentration was calculated by using the relationship, $\xi \approx R_g(\phi/\phi^*)^{-0.76}$. It indicates that ϕ^* depends upon M_w, but ξ is nearly independent of it. ξ ranged from 0.95 nm to 2.6 nm. In all measurements $R_o \geq \xi$ and the ratio R_o/ξ varied from ≈1 to 11. Sufficiently above ϕ^*, the chain entanglement becomes significant and a transition to reptation-like behavior is predicted to occur. The critical concentration for entanglement is given by, $\phi_e \approx (M_e/M_w)^{0.75}$, where M_e is the molecular weight between entanglement in melt. $M_e \approx 2$ kg/mol so that PEG 5K is too short and there would not be enough number of entanglements per chain[29]. For 35K PEG, ϕ_e is about 0.12. In the entangled regime another length scale, tube diameter 'a(ϕ)' needs to be considered, $a(\phi) \approx a(1)\phi^{-0.76}$, where a(1) is the tube diameter in the melt[3]. For PEG a(1)≈4 nm and a(ϕ) ranges between 10-20 nm. Fig. 4.3.1 showed schematically the relative size regimes covered in our experiments (also see Table 4.5.1).

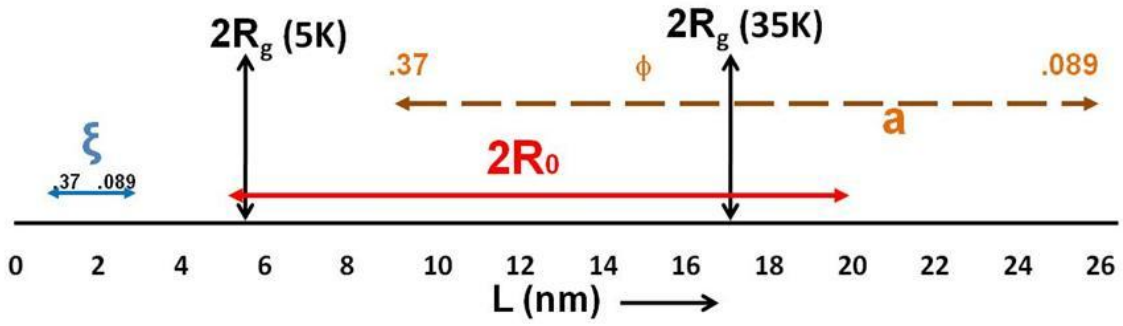

Figure 4.3.1 Schematic of different length-scales covered in the experiments. (Reprinted with permission from Macromolecules 45 (15), 6143-6149. Copyright (2012) American Chemical Society)

In Fig. 4.3.2, we have showed some representative autocorrelation functions collected by FCS and plotted versus logarithmic time lag. Each autocorrelation function

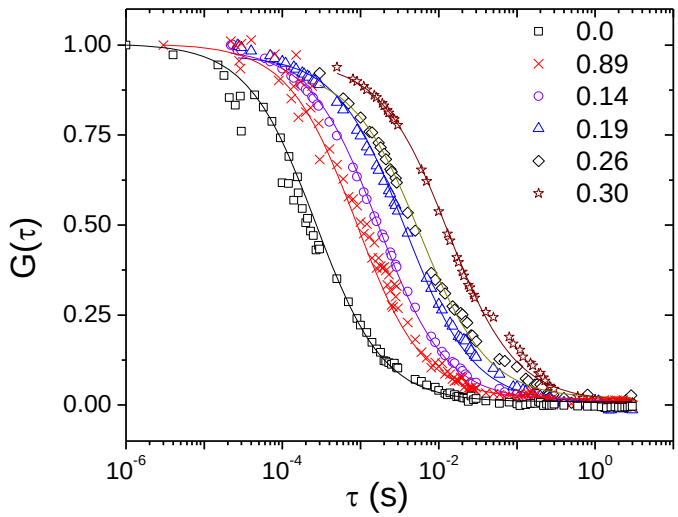

Figure 4.3.2. Normalized autocorrelation curves for Au NP (R_o = 2.5 nm) diffusion in PEG 35K solution at various polymer volume fractions. The curves are shifted to longer time-scale as PEG concentration increases indicating that diffusion coefficient decreases. The solid lines are fit of the curves. (Reprinted with permission from Macromolecules 45 (15), 6143-6149. Copyright (2012) American Chemical Society)

was collected for about 15 minutes. The temperature was kept at room temperature (23 ^{o}C). To minimize the photothermal conversion from the excitation of the gold nanoparticles, the laser power was kept below 1 mW. Our estimation showed that the raise of the local temperature to be less than 0.1 ^{o}C, so the thermal effect did not have any significant impact on the diffusive behavior of particles. The FCS auto correlation data of Au NPs in PEG was fitted using the equation mentioned earlier.

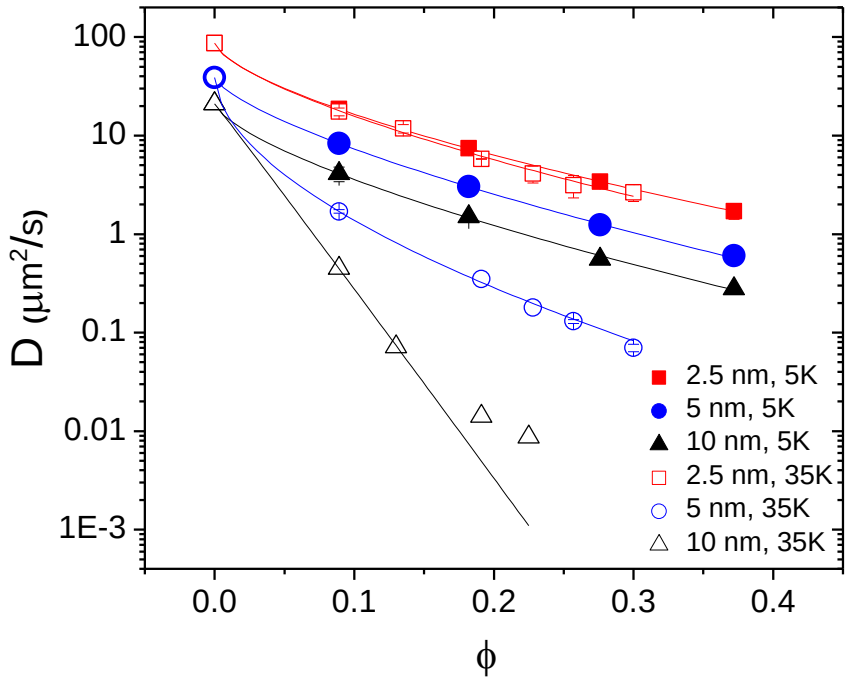

Figure 4.3.3. Diffusion coefficients as a function of polymer volume fraction. The solid lines show fits according to Phillies' equation. The caption indicates particle radii and the polymer molecular weight. The error bars are smaller than the size of the symbols. The fitting parameters are given in Table 4.5.3. (Reprinted with permission from Macromolecules 45 (15), 6143-6149. Copyright (2012) American Chemical Society)

The diffusion coefficients (D) of Au NPs were calculated from the fit. Many different

FCS trials were done for a given nanoparticle size for each polymer concentration on many different days with different samples. Trials were repeated for both molecular weights of PEG. Fig. 4.3.3 shows the plot of D as a function of ϕ for three different nanoparticle sizes (see also Table 4.5.2). Each datum in the graph is the average and the error bars are the standard deviation measured in more than 10 experiments.

First we will compare the scaled diffusion coefficient (D/D_o) data with Phillies equation of stretched exponential function: $D/D_o \sim \exp(-\beta\phi^{\nu})$ with 'β' and 'ν' as adjustable parameters (Figure 4.3.3 and Table 4.5.3)[24]. The fitting deviates from the data at higher concentrations. For PEG 35K at ϕ =0.26 and R_o=10 nm, the measured D is about an order of magnitude faster compared to the fit. At this concentration, $\phi > \phi_e$ and $2R_o > a(\phi)$. We speculate that effect on the particle motion due to network dynamics originating from chain reptation, which is not considered in Phillies model becomes significant at concentrations above ϕ_e. Consistent with some other reports[24, 31], we found that the exponent ν lies between 0.56 to 1, but it does not have any clear dependence on the physical properties of the system, such as molecular weight of the polymer or the particle size. The parameter 'β' is an increasing function of R_o. But it is to be noted here that the actual significance of these scaling exponents still lacks sound theoretical justification.

Next, we compare the measured diffusion coefficient with SE prediction using the bulk solution viscosity (η_m). The macroscopic viscosity information of PEG-water solutions at various concentrations have been obtained from rheology data[32, 59]. The ratio of measured D to calculated D_{SE} is plotted as a function of PEG concentration (Fig.

4.3.4). For 5K PEG, $R_o/R_g \geq 1$ for all particle sizes and we observed $D/D_{SE} \approx 1$ and is independent of polymer concentration. For 35K PEG, the ratio shows positive deviation from unity and the deviation becomes stronger with increasing ϕ and with the ratio R_o/R_g becoming smaller.

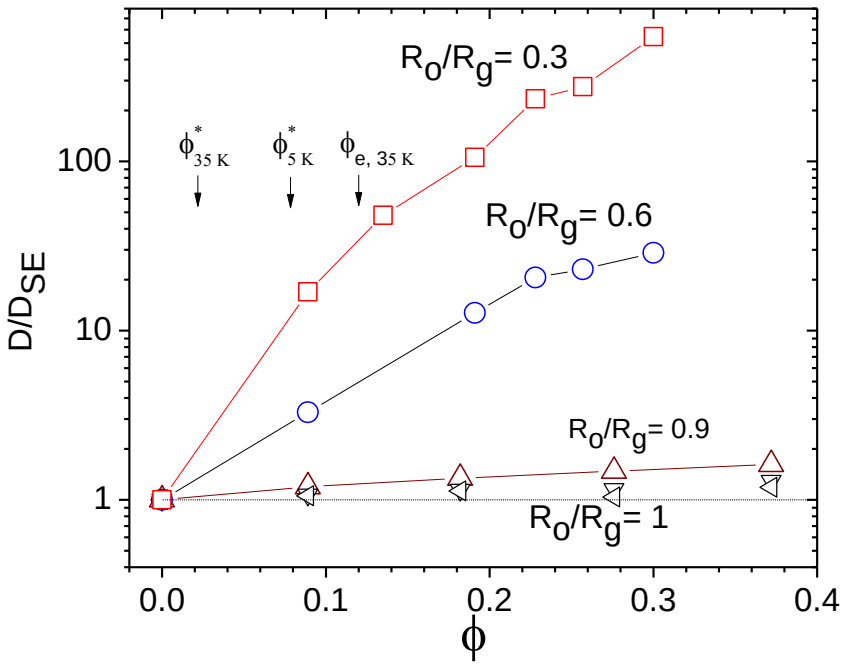

Figure 4.3.4. The ratio D/D_{SE} is plotted as a function of polymer volume fraction. SE behavior corresponds to the horizontal dashed line. As the ratio R_o/R_g becomes larger the ratio approaches unity. Three particular concentrations are denoted. (Reprinted with permission from Macromolecules 45 (15), 6143-6149. Copyright (2012) American Chemical Society)

For the lowest R_o/R_g as probed in our experiments (~0.3), the NPs diffused two to three orders of magnitude faster compared to SE-prediction. If ξ was the crossover length

scale from nano to macroviscosity, all the particles would have experienced the solution viscosity and SE relation would have correctly predicted the diffusion because $R_o \geq \xi$ for all cases investigated here. Thus our results cannot be explained with some previous theories which concluded that ξ is the crossover length scale and D/D_{SE} should be independent of concentration when $R_o > \xi$[8, 28]. But it is in accord with results from computer simulations which characterizes R_g as the crossover length scale[9, 61]. Similar conclusion was also drawn in experiments by Hoyst *et. al.* using various dye and protein molecules but identifying 'R_o' as the probe diameter instead of the radius. Our results do not necessarily contradict experiments by Lodge's group, where a return to SE behavior were obtained with increasing polymer concentration, as those were in the regime of $R_o > R_g$[29]. For $R_o \leq R_g$[59], the relative diffusion coefficients experienced by the particles was scaled as

$$\frac{D_o}{D} = \exp\left(\alpha\left(\frac{R_o}{\xi}\right)^{\delta}\right) \qquad 4.3.1$$

and for $R_o \geq R_g$ as

$$\frac{D_o}{D} = \exp\left(\alpha\left(\frac{R_g}{\xi}\right)^{\delta}\right) \qquad 4.3.2$$

with $\alpha = 1.63 \pm 0.04$ and $\delta = 0.89 \pm 0.02$. Again our results are consistent with Holyst *et al.*, besides the fact that R_o represents particle radius whereas they identified R_o as the particle diameter[32, 59]. The scaled diffusion in these two equations makes SE relation applicable to particles of all sizes as is evident in Fig. 4.3.5.

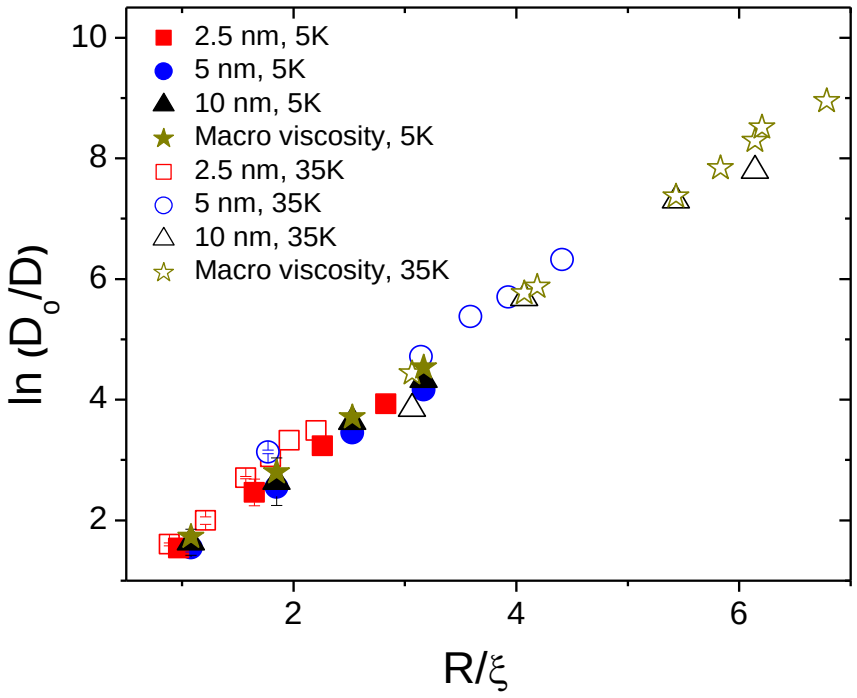

Figure 4.3.5. The normalized plot of D_o/D vs. R/ξ, where $R=R_g$ for $R_o \geq R_g$ and $R=R_o$ for $R_g > R_o$. All data points fall on a single curve. (Reprinted with permission from Macromolecules 45 (15), 6143-6149. Copyright (2012) American Chemical Society)

It is known that the presence of a depletion layer can reduce hydrodynamic resistance force compared to what is expected from the bulk viscosity as the particle moves through a medium of non-adsorbing polymer[16, 17]. In the semidilute regime, the thickness of the depletion zone correlates with ξ, hence it is expected that its' impact will be most significant for motion at the length scale of ξ, which is about 1-3 nm in our experiments. But FCS probes the diffusion set by the length scale of laser focus size (0.5 μm). Assuming a depletion layer thickness of $\ell \sim 2$ nm and a particle (R_o=2.5 nm) within the layer experience the neat solvent viscosity, the crossover time can be estimated as the

$\tau \approx \ell^2/6D_o \sim 10$ ns, which is inaccessible in FCS experiments[59, 65]. The non-uniform viscosity within the depletion layer could also induce slip and reduce the drag by a factor of 2/3[9, 23, 61]. But the deviation from SE prediction that we observed is much stronger.

To explain the observed deviation from SE-predicted diffusion for particle radii, $R_o < R_g$, we consider the role played by the structural relaxation of the polymer matrix[66, 67]. For 35K PEG, the polymer concentrations used in our experiments was about 5-10 times the overlap concentration and they fall in the semidilute entangled regime. The transport properties of the particle could be dominated by the reptation of the chains surrounding the particle[66]. Let us consider a particle with R_o= 2.5 nm radii in 35K PEG solution (R_o/R_g=0.3) at a polymer volume fraction of $\phi \approx 0.2$. We calculated the characteristic diffusion time of the particle, $\tau_d \sim R_o^2/D$, which is ~ 1 μs (D ≈6 $\mu m^2/s$). The characteristic time of polymer mesh relaxation by "constraint release", also called the "tube renewal time" can be estimated by using the relation: $\tau_r \sim 3\eta/G_N^0$, where η is the viscosity, and G_N^0 is the plateau modulus of the polymer solution[33]. We have estimated that at $\phi \approx 0.2$, $G_N^0 \sim 7.5 \times 10^4$ Pa. Taking the viscosity η~1.6 Pa.s, $\tau_r \sim 0.1$ ms. Therefore, $\tau_d << \tau_r$ and mesh is static in the time scale of particle motion and the probe diffusion is not coupled to matrix relaxation[33]. The probe does not experience the macroscopic viscosity of the solution and therefore, $D/D_{SE} \approx 100$. For such situation, hydrodynamic models work relatively well to explain the particle diffusion. In the opposite limit, for a particle with radius, R_o=10 nm in the same polymer solution ($R_o/R_g \approx 1$), $\tau_d \approx 7$ ms with D=0.0141 $\mu m^2/s$. Therefore $\tau_d >> \tau_r$ and the motion of the particle is coupled with the matrix relaxation and $D/D_{SE} \approx 1$ is obtained. The matrix relaxation must be taken into

account to describe probe diffusion in these cases. We have not seen the return to SE behavior in the concentration regime that we explored. A future goal is to extend these measurements at a higher concentration to verify whether SE relation is eventually recovered.

Finally, we compare our data with the recent scaling theory of Cai *et. al*[60]. The choice of the experimental system allowed us to compare two regimes: intermediate size particles ($\xi < 2R_o < a$) and large particles ($2R_o > a$). The theory predicts that the intermediate size particles are affected by the segmental motion of the chains. At short times ($t < \tau_\xi$) particle motion is diffusive and the particle feels the solvent viscosity. In the intermediate time scale, ($\tau_\xi < t < \tau_x$), the motion is subdiffusive and the particle feels a time-dependent viscosity. At longer times ($t > \tau_x$), the motion is diffusive again and the effective viscosity (η_{eff}) felt by the particle is given by a polymer liquid consisting of chains comparable to the particle size, $\eta_{eff} \sim \eta_s(R_o/\xi)^2$. The time scales τ_x and τ_ξ correspond to the relaxation time of a polymer segment with size comparable to particle size $2R_o$ and ξ, respectively. We have estimated that, $\tau_\xi < 1$ ns and $\tau_x < 0.1$ ms, so our experiments measured the long-time diffusion. As $\xi \approx \phi^{-0.76}$, $D(\phi) \sim \phi^{-1.52}$ according to this theory for polymers in good solvent condition. Since both $\xi(\phi)$ and $a(\phi)$ are concentration dependent it is important to consider two crossover concentrations. This first one is ϕ^ξ at which $\xi \approx 2R_o$. For an athermal solvent it can be estimated by the expression, $\phi^\xi \approx \phi^*(R_g/2R_o)^{1.32}$. The other important concentration is ϕ^a at which $a(\phi) \approx 2R_o$. It can be estimated by making use of the expression: $\phi^a \approx (2R_o/a(1))^{-1.32}$. Between ϕ^ξ and ϕ^a, the particle size corresponds to the intermediate size regime. Accordingly, the 2.5 nm radius

Au NPs can be classified as intermediate sized between volume fraction 0.04 to 0.74 (details available in section 4.5. Table 4.5.1). Volume fraction in our experiments was varied from 0.09 to 0.37. It was observed that these particles follow a power law dependence of the measured diffusion on the volume fraction: $D(\phi) \propto \phi^{-1.45\pm0.09}$ (Fig. 4.3.6). Our results are in good agreement with the scaling model according to which the particle diffusion coefficient decreases with solution volume fraction as power -1.52 for athermal solvent[60]. D is expected to be independent of M_w in this regime as long as the tube diameter or polymer size is larger than R_o. For particle with R_o=2.5 nm in 5K PEG solution, $R_o \approx R_g$, so the above condition is approximately satisfied, but we still have observed near-independence of polymer M_w on particle diffusion. In the

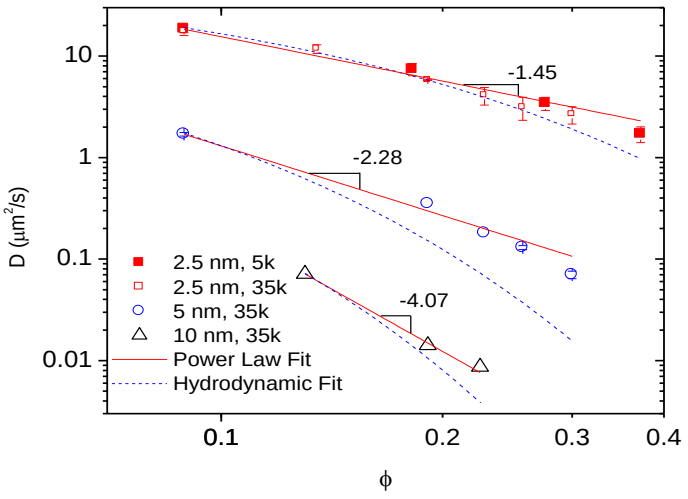

Figure 4.3.6. Power-law dependence of diffusion coefficients on volume fraction. The data for particles with radii, 5 nm and 10 nm in 5K PEG were not included as in these situations, $R_o > R_g$. The figure also showed the hydrodynamic fit, which gives a stretched exponential dependence on polymer volume-fraction with exponent ν=0.76. Table 4.5.3 lists all the fitting parameters used in this figure. (Reprinted with permission from Macromolecules 45 (15), 6143-6149. Copyright (2012) American Chemical Society)

intermediate size regime, the effective viscosity is proportional to the particle surface area, hence D is proportional to R_o^{-3}. To test this prediction, we needed particles of different sizes at a fixed concentration of a particular molecular weight polymer. At volume fraction of ϕ=.089 the 5 nm radii particles fall well in intermediate sized regime. Analyzing the intermediate sized 2.5 nm and 5 nm particles at this concentration for 35 K PEG gives: $D(R_o) \sim R_o^{-3.36}$. Since 5 nm radii particles get into the transition of intermediate to large sized particles with the increase in volume fraction we could not test this scaling relation for other concentrations. These particles (R_o=5 nm) showed a slightly different behavior than that predicted in the literature[60]. It can be attributed to the fact that in the concentration range studied, these particles are at the transition of intermediate and large sized particles. The diffusion still followed a power law dependence on the volume fraction though with a slightly different power: $D(\phi) \propto \phi^{-2.28\pm0.1}$ (Fig. 4.3.6).

The volume fractions equal or above ϕ^a correspond to large particle regime, $2R_o > a(\phi)$. The diffusion for large particles can occur through the reptation of the surrounding polymer chains and from the temporal fluctuation of the local matrix. The motion due to chain reptation is diffusive at long times and is determined by the bulk viscosity (η_m) of entangled liquid. 5K PEG solutions are not entangled at any concentrations, for 35K PEG solution, this regime is obtained above a threshold concentration, $\phi^a \approx 0.12$ for R_o=10 nm. Our data showed D decreases strongly with increasing concentration above ϕ^a. The decrease is well-fitted by the power law, $D(\phi) \sim \phi^{-4.07\pm0.19}$ compared to the theoretical prediction of the exponent -3.93 in athermal solvent. The diffusion coefficient is expected to be inversely proportional to the nanoparticle radius as in SE relation. Since we only

had 10 nm particles in large particle regime, we did not have sufficient data to test this relation. But as our measured diffusion values for the particle show a return to SE behavior, it implies that for even larger particles, this relation would have followed. In Fig. 4.3.6 we have also shown the prediction from hydrodynamic theory[7] which gives the functional form $D/D_o \sim \exp(-\kappa R_o/\xi)$, treating κ as the only adjustable parameter. In this situation, the power law fits better, particularly in the large particle regime. This indicated that polymer motion plays an important role and treating the matrix as fixed in time is inadequate to describe the nanoparticle dynamics in macromolecular solution.

4.4 CONCLUSION

We measured the diffusion of gold nanoparticles of radii 2.5 nm to 10 nm in semidilute poly (ethylene glycol) (PEG)-water solution by using fluctuation correlation spectroscopy. For particles with radii $R_o > R_g$, measured diffusion was similar to that expected by SE relation whereas for particles with radii $R_o \leq R_g$, the diffusion is faster than that estimated from SE relation. The ratio D/D_{SE} increases with polymer concentration and as R_o/R_g becomes smaller. The results were rationalized by comparing the characteristic time of probe diffusion with the time scale of constraint release dynamics for entangled polymer. We compared our results with theories, which are currently available. A reasonably good agreement was found with the recent scaling theory, which takes into account polymer dynamics. Our results will be important for understanding intracellular transport of globular molecules[46] and for the development of novel therapeutic treatments, which rely upon delivery of nanoparticles through complex spatial structures, such as mucin network[6].

4.5 SUPPORTING INFORMATION

Supporting information is available in this section. It consists of one figure and three tables, including the TEM image of gold nanoparticles with histogram analysis, tables for important length scales and other parameters, data for diffusion coefficients as a function of polymer volume fraction and fitting parameters used in analyzing the figures.

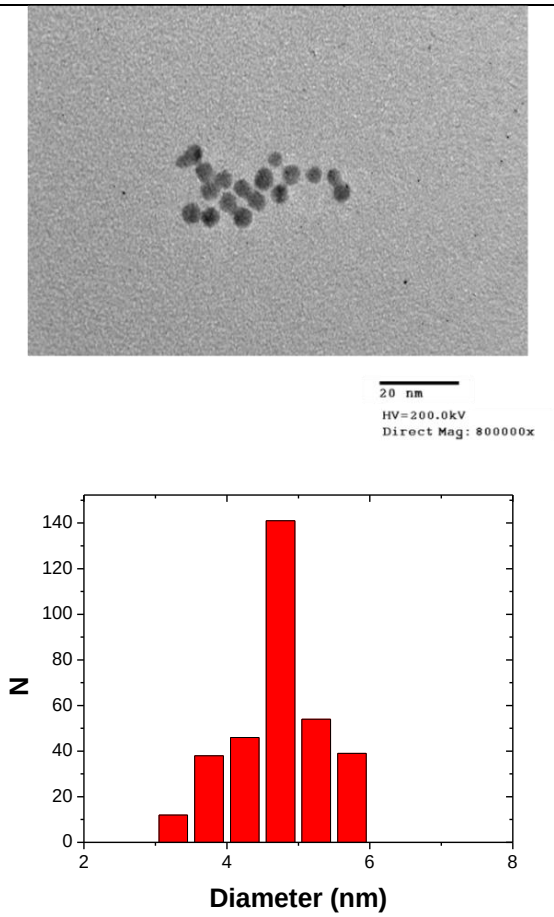

Figure 4.5.1. (a) TEM image of AuNPs deposited on carbon film magnified 800 000×.JEOL-2010 FasTEM Transmission Electron Microscope (TEM) with a LaB6 filament working at 200 kV was employed for imaging. (b) A histogram obtained from measuring the diameters of AuNPs. The average diameter measured is 4.7 ± 0.6 nm. (Kohli 2012)

TABLE 4.5.1: Important parameters

PEG Molecular weight, M_w	5 kg/mol	35 kg/mol
Radius of Gyration $R_g = 0.02\ M_w^{0.58}$ (nm)	2.8	8.64
Volume fraction ϕ range	0.089 - 0.37	0.089 – 0.3
Overlap volume fraction $\phi^* = M_w/(4/3 * \rho * \pi * R_g^3 * N_A)$ ($\rho_{PEG} = 1.126$ g/ml);	.08	.02
Entanglement concentration $\phi_e = M_e/M_w$ (M_e = 2 kg/mol for PEG) [1]	N.A.	0.12
Correlation Length $\xi(\phi) \approx R_g\ (\phi/\phi^*)^{-0.76}$ (nm)	0.9 – 2.6	1.1 – 2.6
Tube diameter $a(\phi) \approx a(1)\ \phi^{-0.76}$ (nm) $a(1) = 4$ nm[1]	N. A.	10.6 – 19.3

Au NPs radius R_o (nm)	$\phi^{\xi} \approx \phi^{*} \left(\frac{R_g}{2R_o}\right)^{1.32}$	$\phi^{a} \approx \left(\frac{2R_o}{a(1)}\right)^{-1.32}$
2.5	0.037	0.74
5	0.015	0.3
10	0.006	0.12

1. Rubinstein, M. and R. H. Colby (2003). Polymer Physics. Oxford ; New York, Oxford University Press

TABLE 4.5.2. Measured Diffusion coefficient values.

(a) Diffusion coefficients (D) of Au NPs (in $\mu m^2/s$) at different volume fractions of PEG 5 kg/mol

ϕ	R_o = 2.5 nm	R_o = 5 nm	R_o = 10 nm
0	87	39	21
0.089	18.6	8.3	4.1
0.182	7.1	3.0	1.5
0.276	3.2	1.24	0.56
0.372	1.5	0.61	0.28

(b) Diffusion coefficients (D) of Au NPs (in $\mu m^2/s$) at different volume fractions of PEG 35 kg/mol

ϕ	R_o= 2.5 nm	R_o = 5 nm	R_o = 10 nm	
0.089	17.5	1.7	ϕ	D
0.135	11.8	-	.089	.45
0.191	5.8	0.35	0.13	.07
0.228	4.1	0.18	0.191	.014
0.257	3.1	0.13	0.225	.008
0.3	2.6	0.07		

TABLE 4.5.3. Fitting parameters

Phillies fit in Figure 4.3.3: $D = D_0 \exp(-b\phi^{\nu})$

R_o (nm), PEG M_w (kg/mol)	b	N
2.5, 5	7.5	0.65
5, 5	8.47	0.70
10, 5	8.58	0.69
2.5, 35	8.07	0.67
5, 35	12.0	0.56
10, 35	44.8	1.01

Power Law Fit in Figure 4.3.6: $D = D_p \phi^{\alpha}$

R_0 (nm)	D_p	A
2.5	0.55	-1.45
5	0.0068	-2.28
10	0.00002	-4.07

Hydrodynamic Fit in Figure 4.3.6: $D = D_0 \exp(-\kappa R_o/\xi)$

R_o (nm)	K
2.5	1.66
5	1.76
10	1.2

CHAPTER 5

NANOPARTICLES DYNAMICS IN BIOPOLYMER SOLUTIONS

5.1 INTERACTION AND DIFFUSION OF GOLD NANOPARTICLES IN BOVINE SERUM ALBUMIN SOLUTIONS.

The Following material was originally published in Applied Physics Letters (2013)[68]

Very recently, gold nanoparticles (AuNPs) have gained a lot of attention for their diagnostic and therapeutic applications.[69-5] These NPs possess numerous unique and attractive properties, such as non-toxicity, size-dependent properties, and their ability to be functionalized.[70] These properties make them a favorable platform for drug delivery. It has been proved experimentally that spontaneous accumulation of protein on AuNPs occurs when these NPs are exposed to protein or serum plasma resulting in a protein layer coating.[36] This in turn alters the size of the drug delivery carrier as seen by the cell, as it will no longer be the size of the NP core but that of the core with the bound proteins, resulting in modified transport properties.[71] Thus understanding the adsorption process and protein-covered NP dynamics when exposed to physiological environments are important.[37, 72, 73]

It has been suggested that the NP size, shape and surface chemistry determines the affinity of a certain protein to bind to its surface.[74,75] This implies that the interaction of protein would not only be different for different types of NPs, but also be different for different sizes and shapes of the same kind of NPs. As a model protein we have selected bovine serum albumin (BSA). So far research has been done to study the interaction of BSA with variety of NPs including small sized (10-20 nm) FePt NPs and quantum dots[38],

medium and large sized AuNPs (20-250 nm)[41]. However, systematic study of interaction of BSA with nanometer-sized AuNPs with radius 2.5-10 nm remains scarce, but would be potentially useful in the areas ranging from Biophysics to drug delivery.[5, 72]

Here, we studied the interactions of these small AuNPs with BSA using fluctuation correlation spectroscopy (FCS) technique. The Brownian diffusion of the NPs was altered by the protein adsorption. This adsorption was studied as a function of NP size and protein concentration. Measured diffusion was compared to Phillies equation of stretched exponential function. A quantitative analysis of the protein binding was also performed.

5.2 EXPERIMENTAL SECTION

Albumin from bovine serum (BSA), fraction v ≥ 96% was purchased from Sigma. Tannic acid stabilized gold nanoparticles of radius 2.5, 5 and 10 nm were purchased commercially from Ted Pella, Inc. The polydispersity of these AuNPs was about 10%, determined by using transmission electron microscopy (TEM). Using a digital balance with resolution of 1 mg, many different concentrations of BSA (0.1 μM to 10 mM), in a phosphate buffer-AuNPs mixture (Ph 7.0) as a solvent, were prepared. The choice of the buffer with this Ph has been justified later in the paper.

Experimental platform was a Zeiss inverted microscope.[76] Near infrared light (wavelength 800 nm) from a femtosecond Ti: Sapphire laser (Mai Tai, Spectra Physics), was focused on the sample through a high numerical aperture (N.A.) objective. Light emitted from the sample was collected through the same objective and passes through a dichroic mirror that transmits light of wavelength below 600 nm. This emitted light was

detected by two single-photon counting modules (Hamamatsu). The output was recorded and analyzed using an integrated data acquisition system (ISS, IL). The number of NPs fluctuates as they diffuse in and out of the laser focus. This fluctuation (F) is quantitatively studied through the autocorrelation function (ACF), G(τ) given by Eq. 5.2.1. If Brownian diffusion is the cause of these fluctuations, the diffusion coefficient (D) can be calculated from the ACF by using Eq. 5.2.2, where G(0) is the magnitude of ACF at short time which is inversely proportional to the number of particles within the laser focus, ω_o is the half-width, and z_o is the half-height of the laser focus. Calibration experiments were performed by correlating luminescence signal from the 2.5 nm radius AuNPs in order to determine the dimensions of the focal point. The size of these NPs was confirmed by conducting TEM measurements. Using SE relation corresponding to the measured size, the calculated diffusion coefficient, D of 87 $\mu m^2/s$ was used to determine that $\omega_o \approx 0.25$ μm and $z_o \approx 1$ μm.

$$G(\tau) = \frac{<\delta F(t).\delta F(t+\tau)>}{<F(t)>^2} \qquad 5.2.1$$

$$G(\tau) = \frac{G(0)}{1+(\frac{8D\tau}{\omega_0^2})\sqrt{1+(\frac{8D\tau}{z_0^2})}} \qquad 5.2.2$$

As mentioned previously, AuNPs were specifically chosen for our experiments owing to their increased therapeutical applications. Some experiments have suggested that these NPs have high photo stability and do not suffer blinking.[69, 76, 77] The size of these NPs can also be tuned as desired, without any change of shape and chemical interaction with the matrix. Although the scattering signal from small NPs is typically

very low, they have high luminescence efficiency upon multi-photon excitation.[76] In all experiments, the laser power was kept below 1 mW to avoid photothermal conversion, which can induce local heating of NPs.

5.3 RESULTS AND DISCUSSION

In Fig. 5.3.1, we have shown some representative autocorrelation functions (ACF), plotted versus logarithmic time lag, collected by FCS. A number of FCS trials were performed for each NP size for each protein concentration. All the data was collected at room temperature 23 ^{o}C. Each ACF was collected for about 10 minutes.

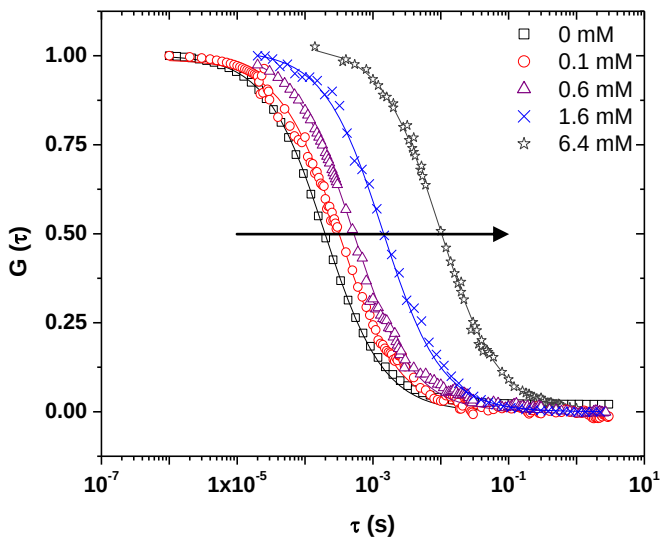

Figure 5.3.1. (Color Online) Normalized autocorrelation curves for AuNP (R= 2.5 nm) diffusing in BSA solution in phosphate buffer at various protein concentrations. Solid lines are fit to the curves using Eq. 5.2.2. Arrow shows direction of increasing concentration.

The data was fitted using Eq. 5.2.2 and the translational diffusion coefficient, D was obtained from the fit. Figure 5.3.2 shows D as a function of protein concentration.

The NPs diffusion coefficient decreases with the increase in BSA concentration as expected. A quantitative analysis was then performed with the obtained data. First, the hydrodynamic radius of the NPs was calculated from the measured diffusion coefficient D, before and after protein adsorption, using Stoke Einstein's (SE) equation. In order to accurately interpret the FCS data we measured the viscosity of the BSA solutions in phosphate buffer with pH 7.0 using a falling ball viscometer. Measured viscosity as a function of protein concentration is also shown in Fig. 5.3.2.

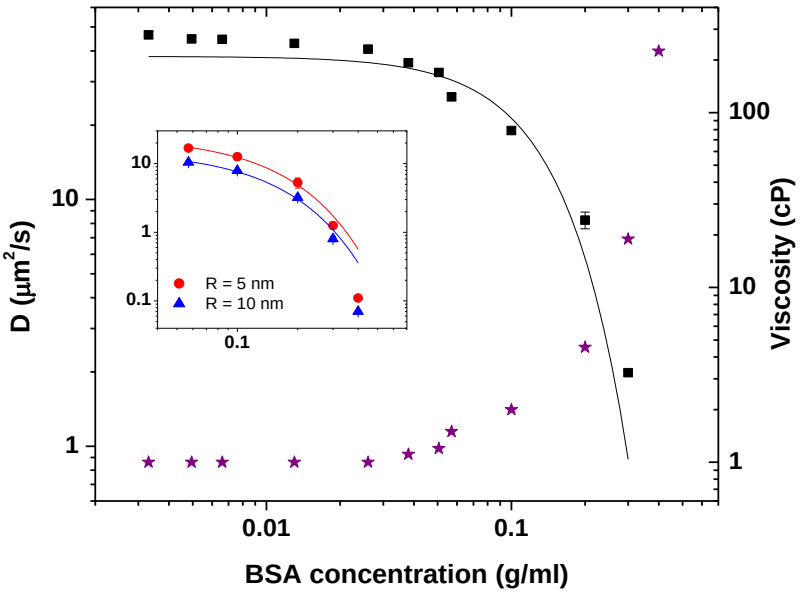

Figure 5.3.2. (Color Online) Diffusion coefficient of R = 2.5 nm AuNPs as a function of protein concentration. The inset shows the measured diffusion for 5 and 10 nm AuNPs at higher concentrations of BSA. Also shown (stars) viscosity as a function of BSA concentration.

BSA exhibits pH dependent conformations with its native (N) state found between pH 4 and 8.[78] The pH 7.0 of the phosphate buffer thus used corresponds to the

N state which can be approximated as an equilateral triangular prism with sides 8 nm and height 3 nm.[39] Table 5.3.1 consists of translational diffusion coefficient, D obtained by autocorrelation analysis, and hydrodynamic radius, R_h calculated using SE relation in the absence and presence of BSA, data shown is for 0.9 mM concentration of BSA. The average change in NP hydrodynamic radius for all concentrations studied comes out to be $\Delta R = 3.8 \pm 0.5$ nm which corresponds to a BSA monolayer formation. No multi-layer formation was observed even at significantly higher protein concentration. For radius 5 and 10 nm AuNPs, we studied only the higher concentrations (0.8 mM - 10 mM) in order to check for any multi layer formation. But, the formation of just a monolayer on the surface of these NPs indicated that for small sized AuNPs the BSA adsorption is size independent.

AuNP Radius(nm)	D_{AuNP} ($\mu m^2/s$)	$D_{AuNP+BSA}$ ($\mu m^2/s$)	$R_{h\ AuNP}$ (nm)	$R_{hAuNP+BSA}$ (nm)
2.5	87±3.5	26.0±0.8	2.51±0.1	5.59±0.2
5	39±1.8	16.86±1.1	5.5±0.3	8.63±0.5
10	21±0.6	10.4±0.5	10.4±0.3	13.9±0.7

Table 5.3.1. Translational diffusion coefficient (D) of AuNPs obtained by autocorrelation analysis, and hydrodynamic radius (R_h) calculated using SE relation in absence and presence of BSA

The diffusion data in Fig. 5.3.2 is fitted with Phillies equation of stretched exponential function: $D/D_0 = \exp(-\beta c^{\nu})$, where D_0 is the diffusion coefficient of the

AuNP in the limit of low protein concentration, β and ν are adjustable parameters. A reasonably good fit was obtained by using the D_0 value corresponding to the AuNP coated with protein monolayer rather than that of bare AuNP. The exponent ν was in marginal agreement with value close to 1 as reported in the literature.[79-29] In all these experiments the size of NPs including the monolayer is greater than the average size of the BSA molecules. The NP diffusion was observed to follow the prediction from Stokes-Einstein relation using the bulk viscosity provided the monolayer thickness was taken into account.[11] This is in agreement with some earlier works, where it has been shown that the macromolecular size (R_g) is the cross-over length scale for NPs experiencing macroviscosity or nanoviscosity.[52,80] Those experiments were preformed for linear polymers, which can entangle in the solution. Together our results imply that the crossover length scale is independent of the shape of the molecules.

Following the concept of Rocker *et. al.*,[38] the Langmuir model can be modified and the dependence of NP radii on protein concentration can be explained as follows:

$$\text{If} \qquad R_h(0) = \sqrt[3]{\frac{3}{4\pi} V_0} \tag{5.3.1}$$

is the hydrodynamic radii of the NP with volume V_0 and it is assumed that N protein (BSA) molecules adsorbed at the surface of the NP, each with volume V_{BSA}, then

$$R_h(N) = \sqrt[3]{\frac{3}{4\pi}(V_0 + NV_{BSA})} \qquad = R_h(0)\sqrt[3]{1 + cN} \text{ , where } c = V_{BSA}/V_0 \tag{5.3.2}$$

Modeling N as,

$$N = \frac{N_{max}}{1+\left(\frac{K_D}{[BSA]}\right)^n} \tag{5.3.3}$$

the hydrodynamic radii of NP as a function of protein concentration can be expressed as follows

$$R_h([BSA]) = R_h(0) \sqrt[3]{1 + \frac{c\, N_{max}}{1 + \left(\frac{K_D}{[BSA]}\right)^n}} \qquad 5.3.4$$

where N_{max} is the maximum number of proteins bound to the NP, K_D is the dissociation coefficient quantifying the NP-protein interaction, and n is the Hill coefficient. Figure 5.3.3 represents the calculated hydrodynamic radii of 2.5 nm AuNPs plotted as a function of BSA concentration. The data is fitted using Eq. 5.3.4. The best fit yields a dissociation coefficient of K_D = 78.6 ± 9.5 μM and a Hill coefficient of n = 0.63 ± 0.03, which being below 1 indicates anticooperative binding. This is also evident from the absence of multilayer formation. Comparison to Langmuir binding isotherm (n=1) is also shown in Fig. 5.3.3. The dissociation coefficient for Langmuir fit is K_D = 14.6 ± 4.3. The inset in Fig. 5.3.3 shows K_D, obtained by the anticooperative binding model, as a function of the NP hydrodynamic radius.

The dissociation coefficient K_D for the 2.5 nm radii NPs being smaller than that obtained by Medina *et. al.*[41], shown as last point in the inset, for the 26 nm radii NPs implies stronger interaction between smaller NPs and BSA. This would indicate the adsorption to be caused by ligand exchange reaction as also suggested by Tsai *et. al.*[42] rather than electrostatic attraction mechanism suggested by other groups[81,82]. The maximum number of protein molecules adsorbed per 2.5 nm radius AuNP as obtained from the fit is N_{max} = 8.4 ± 1. The theoretically calculated N_{max} would be about 3 calculated by dividing the surface area of AuNP ($4\pi*2.5^2$ nm^2) by the area of the

triangular base ($\frac{\sqrt{3}}{4} * 8 * 8\ \mathrm{nm}^2$) of BSA in its N state. This is in reasonably good agreement with the value obtained from the fit.

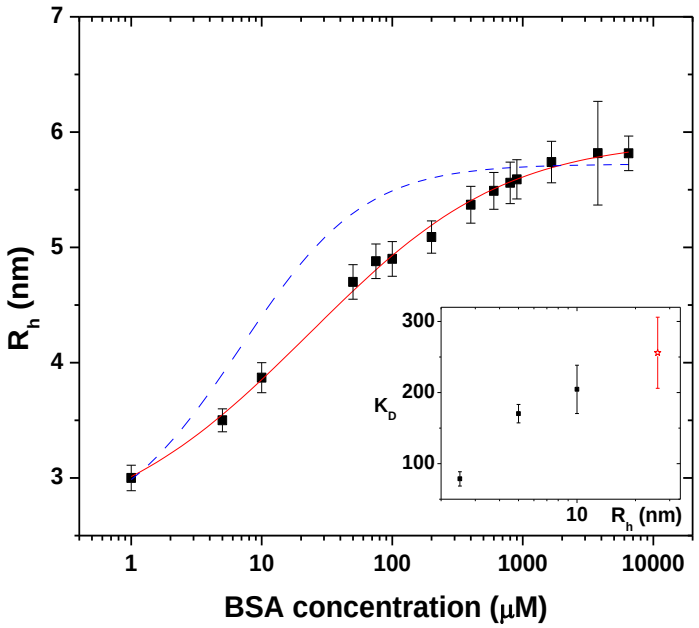

Figure 5.3.3. (Color Online) Hydrodynamic radii of NPs plotted as a function of BSA concentration. Red solid line represents fit of anti cooperative binding model, and blue dashed line shows comparison to Langmuir binding isotherm fitted to first and last 30 percent of data points. The conversion of concentration units is as follows $[BSA]_{g/ml} = [BSA]_{\mu M} * M_w * 10^{-9}$, where M_w is the molecular weight of BSA and is equal to 66,430 g/mol. The inset shows K_D as a function of the hydrodynamic radius R_h.

5.4 CONCLUSION

We demonstrated by performing FCS experiments that BSA forms a protein monolayer on the small sized AuNPs. This monolayer was observed to have attained saturation at a BSA concentration of approximately 0.8 mM. Multi-layer formation was

not observed even at significantly higher BSA concentrations. Average change in NP hydrodynamic radius measured before and after protein adsorption is 3.8 nm. Thickness of the adsorbed layer is independent of NP radius ranging from 2.5 - 10 nm. The NP diffusion followed Stokes-Einstein prediction provided the thickness of the adsorbed layer was accounted for. The adsorption was best described by anticooperative binding model. The estimated N_{max}, was in fairly good agreement with the N_{max} obtained from the fit. Our results will be important in understanding the nanoparticle motion in complex fluids, which is relevant in the areas of bio diagnostics as well as targeted drug delivery.

CHAPTER 6

GOLD NANOPARTICLE DIFFUSION IN BRANCHED POLYMER AND PARTICULATE SOLUTIONS

6.1 CONTRASTING NANOPARTICLE DIFFUSION IN BRANCHED POLYMER AND PARTICULATE SOLUTIONS: MORE THAN JUST VOLUME FRACTION

The Following material has been accepted for publication by Soft Matter.

It is well established that the cell cytoplasm is a crowded aqueous medium with a significant volume fraction occupied by various macromolecules[83]. More insight of the biochemical and biophysical processes should therefore be obtained by carrying out experiments at concentration of macromolecules similar to cellular environment[46]. Diffusion is the most important passive transport mechanism controlled solely by temperature and does not require any external field. Together with active transport processes, it controls various biological processes such as intracellular transport, reaction rates, signaling process, cellular pattern formation, protein assembly, etc[84-90]. Generally as the size of the diffusing species decreases their mobility increases and as the volume fraction of the crowding agents increases their mobility decreases[52]. The crowding agents affect the collisional frequency of the probe particle as well as the hydrodynamic interaction and together they influence the dynamics of the probe. The century-old Stokes-Einstein (SE) relation gives a simple equation to calculate the translational diffusion coefficient (D_{SE}) by using $D_{SE}= k_BT/f\pi\eta_mR_0$, where k_B is the Boltzmann's constant, T is the absolute temperature, η_m is the viscosity of the medium, R_0 is the radius

of the diffusing entity, and the constant f is determined by the boundary condition for flow at the particle surface; f=6 or 4 depending upon "stick" or "slip" boundary conditions.

This equation works remarkably well to describe the diffusion of probe molecules in simple liquids and even self-diffusion in neat liquids. But it is well known in polymer science community that small probe molecule can diffuse orders of magnitude faster in a semidilute or concentrated polymer solution compared to the expectation from SE relation[25, 28, 32, 52, 76]. A good model system to understand the probe diffusion is to use spherical, rigid nanoparticles as probe and homopolymer molecule with varying concentration as crowding agent. Three size regimes for probe diffusion in such systems are well documented[8, 10, 28, 29]. They are generally given as the ratio R_0/ξ, where R_0 is the radius of the probe particle and ξ is the correlation length measured as the average distance of a monomer in one chain to the nearest monomer of the other chains. If $R_0/\xi < 1$, the probe can easily slip through the polymer mesh and it only feels the solvent viscosity (η_0). In the opposite limit, the probe motion is intimately connected to the polymer matrix so that it feels the macroscopic viscosity (η_m) as measured by a rheometer. In the intermediate regime, $R_0/\xi \approx 1$, the probe experiences a local viscosity (η_ϕ), which is between the solvent and bulk viscosity. In this scenario, the crossover length scale (l_c) from η_0 to η_m is the correlation length. There are several experiments conducted in the past few years to determine l_c. Though some of the earlier studies were consistent with the picture of $l_c \approx \xi$[29, 35], more recent work using particles with different sizes indicates that the radius of gyration (R_g) is the crossover length scale[32, 52], which is

typically much larger than ξ. Recent computer simulations also predict R_g as the crossover length scale[9, 10, 59].

A scaling function of the form $F(R_0/\xi)$ has been proposed for the local viscosity (η_ϕ), which depends only upon the ratio R_0/ξ[8, 28]. As ξ depends upon the volume fraction of the polymer in solution (ϕ), but independent of polymer molecular weight (M_w)[8], the scaling function depends only upon ϕ and R_0. Models based upon hydrodynamic interaction between the polymer mesh and particle predict a stretched exponential function, $F(R_0/\xi) \sim \exp[-\beta(R_0/\xi)^\nu]$[12, 28, 31]. This functional form assumes that the diffusion of particles occurs through a statistical pore of size, ξ and involves an activation energy associated with the deformation of the network[8]. Similar stretched exponential function was also obtained in models, which considers the effect of depletion layer around the particle in a non-adsorbing polymer solution[16]. All these models do not explicitly consider the polymer dynamics. Recently, a scaling theory has been used, which took into account the roles of polymer segmental motion and the effect of entanglement dynamics on the particle motion. It predicts power law dependence of scaling function instead of much stronger stretched exponential dependence[60]. In a recent work we have shown that the scaling theory works slightly better especially in the large particle size, when the effects of entanglement and reptation become important[52]. Most of these previous studies have focused on linear polymers.

In this paper, we investigated how the nanoparticle diffusion is affected if a slight branching is introduced in the polymer. We performed experiments using dextran solutions of varying concentrations, a model system, which had been widely used to

study the effect of crowding on diffusion, association rate, etc[88-92]. However, there are several important aspects, which distinguish our work from some earlier studies. First, we compare our results of NP diffusion with the expectation based from SE relation using the bulk viscosity (η_m), which we measured. The results showed strikingly different behavior than linear polymers. Second, we studied the diffusion of NPs in a non-polymeric colloidal system having similar size of dextran and volume fractions, which farther showed the role played by the molecular structure of the crowding agent. Third, our results showed anomalous sub-diffusion of smaller sized (R_0=2.5 nm) nanoparticles in dextran solution but not in any other systems. This implied that the anomalous exponent cannot be used generally as a measure of crowding[91, 93]. Taken together, our results will be important to understand how nanometer-sized particles or macromolecules move within structured fluid and biological systems, which usually consists of molecules of many different size, shape and architecture.

6.2 EXPERIMENTAL SECTION

6.2.1 MATERIALS

We used dextran 70 with an average molecular weight of 70 kDa (Sigma-Aldrich). Ludox TM-50 colloidal silica, 50 wt.% suspension in water was purchased from Sigma-Aldrich. Tannic acid stabilized gold nanoparticles (AuNPs) of radius 2.5 and 10 nm were purchased from Ted Pella, Inc and used as probes. TEM measurements indicate a 10% polydispersity of these NPs. Distilled deionized water (resistivity= 18.2 MΩ.cm) was used as solvent.

6.2.2 METHODS

A digital balance with a resolution of 1 mg was used to prepare different concentrations of dextran in water-AuNP mixture as solvent. Freshly prepared samples were used in all experiments to avoid any aging effect. A falling ball viscometer (Fish-Schurman Corp, N.Y.) was used to measure the viscosity of dextran and particulate solutions. The translational diffusion coefficient (D) of the gold NPs were determined by using the method of fluctuation correlation spectroscopy (FCS) also known as fluorescence correlation spectroscopy[52, 76]. Briefly the near infrared light (wavelength 800 nm) from a pulsed laser was focused into the sample through a high N.A. objective. The fluctuation in photon counts as the gold NPs move into or out of the laser focus is collected through two single-photon counting modules (Hamamatsu). The data is cross-correlated and from the resulting autocorrelation function, $G(\tau)$ diffusion coefficient D was calculated by using the equation:

$$G(\tau) = \frac{G(0)}{1+(\frac{8D\tau}{\omega_0^2})\sqrt{1+(\frac{8D\tau}{z_0^2})}}. \qquad 6.2.1$$

Here, G(0) is the magnitude of the autocorrelation function at short time ($\tau \to 0$) which is inversely proportional to the number of particles within the laser focus, ω_o is the half-width, and z_o is the half-height of the laser focus. By performing a calibration experiment, we determined that $\omega_o \approx 0.33$ μm and $z_o \approx 2$ μm. The laser power was kept below 1 mW to reduce local photothermal effect[76].

6.3 RESULTS AND DISCUSSION

The crowded medium was mimicked by using dextran solutions of various volume fractions up to 30% (≈40 wt%), which is close to the volume occupied by various macromolecules inside a cell cytoplasm[83]. Dextran is a flexible, slightly branched polysaccharide consisting of glucose subunits. It assumes an almost random coil conformation in dilute solutions above a molecular weight, $M_w \approx 2$ kDa[94]. Experiments have shown about 1 branch in every 25 subunits with most of the branches few residues long[92, 95]. Dextran has been proven to be biocompatible and clinically safe. We have chosen dextran 70, because parenterally administered dextran uses solutions of M_w between 40 kDa and 70 kDa. These molecular weight dextrans are also ideal for coating iron oxide or gadolinium particles used as a contrast agent in MRI. We compare the probe particle diffusion in dextran with another crowded system composed of unlabelled Ludox particles of radius, $R_p \approx 10$ nm. It is comparable to the radius of gyration, $R_g \approx 8$ nm of the dextran molecules used[92]. But in contrast to Ludox particles, which are rigid and impenetrable spheres, dextran molecules are soft and structured. This is reflected in differences in the probe diffusive behavior and the rheological properties of the solution as will be discussed later. We used gold NPs as a probe because these are increasingly being used for their diagnostic and therapeutic applications, such as a drug delivery agent. They are non-toxic and can be functionalized routinely using thiol chemistry. Their other useful properties, especially relevant for our experiments, are high luminous efficiency and no photobleaching or blinking, which are common problems associated with fluorescent dyes and semiconductor quantum dots. Gold nanoparticle concentration

was always kept at ≈100 nM to achieve single-molecule sensitivity for FCS experiments. Two different sizes (R_0=2.5 nm and 10 nm) of these NPs were chosen to investigate the most interesting size regimes from polymer science perspective, i.e., for smaller sized AuNPs, $R_g > R_0 \approx \xi$ and for larger sized NPs, $R_g \approx R_0 > \xi$. These two size regimes allowed us to determine the crossover length scale for branched polymers and compare our results with probe diffusive behavior in linear polymer solutions. Control experiments indicated no specific interactions between gold NPs and the crowding agents (dextran and ludox particles) used, which would have lead to irreversible adsorption on NP surface.

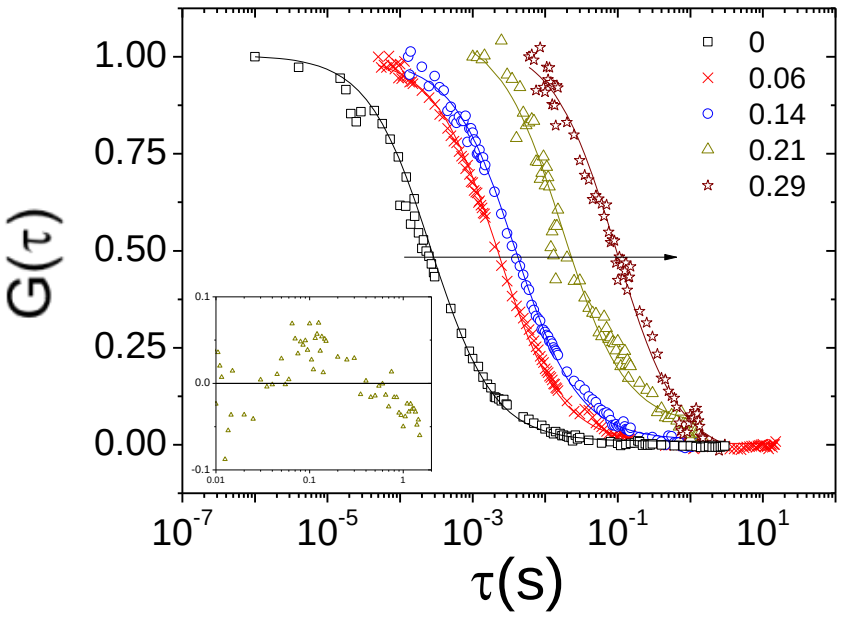

Figure 6.3.1. Autocorrelation function of 2.5 nm radii gold nanoparticles diffusing in dextran 70 solution at various volume fractions as indicated. Data was collected for 15 minutes. The arrow points towards higher concentration. The solid lines are fitting of the data with normal diffusion (Eq. 1). The fitting deviates at two highest volume fractions (ϕ=0.21 and 0.29), which is more prominent at longer time scales. (Inset) Residual of fitting for volume fraction, ϕ=0.21 and τ >0.01 s is shown.

Figure 6.3.1 displays representative normalized autocorrelation functions (ACF) for smaller AuNPs (R_0=2.5 nm) in dextran solutions of volume fraction ϕ = 0.06 to 0.29. It is evident from the figure that the mean decay time (τ_d) of the ACF increases with an increase in the polymer concentration indicating slower diffusion coefficient. This is a result of the increase of the viscosity of the solution. The ACF are fitted using Eq. 6.2.1 to obtain the translational diffusion D. The fitting deviates for two higher concentrations (ϕ=0.21 and 0.29) as shown in the residual plot (Fig. 6.3.1 inset). The data points are not distributed randomly about the fitting, especially at longer time scales. It has been observed previously that in crowded macromolecular environment, the diffusion can deviate from simple model as was used in Eq. 6.2.1[76, 91, 92]. In such situations, the data needs to be fitted with anomalous sub-diffusion model, where the mean-square-displacement (MSD) shows a fractional power law dependence, $\langle r^2(t)\rangle \sim t^{\alpha}$ (α <1) rather than linear dependence on time (t). The anomalous exponent (α) can be used as a measure of subdiffusion. The linear dependence (α=1) correspond to normal diffusion. The autocorrelation function for anomalous diffusion is fitted with the equation[91-93]:

$$G(\tau) = \frac{G(0)}{1 + (\frac{8D_a\tau}{\omega_0^2})^{\alpha}\sqrt{1 + (\frac{8D_a\tau}{z_0^2})^{\alpha}}}. \qquad 6.3.1$$

The diffusion in this situation cannot be described by a single diffusion coefficient. But we can define an apparent diffusion coefficient (D_a), which describes the diffusion at the length scale of the laser focus ($\sim\omega_o$) and at time scale of mean decay time ($\sim\tau_d$). For the two lowest concentrations, ϕ=0.06 and 0.14 the fitting of the data with anomalous model is not different from using a fixed α=1. In Fig. 6.3.2 we have shown

the fitting of ACF for ϕ=0.21 using Eq. 6.3.1 and the residual is shown in the inset. The reduced χ^2 becomes 30% less and the distribution of residuals at longer times becomes more random compared to normal fitting (Eq. 6.2.1). Similar analysis of autocorrelation functions were performed with other systems (Figure 6.5.1).

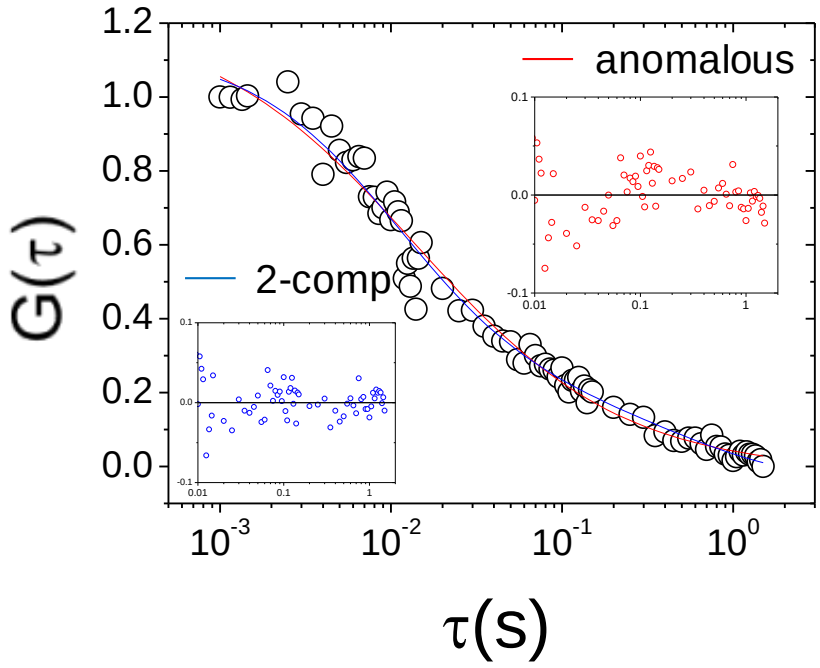

Figure 6.3.2. Anomalous (red line) and two-component (blue line) fits for the data of Fig. 6.3.1 with ϕ=0.21. The anomalous fitting gives α=0.75 and D=1.1 $\mu m^2/s$. The two component fitting gives a fast and slow component with values, D_{fast}=1.42 $\mu m^2/s$ and D_{slow}=0.027 $\mu m^2/s$. (Insets) Corresponding residuals are shown for τ > 0.01 s.

We also considered two-component model to fit our data. This model is particularly suitable for studying binding interaction in situation when a small probe molecule/particle binds with a much bigger entity. In this case, the fast component of diffusion corresponds to probe diffusion and the slow component originates from the

diffusion of bound complex[89]. The fitting quality of data with this model for R_0=2.5 nm in dextran solution of ϕ=0.21 is similar to the anomalous model (Fig. 6.3.2). However, we will not consider the two-component model farther because we do not except any strong interaction between gold and dextran. In addition, we did not observe anomalous diffusion for bigger AuNPs, which has the same surface chemistry as the smaller ones.

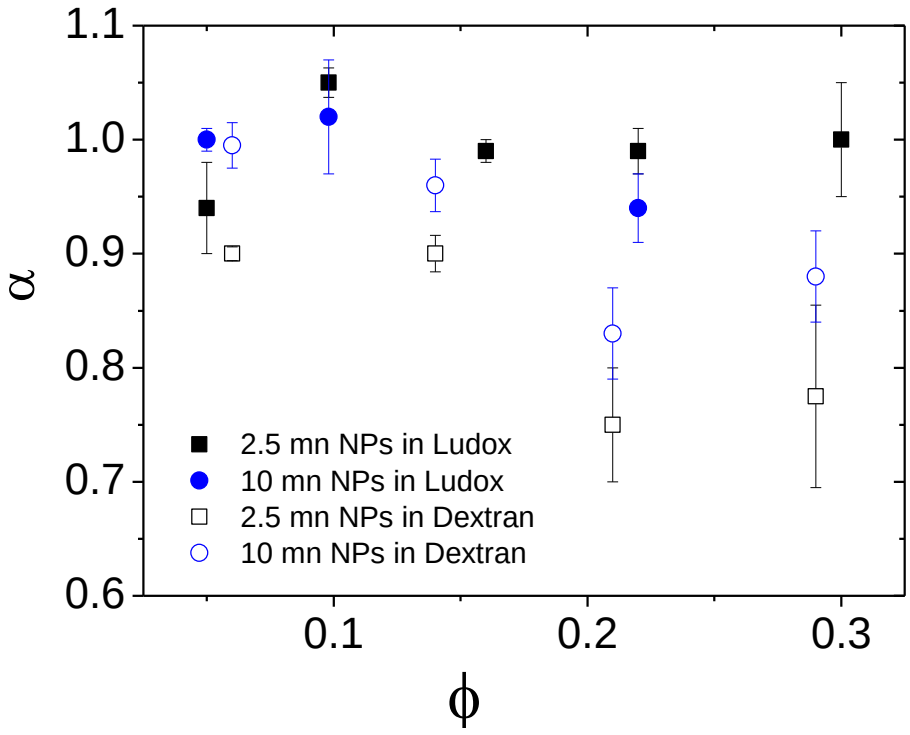

Figure 6.3.3. Anomalous exponent (α) as a function of volume fraction for dextran (open symbols) and Ludox (filled symbols). The exponents were obtained by fitting with Eq.6.3.1 (main text). The error bars were calculated from the average of five measurements.

In Fig. 6.3.3, α vs. ϕ was plotted by fitting all ACFs with the anomalous model. Gold NP diffusion in varying volume fraction of Ludox silica particles showed normal

diffusive behavior with $\alpha \approx 1$. Because of the statistical noise, only for $\alpha < 0.85$ we can confidently claim anomalous diffusion. The data in Fig. 6.3.3 indicates clearly of subdiffusion for smaller AuNP particles in dextran at high volume fractions. However, given the experimental uncertainty, we were unable to observe any systematic dependence of anomalous exponent with concentration. The bigger NPs in dextran showed normal or slightly anomalous behavior.

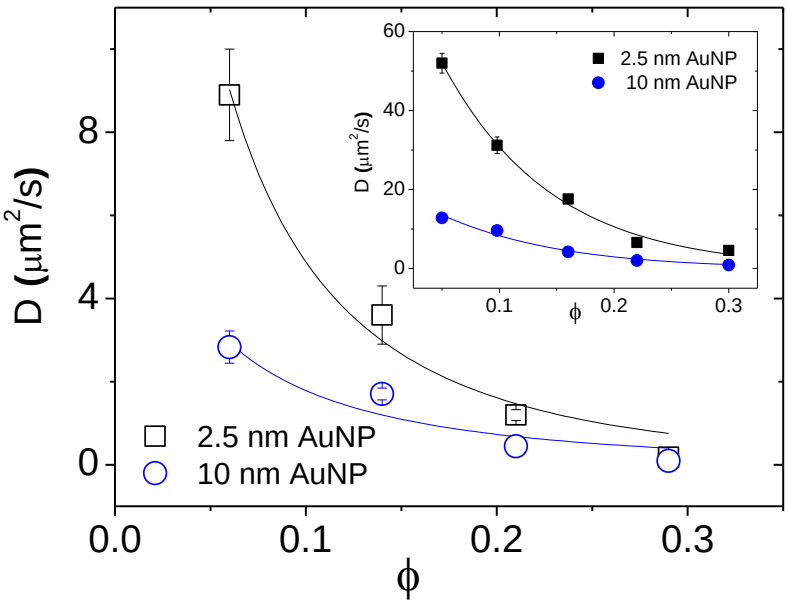

Figure 6.3.4. Diffusion coefficient (D) of two different sized AuNPs plotted as a function of various volume fraction of dextran (main figure) and Ludox (inset) solutions. The solid lines are stretched exponential fit as given by Phillies equation. The values of the fitting parameters are listed in Table 6.5.1.

In Figure 6.3.4, we plotted D (or D_a for anomalous diffusion) as a function of volume fraction. We fitted the data with a stretched exponential function: $D/D_0 = \exp(-\beta\phi^{\nu})$, also called Phillies fit[25], where D_o is the diffusion coefficient of AuNPs in the neat

solvent (water), β and ν are adjustable parameters. A reasonably good fit was obtained in all systems even for higher concentrations. The smaller NPs in dextran at the highest concentration showed some deviation from the fitting, which has been explained later. The exponent ν in dextran solution (ν≈0.45) has been observed to be smaller compared to Ludox solution (ν≈1). For probe diffusion in linear polymer in good solvent ν≈0.75 expected[31], but for dextran ν values between 0.5 to 1.5 have been reported[92]. Some experiments have observed β increases with probe size[31], but we observed no clear trend for dextran 70. The physical significance of parameters in Phillies equation is still not clear. The values of β and ν for all fittings were given in Table 6.5.1. The stretched exponential fitting considers the hydrodynamic interaction, but ignores the fluctuation of polymer mesh size because of polymer motion. In case of probe diffusion in linear polymer (polyethylene glycol) solutions, it has been observed that the mobility could be an order of magnitude faster compared to prediction from stretched exponential fitting[52]. This can be explained by taking into account polymer motion, which opens up additional mechanism for particle diffusion[60]. In dextran solutions, our data indicates polymer dynamics do not play significant role in probe mobility in the concentration and the size regime studied. As both Ludox and dextran data can be fitted equally well with the stretched exponential fitting, this points towards similar mechanism for probe diffusion in both solutions. We will argue later that probe particles view the matrix in dextran solution as consisting of soft colloids. This point will be strengthened farther in explaining the adherence to the SE relation.

The bulk viscosity (η_m) of the dextran and Ludox solutions was measured using a falling ball viscometer. The measured viscosity as a function of concentration for dextran is shown in Fig. 6.3.5 inset. The viscosity of the dextran solution is consistently higher compared to Ludox because of higher pervaded volume by the polymer (Figure 6.5.2). For both dextran and ludox particles, the viscosity data can be fitted with stretched exponential function. Above the overlap volume fraction (ϕ^*), which marks the onset of semidilute regime, the chains begin to overlap and viscosity starts to rise rapidly. Thus ϕ^* can be estimated from the change in slope of the viscosity vs concentration in log-log plot (Fig. 6.3.5 inset), which for dextran yields $\phi^* \approx 0.033$. From ϕ^* we calculated the intrinsic viscosity, $[\eta] \sim 1/c^* \approx 0.22$ dl/g, where c* represents the overlap concentration. $[\eta]$ is related to the polymer molecular weight (M_w) by Mark-Houwink-Sakurada (MHS) relationship $[\eta]=KM_n^{\beta}$, where for dextran in water $K=8.525 \times 10^{-4}$ dl/g and $\beta=0.522$ are constants[96]. This gives the number average molecular weight, (M_n) ≈ 47 kDa. Viscosity measurement allowed us to compare the diffusion coefficient of the AuNPs with the Stokes-Einstein (SE) prediction. Our results indicate that the diffusing NPs obey the SE relation for both systems at all concentrations, as evident from Fig. 6.3.5.

To interpret this result and to estimate the crossover length scale from nanoviscosity to macroviscosity, we need to calculate the important length scales of the system. As $\phi^* \approx 0.033$, all the measurements (ϕ=0.06-0.29) were carried out in the semidilute regime. The average radius of gyration R_g of the dextran 70 in water corresponds to $R_g \approx 8.2$ nm[94]. Thus, R_0/R_g ratios were between 0.3 and 1.2 corresponding to the R_0 values of 2.5 and 10 nm. The correlation length (ξ) as a function of polymer

concentration was calculated by using the relationship[8], $\xi \approx R_g(\phi/\phi^*)^{-0.76}$. $\xi(\phi)$ ranged from 1.6 nm to 5.2 nm. Thus the measurements covered the regime $R_0 \approx \xi$ as well as $R_0 > \xi$ as the ratio R_0/ξ varied from ≈0.5 to 6. The chain entanglement becomes significant

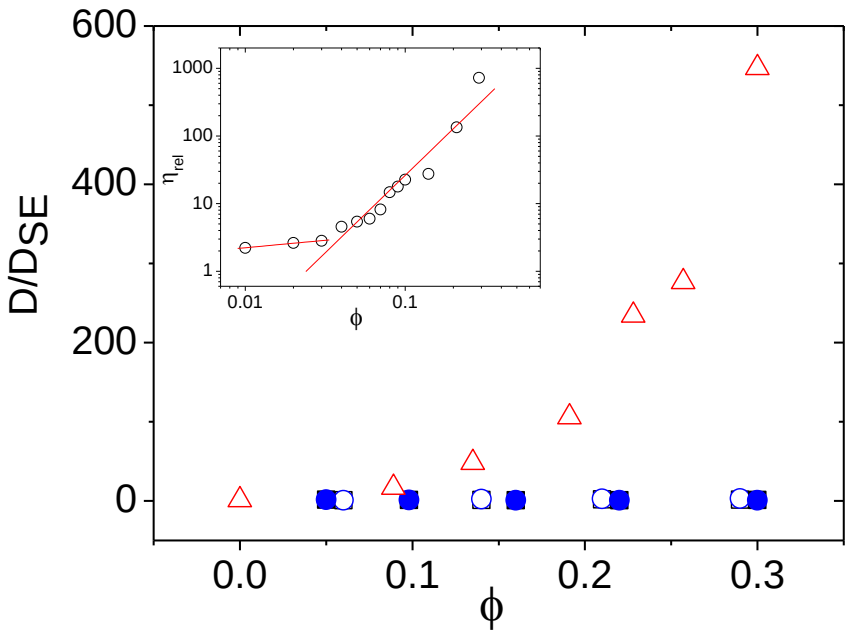

Figure 6.3.5. (Inset) Viscosity of dextran 70 solution vs. volume fraction in log-log plot. The vertical axis is normalized with respect to the solvent viscosity. The intersection of the two straight lines gives the overlap volume fraction (ϕ^*) ≈0.033. (Main figure) The ratio D/D_{SE} plotted as a function of volume fraction; 2.5 nm AuNPs in dextran (R_0/R_g=0.3, open square) and in Ludox (R_0/R_p=0.25, filled square); 10 nm AuNPs in dextran (R_0/R_g=1.2, open circle) and in Ludox (R_0/R_p=1, filled circle). Also shown for comparison D/D_{SE} for 2.5 nm AuNP in a linear polymer polyethylene glycol (PEG) of M_w= 35 kg/mol (R_0/R_g=0.3, open triangle)[10]. PEG data has been adapted with permission from Macromolecules 2012, 45, 6143-6149. Copyright (2012) American Chemical Society

only at volume fractions sufficiently above ϕ^*. The critical concentration for entanglement is given by, $\phi_e \approx (M_e/M_w)^{0.75}$, where M_e is the molecular weight between entanglement in melt. For dextran, $M_e \approx 75$ kg/mol which implies that the dextran sample

used in our experiments does not possess enough number of entanglements. Therefore, entanglement dynamics does not play significant role in particle diffusion. The crowded nonpolymeric nanoparticle system was so chosen to have the radius (R_p) of approximately 10 nm, which gives similar R_0/R_p ratios as for the dextran system. Since it is a solution consisting of only unlabelled spherical particles, presence of entanglements is completely ruled out.

Our results in Fig. 6.3.5 indicated that in branched polymer and in Ludox particle systems, SE relation is followed in the size regime we investigated. This is contrary to our findings with the diffusion of these NPs for similar R_0/R_g in linear polymers where we had observed a strong deviation. NPs in polyethylene glycol (PEG) solutions can diffuse orders of magnitude faster compared to the expectation based from SE relation using macroscopic viscosity and the ratio depends upon the volume fraction if $R_0/R_g < 1$[52]. But as R_0/R_g ratio approaches 1, the SE prediction is also increasingly followed. Thus, it can be concluded that in case of branched polymers, R_g is not the crossover length scale for particles experiencing nanoviscosity or macroviscosity, but it has to be smaller then R_g.

Therefore we need to explain two striking results, i.e., the difference in the crossover length scale for branched polymer compared to linear polymer and the observation of anomalous diffusion for 2.5 nm AuNP particles in dextran, but not in other systems. As the observation of heterogeneous dynamics is a hallmark of systems near the glass transition[97], we have estimated the glass transition temperature (T_g) of the dextran solution using Fox equation[98]. For the highest volume fraction studied ($\phi \approx 0.29$) we

determine that $T_g \approx -119\ ^0C$[99] , which is much below the room temperature (23 ^{0}C) where the measurements were carried out. So alternate explanation need to be sought. We considered the detailed structure of the dextran molecules. It has been observed that even a small amount of branching can affect physical and dynamical properties of dextran molecules[92]. For example, rheologically dextran behaves as Newtonian fluid, i.e., the flow rate is independent of shear stress. We also point out that previous experiments concluded that a soft sphere model is a suitable description of the molecular structure of dextran in water[94, 95]. To be more specific, hydrodynamically dextran behaves as prolate ellipsoid of revolution and for dextran 70, the ratio of semimajor and semiminor axis is ≈9[95]. As the molecular weight increases the ratio decreases and the molecule approaches closes to spherical symmetry. Some other group have determined the fractal dimension (d_f) of dextran as ~2.3 which is different from what is expected for ideal chain (d_f=2) or expanded coils in good solvent condition ($d_f < 2$)[33, 95]. This soft sphere model of dextran supports the essential results of Fig. 6.3.5, which showed similar D/D_{SE} for both Ludox and dextran solutions. This can also explain why the stretched exponential fit of Fig. 6.3.4, which ignores the polymer dynamics can explain dextran data reasonable well.

As mentioned earlier, the correlation length (ξ) depends upon concentration and is ≈ 2 nm for high dextran volume fraction. Though this is comparable to AuNP particles of 2.5 nm radii, we do not attribute anomalous dynamics to correlation length becoming comparable to the particle size. Plot of the exponent, α vs. R_o/ξ did not show any correlation (Figure not shown). In addition for a wide range of particle sizes, linear polymer solutions always exhibited normal diffusion (Chapter 4). We will argue, instead,

that the anomalous dynamics is due to the presence of branching. Even though the branching occurs randomly, on the average there are about 5% branching in dextran[95]. So there are approximately 20 residues of glucose unit between consecutive branches. Taking the size of a glucose molecule as ~1 nm, on the average the distance between branches is about 20 nm. As branching increases the local segmental density, the smaller AuNPs (R_0=2.5 nm) can penetrate deep inside the chain but not the bigger NPs (R_0=10 nm). The effect of branches is then to create a trap for the smaller nanoparticles. The trap, however, is not fixed in time because of the local segmental motion. In some ways, this is analogous to glass forming colloidal systems, where the transient caging formed by the other particles can trap the tracer particle for a long time. Particle tracking experiments in such situations revealed subdiffusion above a certain volume fraction[100]. We can expect a similar behavior where the branching can trap the smaller particles and thus give rise to anomalous diffusive behavior. The larger sized particles cannot be trapped and feel on the average a homogeneous medium. Therefore, weak or no anomalous subdiffusion was observed for those (Fig. 6.3.3). Indeed previous experimental work observed that trapping of molecules for random periods of times inside dendritic spines can cause anomalous diffusion[101]. Computer modeling predicts a larger degree of subdiffusion in spiny dendrites compared to smooth dendrites and the value of anomalous exponent correlates with spine density. We note that microrheology experiments have shown that coupling of the probe and segmental motion of the chains can also give a mean-square-displacement (MSD), which follows the power law $\langle r^2(t)\rangle \sim t^{3/4}$ instead of t^1 as for a freely diffusing Brownian particle[91]. This has been observed for particles embedded in

semiflexible polymer network such as actin gels[102]. Normal diffusive behavior in system with Ludox particles was observed because no caging effect is expected even for the maximum volume fraction studied (ϕ~0.3), which is much smaller than the glass forming volume fraction (ϕ_g~0.58 for hard spheres).

6.4 CONCLUSION

The goal of this study was to investigate the role played by the molecular structure of the crowding agent in determining the diffusive behavior of probe particle or molecule. We selected dextran molecule which is coil like with randomly distributed branches. It can form a fluctuating polymer network with pore size that decreases with increasing volume fraction. The other crowding agent was silica spheres with similar size of dextran molecules but it should not form a network. We compared the diffusion of gold nanoparticles in these two systems. For both cases we observed that diffusion coefficient followed a stretched exponential function of concentration and can be predicted from Stokes-Einstein relation using the bulk viscosity, which are very different than linear polymer. This can be explained by assuming that hydrodynamically dextran behave as soft colloid. But the presence of branches in itself reveals important differences. The smaller nanoparticles can be transiently trapped within the branch giving rise to anomalous subdiffusion at high concentrations. But the bigger NPs do not show any such behavior and demonstrate normal diffusive behavior. This implies that anomalous behavior is not simply a function of volume fraction of the crowding agent. The detailed structure of the molecules needed to be taken into account and each type of macromolecule can affect the diffusive behavior in different manner. The results will be

important to understand the passive transport processes within complex media such as cellular matrix, mucus and in neurons possessing spiny dendrites.

6.5 SUPPORTING INFORMATION

Supporting information is available below.

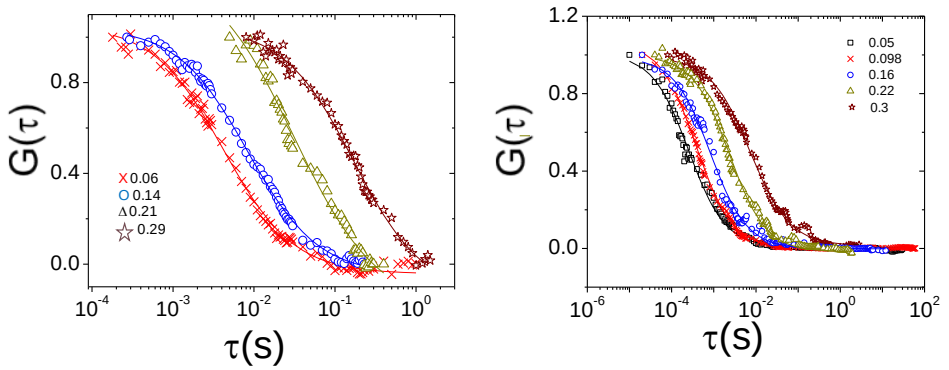

Figure 6.5.1. (Left) Diffusion of 10 nm AuNP particles in various volume fractions of dextran solutions. (Right) Diffusion of 2.5 nm AuNP particles in various volume fractions of Ludox particles. All fittings are with anomalous subdiffusion model. The fitting gives $\alpha \approx 1$ in all cases.

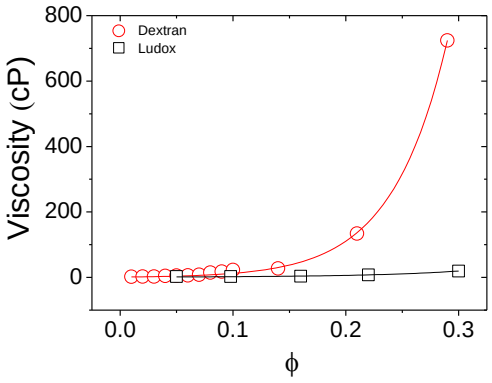

Figure 6.5.2. Viscosity as a function of volume fraction for dextran and Ludox solutions. The solid line is a stretched exponential fitting. $\eta = \eta_s \exp(a\phi^b)$, where η_s is the solvent (water) viscosity, 'a' and 'b' are adjustable parameters. For Ludox solution, a=12.7 and b=1.2 and for dextran solutions a=20.2 and b=0.9.

Table 6.5.1.

Phillies fit: $D = D_0 \exp(-\beta\phi^{\nu})$

Dextran

Particle radius, R_0 (nm)	β	ν
2.5	8.5±1.3	0.47±0.06
10	6.9±2.0	0.45±0.11

Ludox

Particle radius, R_0 (nm)	β	ν
2.5	10.9±1.3	1.01±0.05
10	11.2±2.9	1.08±0.12

CHAPTER 7

CONCLUSION AND FUTURE RESEARCH

The experiments comprising my dissertation have focused on nanoparticle dynamics in synthetic and bio-polymer solutions. As mentioned earlier in the thesis, understanding the transport properties of nanoparticles in macromolecular solutions is significant for several interdisciplinary fields of studies; colloidal physics, biophysics, microrheology etc.; as well as relevant for many technological applications. The optical measurements of FCS, conducted for these experiments, were performed by myself under the supervision of my advisor, Dr. Ashis Mukhopadhyay. Important observations of these experiments have been reported in chapters 4 through 6. In this concluding chapter, I will summarize the findings of these research projects as well as discuss the future research plans.

Owing to their mesoscopic length scale, soft matter systems are susceptible to thermal fluctuations. The dynamics of these systems are driven by Brownian motion, but the inherent length scales associated with the diffusing medium can also alter the system dynamics significantly. The Stokes-Einstein (SE) relation was developed for dynamics of mesoscopic objects in a homogeneous environment of relatively smaller solvent molecules. Its applicability becomes complicated in case of concentrated polymer solutions where various length scales are involved. We had observed that the R_o = 2.5 nm AuNPs diffused two to three orders of magnitude faster than that predicted by SE relation in 35 kDa PEG solutions (R_g = 8.6 nm). The ratio D/D_{SE}, in this linear polymer solution, showed positive deviation from unity with the deviation getting stronger with an increase

in concentration, and with a decrease in the ratio of R_o/R_g. The small sized AuNPs probed the nanoviscosity of the polymer solution rather than the overall bulk viscosity. The SE relation was observed to recover with particle size approaching the polymer size. It was concluded that the radius of gyration of the polymer is the crossover length scale for particles experiencing nanoviscosity or macroviscosity. The diffusion data was well fitted with the power law dependence on concentration as suggested by the recent scaling theory by Cai *et al.*

AuNP diffusion in biopolymer bovine serum albumin (BSA) demonstrated that BSA adsorbs on the surface of small sized AuNPs. The average change in NP hydrodynamic radius measured before and after protein adsorption was approximately 3.8 nm which corresponded to a BSA monolayer. Multi-layer formation was not observed even at significantly higher BSA concentrations. An anticooperative binding model best described the protein adsorption. The thickness of the adsorbed layer was independent of NP radius ranging from 2.5 - 10 nm. In addition, the NP diffusion was observed to have followed Stokes-Einstein prediction provided the thickness of the adsorbed layer was accounted for.

We also compared the diffusion of gold nanoparticles in solutions of randomly branched dextran to a solution of silica spheres with size similar to dextran. For both these cases, we observed that diffusion coefficient followed a stretched exponential function of concentration and followed Stokes-Einstein relation using the bulk viscosity irrespective of R_o/R_g values. This behavior was contrary to that of linear polymers . It was justified by considering that hydrodynamically dextran behaved as soft colloid.

Small sized AuNPs exhibited anomalous subdiffusion at higher concentrations of dextran solutions caused by the transient trapping of these NPs within the branches, whereas the bigger NPs did not show any such behavior and demonstrate normal diffusive behavior. No such behavior was observed in Ludox solutions either. Thus, the molecular structure of the crowding agent played a significant role in determining the diffusive behavior of probe particle.

My future goal will be to synthesize anisotropic nanoparticles and investigate their dynamics in complex solutions. Anisotropy in a particle can either be naturally inherited, like gold nanoparticles or induced by synthesizing Janus particles. These particles exhibit two faces in the sense that the properties of the two hemispheres are chemically different.[103] There is no centrosymmetry in the architecture of these particle making their synthesis challenging although recently some progress has been made in their preparation.[104] Many demanding problems involving production of dual functionalized devices in material science, biomedicine and other fields can be tackled with the advanced properties of these particles, thus making study of their dynamics significant. Particles will be prepared by half coating non-conducting cores such as silica or polystyrene with a metal. The FCS set up will be modified in order to measure rotational diffusion. A linear polarizer and a quarter-wave plate will be placed in the path of incident light to obtain circularly polarized light. A polarizing beam splitter will be used to provide polarized light to each of the photo multiplier tubes. In our experiments, we will investigate the dynamics of these anisotropic particles as a function of their size, polymer molecular weight, and temperature.

APPENDIX A: FCS WORK IN COLABORATION

The following is the summary of the research publication, that I had co-authored, with the focus on my contribution towards the same.[105] Magnetic oxide nanoparticles possess the potential to develop new biomedical applications including magnetic hyperthermia, magnetic resonance imaging contrast agents, targeted-drug delivery, among others.[106, 107] Iron oxide nanoparticles exhibit a number of properties; such as biocompatibility, superparamagnetic response etc.; which make them attractive for such applications.[108, 109] These magnetic nanoparticles are often required to be coated with suitable polymer to prevent agglomeration as well as to provide additional functionality to the system.[110] Dextran coated magnetic nanoparticles have been used in a number of clinical trials, and have been shown to circulate for long times with no reported toxicity; thus, making them an apt choice for our experiments.[111, 112]

The effective hydrodynamic diameter of the polymer coated nanoparticles is an important parameter in biomedical applications. It is generally determined by measuring the diffusion coefficient of the system in solution and using Stokes Einstein relation to determine the particle size. For this research project three different techniques, dynamical light scattering (DLS), fluorescence correlation spectroscopy (FCS), and magnetic susceptibility were particularly employed to determine the size of the dextran coated iron oxide nanoparticles. The core size of the Fe_3O_4 nanoparticles was determined by TEM measurements to be 12 ± 2 nm. My contribution was mainly towards the fluorescence correlation spectroscopy measurements to determine the size of polymer coated Fe_3O_4 NPs.

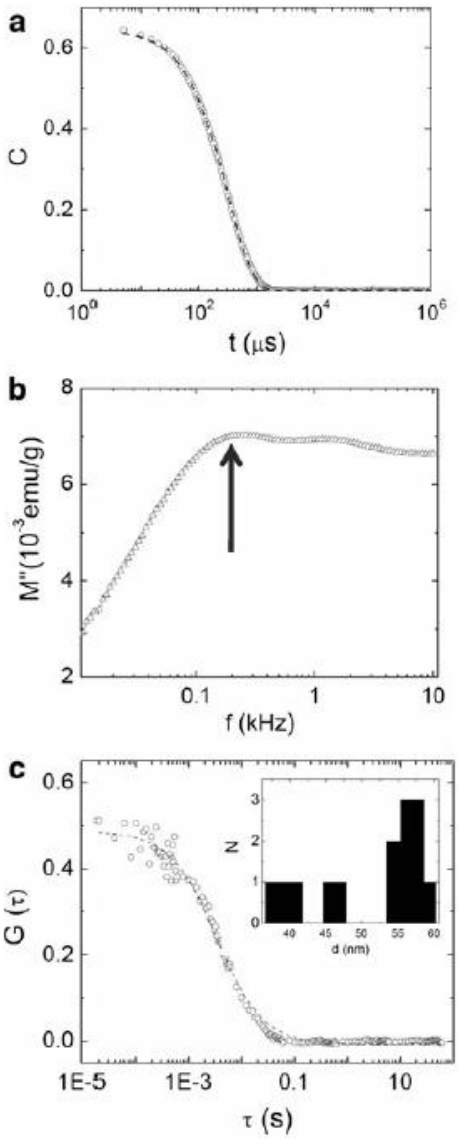

Figure A-1.1: (a) Autocorrelation curves by DLS for 5 kDa dextran coated NPs. (b) AC magnetic susceptibility measurements for 60-90 kDa dextran coated NPs. (c) Representative ACF for FCS measurements of 15-20 kDa dextran coated NPs Inset shows size distribution of NPs with repeated FCS measurements (Regmi 2011).

Fluorescence correlation spectroscopy measurements were conducted for iron oxide nanoparticles coated with 15-20 kDa dextran attached to the dye, FITC, with a solution volume fraction of .004%. A number of autocorrelations functions (ACF) were

collected. Figure A-1.1(c) shows a representative ACF collected by FCS and plotted versus logarithmic time lag. The ACF were fitted with the following model

$$G(\tau) = \frac{G(0)}{1+(\frac{8D\tau}{\omega_0^2})\sqrt{1+(\frac{8D\tau}{z_0^2})}} \qquad \text{A-1.1}$$

where G(0) is the magnitude of the autocorrelation function at short time ($\tau = 0$), ω_o is the half-width in the lateral direction, and z_o is the half-height in the axial direction of the laser focus. By performing a calibration experiment with dye molecule rhodamine 6G, we determined that $\omega_o \approx 0.45$ μm and $z_o \approx 2$ μm. The diffusion coefficient as obtained from the fit was D = 7.7 $\mu m^2/s$. Applying generalized Stokes-Einstein relation, the size of the dextran coated nanoparticles was estimated to be 57 nm. A statistical distribution of the nanoparticle size, shown as a histogram in the inset of figure A-1.1(c), was determined by repeating the FCS measurements on a number of different nanoparticles. The hydrodynamic diameter corresponding to a majority of the sample nanoparticles was estimated to lie in the range 55 ± 5 nm although the distribution obtained was not Gaussian.

The results of FCS measurements were inconsistent with the size measurements obtained from the other techniques used, DLS and magnetic susceptibility as a function of frequency.[105] The particle size, as determined by DLS, varied from 91 nm for nanoparticles coated with 5 kDa dextran to 132 nm for 670 kDa dextran. The magnetic susceptibility measurements reported the size to range from 105 nm for 5 kDa dextran to 136 nm for 670 kDa sample.

The physically expected value for the diameter of the surfaced nanoparticles was estimated by assuming that the maximum size would correspond to that of the core diameter plus twice the length of stretched dextran chain. The chain length of 20 kDa dextan was obtained from the literature to be 22 nm. The average core diameter determined by analyzing TEM data was 12 nm, resulting in an estimated maximum coated particle size of 56 nm. Thus, compared to other techniques, there was better agreement between FCS measurements and the expected hydrodynamic diameter.

It was argued that FCS studies on properly prepared samples provided a relatively accurate size estimate compared to other measurement techniques which overestimated the size by a factor of two. [105]

APPENDIX B: CURRENT WORK

FCS experiments were performed to investigate temperature dependence of translational diffusion of gold nanoparticles in linear polymer solutions. First the diffusion of these gold nanoparticles in pure water was observed as a function of temperature. Following this, temperature scan of AuNP diffusion in one particular concentration of polymer solution was conducted. Similar experiments were performed for different concentrations (wt%) of polymer solutions as well as for different sized gold nanoparticles. Poly(ethylene glycol) of M_w 5 kDa and AuNPs of radius 2.5 and 10 nm were used.

Since the diffusion was thermally activated, we calculated the corresponding activation energy, E_{act}, using

$$D = D_o \exp(-E_{act}/k_B T) \qquad \text{B-1.1}$$

Figure B-1.1 (a), (b) and (c) shows temperature dependence of particle diffusion coefficient. The corresponding activation energy can be calculated from the slope of ln D vs 1/T curve, as represented in figure B-1.1(d).

In the limited temperature range of our experiments, the ln D vs 1/T (k^{-1}), was well fitted with a straight line. The estimated E_{act} values for all experiments ranged from 0.1 to 0.6 eV/ molecule. For comparison we had also estimated the E_{act} for a dye molecule R6G which was approximately 0.04 eV/molecule. The E_{act} of dye molecule being smaller than that of AuNP implies that the energy barrier that the dye molecule should overcome to carry out a diffusion step is lower than that for AuNP. This can be attributed to the dye

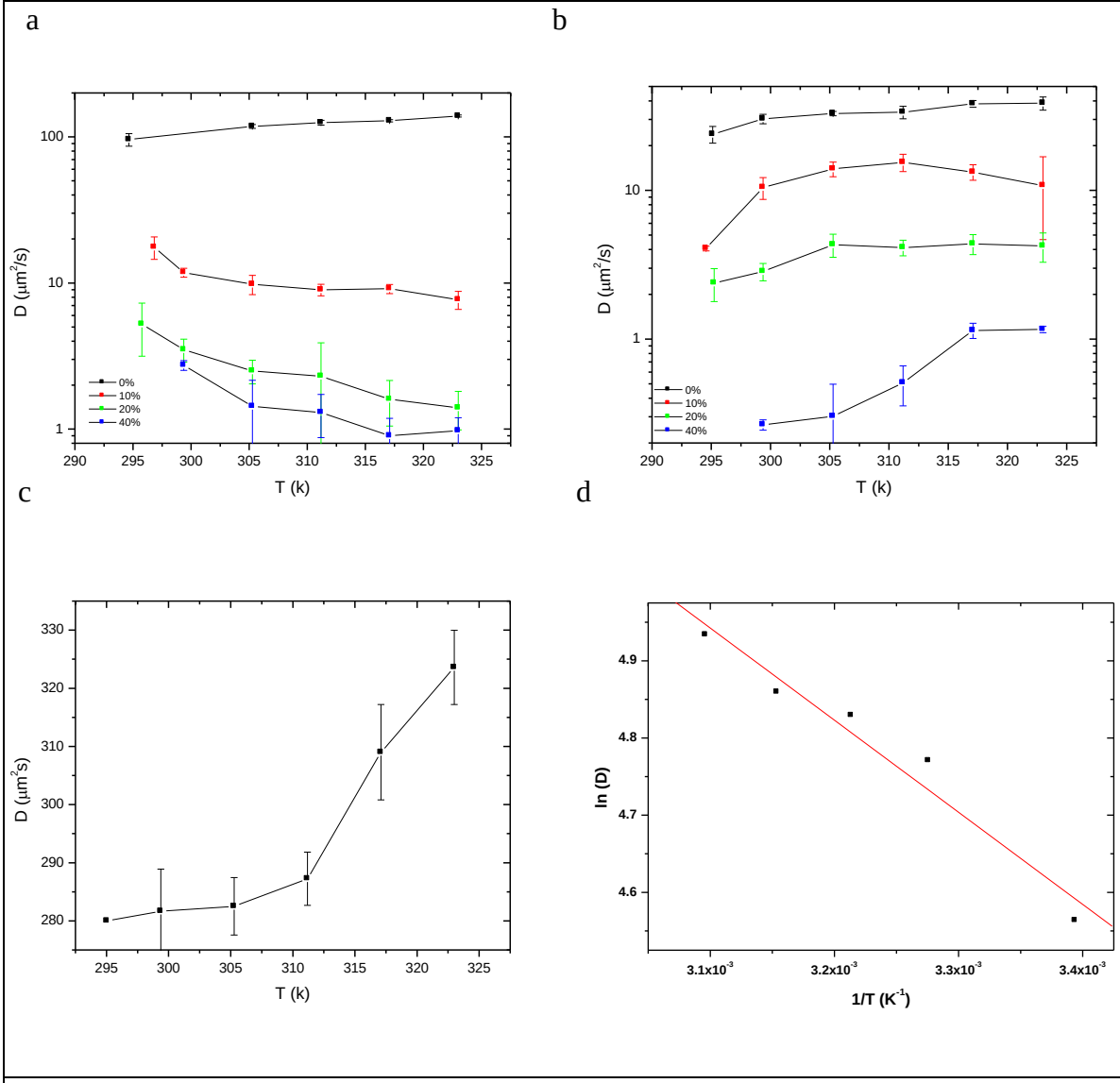

Figure B-1.1: Translational diffusion coefficient D ($\mu m^2/s$) vs Temperature (K) for (a) 2.5 nm radius AuNPs in PEG 5 kDa, (b) 10 nm radius AuNps in PEG 5 kDa (c) Rhodamine6G in water. The legend in graph a and b represent wt% of PEG in solvent. (d) Semi log plot of translational diffusion D vs 1/T (K^{-1}) for AuNP 2.5 nm in water. Solid line is the Arrhenius fit to obtain activation energy.

molecule being smaller in size than the AuNPs. The results obtained so far look interesting although a detailed analysis of this experimental data is yet to be done.

REFERENCES

1. R. A. L. Jones, Oxford University Press (2002).

2. I. W. Hamley, Wiley (2007).

3. M. Rubinstein and R. H. Colby, *Polymer Physics.* (Oxford University Press, New York, 2003).

4. S. Gupta, Q. L. Zhang, T. Emrick, A. C. Balazs and T. P. Russell, Nature Mater. **5**, 229-233 (2006).

5. P. K. Jain, I. H. El-Sayed and M. A. El-Sayed, Nano Today **2** (1), 18-29 (2007).

6. Y. Cu and W. M. Saltzman, Nat. Mater. **8**, 11-13 (2009).

7. M. J. Solomon and Q. Lu, Curr. Opin. Colloid Interface Sci. **6**, 430-437 (2001).

8. P.-G. de Gennes, *Scaling Concepts in Polymer Physics*. (Cornell University Press, Ithaca, NY, 1979).

9. J. Liu, D. Cao and L. Zhang, J. Phys. Chem. C **112**, 6653-6661 (2008).

10. V. Ganesan, V. Pryamitsyn, M. Surve and B. Narayanan, J. Chem. Phys. **124**, 221102 (2006).

11. L. H. Cai, S. Panyukov and M. Rubinstein, Macromolecules **44** (19), 7853-7863 (2011).

12. R. I. Cukier, Macromolecules **17**, 252-255 (1984).

13. M. Kruger and M. Rauscher, J. Chem. Phys. **131**, 094902-094909 (2009).

14. G. D. J. Phillies, G. S. Ullmann, K. Ullmann and T. H. Lin, J. Chem. Phys. **82**, 5242-5246 (1985).

15. T. Odijk, Biophys. J. **79**, 2314-2321 (2000).

16. T. H. Fan, J. K. G. Dhont and R. Tuinier, Phys Rev E **75** (1) (2007).

17. R. Tuinier and T. H. Fan, Soft Matter **4** (2), 254-257 (2008).

18. A. G. Ogston, Trans. Faraday Soc. **54**, 1754-1757 (1958).

19. A. G. Ogston, B. N. Preston, J. M. Snowden and J. D. Wells, Proc. R. Soc. London, A **333**, 297-316 (1973).

20. A. R. Altenberger and M. Tirrell, J. Chem. Phys. **80**, 2208-2213 (1984).

21. L. Johansson, C. Elvingson and J. E. Lofroth, Macromolecules **24**, 6024-6029 (1991).

22. B. Amsden, Macromolecules **32**, 874-879 (1999).

23. F. Brochard Wyart and P. G. de Gennes, Eur. Phys. J. E **1**, 93-97 (2000).

24. G. D. J. Phillies, Macromolecules **20**, 558-564 (1987).

25. G. D. J. Phillies and D. Clomenil, Macromolecules **26** (1), 167-170 (1993).

26. K. Kremer and G. S. Grest, J. Chem. Phys. **92**, 5057 (1990).

27. M. Kroger, W. Loose and S. Hess, J. Rheol. **37**, 1057.

28. D. Langevin and F. Rondelez, Polymer **19** (8), 875-882 (1978).

29. J. Won, C. Onyenemezu, W. G. Miller and T. P. Lodge, Macromolecules **27** (25), 7389-7396 (1994).

30. X. Ye, P. Tong and L. J. Fetters, Macromolecules **31** (17), 5785-5793 (1998).

31. A. Michelman-Ribeiro, F. Horkay, R. Nossal and H. Boukari, Biomacromolecules **8** (5), 1595-1600 (2007).

32. R. Holyst, A. Bielejewska, J. Szymanski, A. Wilk, A. Patkowski, J. Gapinski, A. Zywocinski, T. Kalwarczyk, E. Kalwarczyk, M. Tabaka, N. Ziebacz and S. A. Wieczorek, Phys Chem Chem Phys **11** (40), 9025-9032 (2009).

33. Y. Cheng, R. K. Prud'homme and J. L. Thomas, Macromolecules **35** (21), 8111-8121 (2002).

34. T. H. Lin and G. D. J. Phillies, J Phys Chem-Us **86** (20), 4073-4077 (1982).

35. P. Tong, X. Ye, B. J. Ackerson and L. J. Fetters, Phys Rev Lett **79** (12), 2363-2366 (1997).

36. K. Vangala, F. Ameer, G. Salomon, V. Le, E. Lewis, L. Yu, D. Liu and D. Zhang, J. Phys. Chem. C **116** (5), 3645-3652 (2012).

37. E. Casals and V. F. Puntes, Nanomedicine **7** (12), 1917-1930 (2012).

38. C. Rocker, M. Potzl, F. Zhang, W. J. Parak and G. U. Nienhaus, Nature nanotechnology **4** (9), 577-580 (2009).

39. X. M. He and D. C. Carter, Nature **358** (6383), 209-215 (1992).

40. S. H. Brewer, W. R. Glomm, M. C. Johnson, M. K. Knag and S. Franzen, Langmuir **21**, 9303-9307 (2005).

41. S. Dominguez-Medina, S. McDonough, P. Swanglap, C. F. Landes and S. Link, Langmuir **28** (24), 9131-9139 (2012).

42. D. H. Tsai, F. W. Delrio, A. M. Keene, K. M. Tyner, R. I. Maccuspie, T. J. Cho, M. R. Zachariah and V. A. Hackley, Langmuir (2011).

43. R. Rigler and E. S. Elson, Springer (2001).

44. D. E. Madge, E. L. Elson and W. W. Webb, Phys. Rev. Lett. **29**, 705-708 (1972).

45. O. Krichevsky and G. Bonnet, Rep. Prog. Phys. **65**, 251–297 (2002).

46. H.-X. Zhou, G. Rivas and A. P. Minton, Annu. Rev. Biophysics. **37**, 375-397 (2008).

47. K. M. Berland, P. T. C. So and E. Gratton, Biophys. J. **68**, 694-701 (1995).

48. P. Schwille and E. Haustein, (2002).

49. H. E. and S. P., Annu. Rev. Biophys. Biomol. Struct. **36**, 151-169 (2007).

50. G. J. Brakenhoff, M. Muller and R. I. Ghauharali, Journal of Microscopy. **183**, 140-144 (1996).

51. P. T. C. So, T. French, W. M. Yu, K. M. Berland, C. Y. Dong and E. Gratton, Chemical Analysis Series **137**, 351-374 (1996).

52. I. Kohli and A. Mukhopadhyay, Macromolecules **45** (15), 6143-6149 (2012).

53. W. B. Russel, D. A. Saville and W. R. Schowalter, *Colloidal Dispersions*. (Cambridge University Press, Cambridge, U. K., 1989).

54. J. Liu, L. Zhang, D. Cao and W. Wang, Physical chemistry chemical physics : PCCP **11** (48), 11365-11384 (2009).

55. L. Masaro and X. X. Zhu, Prog Polym Sci **24** (5), 731-775 (1999).

56. R. Omari, A. Aneese, C. Grabowski and A. Mukhopadhyay, J. Phys. Chem. B **113**, 8448-8451 (2009).

57. G. H. Koenderink, S. Sacanna, D. G. A. L. Aarts and A. P. Philipse, Phys. Rev. E **69**, 021804 (2004).

58. G. S. Ullmann, K. Ullmann, R. M. Lindner and G. D. J. Phillies, J Phys Chem-Us **89** (4), 692-700 (1985).

59. N. Ziebacz, S. A. Wieczorek, T. Kalwarczyk, M. Fiakowski and R. Holyst, Soft Matter **7** (16), 7181-7186 (2011).

60. L.-H. Cai, S. Panyukov and M. Rubinstein, Macromolecules **44**, 7853–7863 (2011).

61. S. A. Egorov, J Chem Phys **134** (8) (2011).

62. C. N. Onyenemezu, D. Gold, M. Roman and W. G. Miller, Macromolecules **26** (15), 3833-3837 (1993).

63. C. Grabowski and A. Mukhopadhyay, Appl. Phys. Lett. **94**, 021903 (2009).

64. K. Devanand and J. C. Selser, Macromolecules **24**, 5943-5947 (1991).

65. A. Ochab-Marcinek and R. Holyst, Soft Matter **7** (16), 7366-7374 (2011).

66. W. W. Graessley, Adv. Polym. Sci. **47**, 67-117 (1982).

67. V. Pryamitsyn and V. Ganesan, Phys Rev Lett **100** (12) (2008).

68. I. Kohli, S. Alam, B. Patel and A. Mukhopadhyay, Appl. Phys. Lett. **102**, 203705 (2013).

69. N. J. Durr, T. Larson, D. K. Smith, B. A. Korgel, K. Sokolov and A. Ben-Yakar, Nano Letters **7** (4), 941-945 (2007).

70. X. Shi, D. Li, J. Xie, S. Wang, Z. Wu and H. Chen, Chin. Sci. Bull. **57** (10), 1109-1115 (2012).

71. M. A. Dobrovolskaia, A. K. Patri, J. Zheng, J. D. Clogston, N. Ayub, P. Aggarwal, B. W. Neun, J. B. Hall and S. E. McNeil, Nanomedicine : nanotechnology, biology, and medicine **5** (2), 106-117 (2009).

72. P. Aggarwal, J. B. Hall, C. B. McLeland, M. A. Dobrovolskaia and S. E. McNeil, Advanced Drug Delivery Reviews **61** (6), 428-437 (2009).

73. J. B. Hall, M. A. Dobrovolskaia, A. K. Patri and S. E. McNeil, Nanomedicine **2** (6), 789-803 (2007).

74. M. Lundqvist, J. Stigler, G. Elia, I. Lynch, T. Cedervall and K. A. Dawson, Proc Natl Acad Sci U S A **105** (38), 14265-14270 (2008).

75. S. Chakraborty, P. Joshi, V. Shanker, Z. A. Ansari, S. P. Singh and P. Chakrabarti, Langmuir **27** (12), 7722-7731 (2011).

76. C. A. Grabowski, B. Adhikary and A. Mukhopadhyay, Applied Physics Letters **94** (2) (2009).

77. R. A. Farrer, F. L. Butterfield, V. W. Chen and J. T. Fourkas, Nano Letters **5** (6), 1139-1142 (2005).

78. G. J. Brownsey, T. R. Noel, R. Parker and S. G. Ring, Biophysical journal **85** (6), 3943-3950 (2003).

79. G. D. J. Phillies, Macromolecules **20**, 558-564 (1987).

80. R. Holyst, A. Bielejewska, J. Szymanski, A. Wilk, A. Patkowski, J. Gapinski, A. Zywocinski, T. Kalwarczyk, E. Kalwarczyk, M. Tabaka, N. Ziebacz and S. A. Wieczorek, Physical Chemistry Chemical Physics **11** (40), 9025-9032 (2009).

81. E. Casals, T. Pfaller, A. Duschl, G. J. Oostingh and V. Puntes, ACS nano **4** (7), 3623-3632 (2010).

82. S. H. Brewer, W. R. Glomm, M. C. Johnson, M. K. Knag and S. Franzen, Langmuir **21** (20), 9303-9307 (2005).

83. K. Luby-Phelps, Int. Rev. Cytol. **192**, 189-221 (2000).

84. N. Kozer , Y. Y. Kuttner, G. Haran and G. Schreiber, Biophys. J. **92**, 2139-2149 (2007).

85. R. Macnab, Science **290**, 2086-2087 (2000).

86. H. Berry, Biophys. J. **83**, 1891-1901 (2002).

87. F. Crick, Nature **225**, 420-422 (1970).

88. K. Sasahara, P. McPhie and A. P. Minton, J. Mol. Biol. **326**, 1227-1237 (2003).

89. S. P. Zustiak, R. Nossal and D. L. Sackett, Biophysical journal **101** (1), 255-264 (2011).

90. I. Pastor, E. Vilaseca, S. Madurga, J. L. Garces, M. Cascante and F. Mas, The journal of physical chemistry. B **115** (5), 1115-1121 (2011).

91. D. S. Banks and C. Fradin, Biophysical journal **89** (5), 2960-2971 (2005).

92. A. B. Goins, H. Sanabria and M. N. Waxham, Biophysical journal **95** (11), 5362-5373 (2008).

93. M. Weiss, M. Elsner, F. Kartberg and T. Nilsson, Biophysical journal **87** (5), 3518-3524 (2004).

94. J. Smit, J. A. P. P. van Dijk, M. G. Mennen and M. Daoud, Macromolecules **25**, 3585-3590 (1992).

95. E. Nordmeier, J. Phys. Chem. **97**, 5770-5785 (1993).

96. E. Antoniou and M. Tsianou, Journal of Applied Polymer Science **125** (3), 1681-1692 (2012).

97. M. D. Ediger, Annu. Rev. Phys. Chem. **51**, 99-128 (2000).

98. T. G. Fox and S. LOSHAEK, Journal of polymer science **15** (80), 371-390 (1955).

99. D. Z. Icoz, C. I. Moraru and J. L. Kokini, Carbohyd. Polym. **2**, 120-129 (2005).

100. E. R. Weeks and D. A. Weitz, Phys. Rev. Lett. **89**, 095704 (2002).

101. F. Santamaria, S. Wils, E. De Schutter and G. J. Augustine, The European journal of neuroscience **34** (4), 561-568 (2011).

102. F. Amblard, A. C. Maggs, B. Yurke, A. N. Pargellis and S. Leibler, Phys. Rev. Lett. **77**, 4470-4473 (1996).

103. A. Perro, S. Reculusa, S. Ravaine, E. Bourgeat-Lami and E. Duguet, J. of Mat. chem. **15**, 3745 (2005).

104. A. Walther and A. H. E. Muller, Soft Matter **4**, 663 (2008).

105. R. Regmi, V. Gumber, v. Subba Rao, I. Kohli, C. Black, C. Sudakar, P. Vaishnava, V. Naik, R. Naik, A. Mukhopadhyay and G. Lawes, J. nanopart. Res. **13**, 6869 (2011).

106. Q. A. Pankhurst, J. Connolly, S. K. Jones and J. Dobson, J. Phys. D: Appl. Phys. **36**, R167 (2003).

107. P. Tartaj, M. D. P. Morales, S. Veintemillas-Verdaguer, T. Gonzalez-Carreno and C. J. Serna, J. Phys. D: Appl. Phys. **36**, R182 (2003).

108. C. Wilhelm, C. Bilotey, J. Roger, J. N. Pons, J.-C. Bacri and F. Gazeau, Biomaterials **24**, 1001 (2003).

109. C. C. Berry, S. Wells, S. Charles, G. Aitichison and C. A.S.G., Biomaterials **25**, 5405 (2004).

110. A. Villanueva, M. Canete, A. G. Roca, M. Calero, S. Veintemillas-Vergaguer, C. J. Serna, M. P. Morales and R. Miranda, Nanotechnology **20**, 115103 (2009).

111. Y. Anzai, K. E. Blackwell, S. L. Hirschowitz, J. W. Rogers, Y. Sato, W. T. Yuh , V. M. Runge, M. R. Morris, S. J. McLachlan and R. B. Lufkin, Radiaology **192**, 709 (1994).

112. A. Moore, E. Marecos, A. Bogdanov and R. Weissleder, Radiology **214**, 568 (2000).

ABSTRACT

DIFFUSION OF NANOPARTICLES IN SYNTHETIC AND BIOPOLYMER SOLUTIONS

by

INDERMEET KOHLI

AUGUST 2013

Advisor: Dr. Ashis Mukhopadhyay

Major: Physics

Degree: Doctor of Philosophy

Soft matter systems of colloidal particles, polymers, amphiphiles and liquid crystals are ubiquitous in our everyday life. Food, plastics, soap and even human body is comprised of soft materials. Research conducted to understand the behavior of these soft matter systems at molecular level is essential for many interdisciplinary fields of study as well as important for many technological applications.

We used gold nanoparticles (Au NPs) to investigate the length-scale dependent dynamics in semidilute poly(ethylene glycol) (PEG)-water, bovine serum albumin (BSA)-phosphate buffer, dextran and particulate solutions. In case of PEG-water solutions, fluctuation correlation spectroscopy was used to measure the diffusion coefficients (D) of the NPs as a function of their radius, R_o (2.5-10 nm), PEG volume fraction, ϕ (0-0.37) and molecular weight, M_w (5 kg/mol and 35 kg/mol). Our results

indicate that the radius of gyration, R_g of the polymer chain is the crossover length scale for the NPs experiencing nanoviscosity or macroviscosity.

In BSA-phosphate buffer solutions, we observed a monolayer formation at the NP surface with a thickness of 3.8 nm. The thickness of the adsorbed layer was independent of NP size. Best fit was obtained by the anticooperative binding model with the Hill coefficient of n = 0.63. Dissociation constant (K_D) increased with particle size indicating stronger interaction of BSA with smaller sized NPs.

We also contrasted the diffusion of gold nanoparticles (AuNPs) in crowded solutions of randomly branched polymer (dextran) and rigid, spherical particles (silica) to understand the roles played by the probe size and structure of the crowding agent in determining the probe diffusion. AuNPs of two different sizes (2.5 nm & 10 nm), dextran of molecular weight 70 kDa and silica particles of radius 10 nm were used. Our results indicated that the AuNP diffusion can be described using the bulk viscosity of the matrix and hydrodynamically dextran behaved similar to soft colloid. In all situations, we observed normal diffusion except for 2.5 nm sized AuNP particles in dextran solution at higher volume fraction. This was caused by transient trapping of particles within the random branches. The results showed the importance of macromolecular architecture in determining the transport properties in intracellular matrix and in cells with spiny dendrites.

AUTOBIOGRAPHICAL STATEMENT

Education:

- 2008-2013, Wayne State University, Detroit MI: Doctor of Philosophy in Condensed Matter Physics
- 2001-2005, Punjabi University - Patiala, Punjab, India: Bachelor of Science in Physics, Chemistry, Mathematics and Education

Publications:

- Indermeet Kohli and Ashis Mukhopadhyay, "Contrasting Nanoparticle Diffusion in Branched Polymer and Particulate Solutions: More Than Just Volume Fraction", Manuscript under review at Soft matter, July 2013.
- Indermeet Kohli, Sharmine Alam, Bhavdeep Patel and Ashis Mukhopadhyay, "Interaction and Diffusion of Gold Nanoparticles in Bovine Serum Albumin Solutions", Appl. Phys. Lett. (2013) **102**, 203705
- Indermeet Kohli and Ashis Mukhopadhyay, "Diffusion of Nanoparticles in Semidilute Polymer Solutions: Effect of Different Length Scales", Macromolecules (2012) **45** (15), 6143–6149
- R. Regmi, V. Gumber, V. Subba Rao, I. Kohli, C. Black, C. Sudakar, P. Vaishnava, V. Naik, R. Naik, A. Mukhopadhyay, G. Lawes, "Discrepancy between different estimates of the hydrodynamic diameter of polymer-coated iron oxide nanoparticles in solution", J. Nanopart Res (2011) **13**, 6869–6875